



Recent progress in low-voltage cathodoluminescent materials: synthesis, improvement and emission properties

| | |
|-------------------------------|--|
| Journal: | <i>Chemical Society Reviews</i> |
| Manuscript ID: | CS-REV-03-2014-000109.R1 |
| Article Type: | Review Article |
| Date Submitted by the Author: | 03-May-2014 |
| Complete List of Authors: | Li, Guogang; China University of Geosciences, Faculty of Materials Science and Chemistry lin, j; Changchun inst appl chem, rare earth lab |
| | |

Cite this: DOI:

www.rsc.org/xxxxxx

REVIEW

Recent progress in low-voltage cathodoluminescent materials: synthesis, improvement and emission properties

Guogang Li^{ab} and Jun Lin*^a

^a State Key Laboratory of Rare Earth Resource Utilization, Changchun Institute of Applied Chemistry, Chinese Academy of Sciences, Changchun 130022, P. R. China. E-mail: jlin@ciac.ac.cn; Fax: (+86) 431-85698041

^b Faculty of Materials Science and Chemistry, China University of Geosciences, Wuhan 430074, P. R. China. E-mail: ggli8312@gmail.com

* Author to whom any correspondence should be addressed.

10

Nowdays there are several technologies used for flat panel displays (FPDs), and developing FPDs with enhanced energy efficiency and improved display quality is strongly stimulated. Field emission displays (FEDs) have been considered as one of the most promising next generation flat panel display technologies due to its excellent display performances and low energy consumption. During the development of FEDs, phosphors are irreplaceable components. In the past decade, the exploring of highly efficient low-voltage cathodoluminescent materials, namely FED phosphors, has been becoming the focus of enhancing energy efficiency and realizing high-quality display. This review summaries the recent progress in chemical synthesis and improvement of novel and rare-earth and transition metal ions activated inorganic cathodoluminescent materials with powder and thin film forms. Discussion is focused on the modification of morphology, size, surface, composition, conductivity of phosphors and corresponding effects on their cathodoluminescent properties. Special emphases are given to the selection of host and luminescent centers, the adjustment of emission colors through doping concentration optimization, energy transfer and mono- or co-doping activator ions, the improvement of chromaticity, color stability and color gamut as well as the saturation behavior and the degradation behavior of phosphors under the excitation of low-voltage electron beam. Finally, the research prospects and future directions of FEDs phosphors are discussed with recommendations to facilitate the further exploration of new and highly efficient low-voltage cathodoluminescent materials.

Keywords: Field emission displays, Cathodoluminescence, Rare earth, Phosphor, Thin film.

1. Introduction

Currently, quite a few technologies are being developed for flat panel displays (FPDs), including plasma display panels (PDPs), electroluminescence (EL) devices, field emission displays (FEDs) and liquid crystal displays (LCDs) and so on. Now people have more and more requirements for image quality. Therefore, developing display panel technologies with enhanced energy efficiency and improved display quality is strongly stimulated.¹ Of these display technologies, in recent years, FEDs have been investigated for the development of full color flat panel display, which is considered as one of the most promising technologies for next generation FPDs due to their potential advantages in aspects of display quality (brightness, contrast ratio, angle of viewing, response time), power consumption, stability, lifetime, etc.²⁻⁴ For FED, its basis is an array of field emitter tips cathodes aligned opposite to the phosphor anode, as shown in Scheme 1. Therefore, the development of FEDs mainly depends on the following aspects: field emitter arrays (namely electron-emitting microcathode arrays), the packaging of FEDs devices and luminescent materials.⁵ The field emitter arrays may be manufactured using a variety of materials (Mo, W, Ta, ZnO,

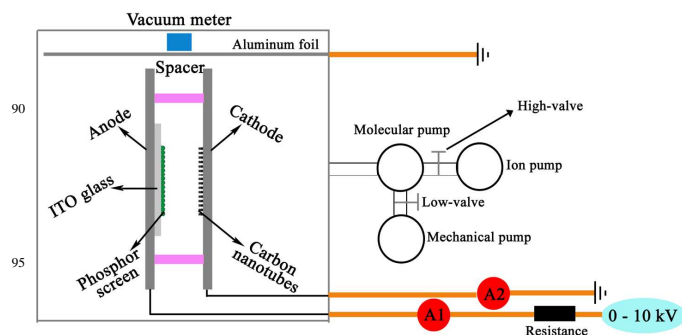
Silicon-based and Carbon-based materials etc.) by the photolithography with thin film deposition and etching.⁵ Moreover, the cathode technology is advanced and its development affects the energy efficiency of FEDs. Because a number of issues exist in the packaging of FEDs devices, including frit seals, spacers to maintain cathode/anode distances, dielectric breakdown, plasma discharge, and vacuum generation and maintenance, the packaging of FEDs is also necessary for the improvement of the display performance. While luminescent materials (or phosphors) are indispensable components of FEDs devices, whose luminescent efficiencies and properties not only determine the quality of images but also affect the energy efficiency of display devices.⁶⁻⁹ Therefore, selection of the phosphors for the anode is critical for FEDs. In order to make FEDs come into market, it is clear that continued improvements are required in microcathode arrays and packaging technologies, especially for the phosphors. Consequently, in the past decade, the exploring and development of highly efficient low-voltage cathodoluminescent materials and improvement of existing FEDs phosphors have been becoming the focus of FEDs devices.¹⁰⁻²²

Basically, the operation principle of FEDs is similar to that of conventional cathode ray tubes (CRTs) in which the images originate from the excitation of electrons on phosphors (Scheme

1). However, requirements for phosphors applied in FEDs are greatly different from those used in CRTs due to the lower accelerating voltages and the higher current densities. Firstly, FEDs phosphors should decrease or avoid the release of gasses in the FED devices that is connected with progressive degradation of vacuum level in the display space to extend its operating time.²³⁻²⁶ Secondly, for FEDs phosphors, the excellent cathodoluminescent properties such as high emission intensity, high luminous efficiency, high saturation current density, high color purity and good stability and durability under low accelerating voltages (≤ 7 kV) and high current density (≥ 100 $\mu\text{A}/\text{cm}^2$) are essential.²⁷⁻²⁹ Based on the above reasons, the selection of suitable hosts and luminescent centers is very important for synthesis of FEDs phosphors.³⁰ As activator ions, rare earth (RE) ions have been playing an important role in modern lighting and display fields due to the abundant emission colors in the whole visible light range owing to their $4f \rightarrow 4f$ or $5d \rightarrow 4f$ transitions.³¹ In addition, transition metal ion (Mn^{2+}), Bi^{3+} ion and some groups (e.g. WO_4^{2-} , MoO_4^{2-} , GeO_4^{4-} , SnO_6^{2-} , TiO_6^{2-} , NbO_4^{2-}) are also efficient luminescent centers.³²⁻³⁹ For host materials, so far many efficient sulfide-based phosphors such as $\text{Y}_2\text{O}_2\text{S}:\text{Eu}^{3+}$, $\text{Gd}_2\text{O}_2\text{S}:\text{Tb}^{3+}$, $\text{SrGa}_2\text{S}_4:\text{Eu}^{3+}/\text{Ce}^{3+}$, $(\text{Zn}/\text{Cd})\text{S}:\text{Cu}, \text{Al}$, and $\text{ZnS}:\text{Ag}, \text{Cl}$, etc. have been explored as efficient low-voltage cathodoluminescent materials.⁴⁰⁻⁴³ Unfortunately, sulfide phosphors are easily decomposed and emit sulfide gases under electron bombardment due to dissociation of the cation-sulfur bonds, subsequently damage emission tips, shorten the device lifetime and simultaneously contaminate environment, which deny the practical application in FEDs devices.^{44, 45} For the same reasons, $\text{ZnS}:\text{Mn}$ nanomaterials, CdSe/ZnS quantum dots composites need to be eliminated, and the influence of other gasses on FED operation should also be avoided.⁴⁶⁻⁴⁸ In avoid of the abovementioned defects, oxide-based phosphors including rare-earth and transition metal ions doped garnets, oxides, silicates, phosphates, vanadates, perovskites, etc.⁴⁹⁻⁶² have gained increasing concerns due to their better thermal stability, chemical stability and environmental friendliness compared with sulfides. However, most of these phosphors are insulators and negative loading is easy to accumulate on the grain surface in phosphor layer, which decreases cathodoluminescent efficiency. That is why the electrical conductivity of FED phosphors should be high enough to avoid charge accumulation.²⁷ In order to overcome this drawback, in recent years many semiconductor-based materials such as ZnO , Ga_2O_3 , $(\text{Gd}, \text{Lu})_3\text{Ga}_5\text{O}_{12}$, $\text{Zn}(\text{Ga}, \text{In})_2\text{O}_4$, $(\text{Ca}, \text{Sr})\text{In}_2\text{O}_4$, $\text{Zn}_3\text{Ta}_2\text{O}_8$, Zn_2GeO_4 , GaGe_2O_5 , Mg_2SnO_4 , ZnGeN_2 , etc. are explored as low-voltage cathodoluminescent materials through the efficient doping of RE^{3+} , Mn^{2+} and Bi^{3+} ions.^{17, 43, 63-75} Besides, the current low voltage cathodoluminescent materials also suffer rough surfaces, irregular shape and size distribution, poor adherence to substrates, poor preparing of phosphor screens (thin films) from phosphor powders, simultaneously the color saturation and color index need be further improved to enhance display quality.^{15, 76, 77} All these considerations and the ever-growing demand for highly efficiently low voltage cathodoluminescent materials in FEDs prompt researchers to reach a cognitive that more attention should be paid to improve existing phosphors and develop newly efficient low voltage cathodoluminescent materials.

On another level, in modern chemistry and materials science, the tremendous advances in the synthetic control of morphology, size, dimensionality and composition allows researchers to tailor chemical and physical properties of materials and thus, the rational control over these factors has motivated scientific and technological efforts in recent years.⁷⁸⁻⁸⁵ The morphology, size,

composition, surface, and crystallization can influence the cathodoluminescent properties of phosphors.²⁷ To date, many efforts have been made to explore excellent approaches for the fabrication of a variety of inorganic luminescence materials to improve their performance in applications. Among them, the soft-chemical methods are intensively pursued as effective and convenient approaches to prepare various inorganic cathodoluminescent materials with controllable shape, size, surface form, composition and luminescent properties.^{15, 66, 86-97} In this critical review, we summaries the recent progress in chemical synthesis and improvement of existing and new phosphors including RE^{3+} ions and transition metal ions activated inorganic oxide-based luminescence materials, semiconductor-based luminescence materials, self-activated luminescent materials etc. We discuss the modifications and optimizations in morphology, size, composition, conductivity of phosphors and their cathodoluminescent properties. Some emphases are also focused on the studies of selection of hosts and luminescent centers, enhancement of efficiency through energy transfer, adjustment and design of emission colors, improvement of color index and color gamut as well as color stability and degradation behavior of phosphors.



Scheme 1 A schematic model of analogue FED device. (reproduced with the permission from ref. 94, copyright 2011, Optical Society of America)

2. Improvement and development of FEDs phosphor powders

2.1 Improvement of phosphor powders

It is well known that the most common form of phosphors is powders, which are mixed with organic binders to spread on a substrate for display and lighting applications.⁶⁻⁸ Conventionally, phosphor powders are prepared by the solid reaction process, i.e., direct mixing of precursor components (oxides and inorganic salts etc.) and firing them at high temperature for long time with repeat grinding process. This process usually suffers from waste of energy ($>1000^\circ\text{C}$, >10 h in general), contamination of impurities, and inhomogeneous composition and morphology (>3 μm particles with irregular shapes, wide size distribution, and serious aggregation) for the final phosphor products, which might result in a damage of luminescent performance of phosphors.⁹⁸ Because of the morphology, size, composition, surface, and crystallization have great effects on the cathodoluminescent properties of phosphors, many efforts have been made to explore suitable methods to control these factors for improving their cathodoluminescent performance, which has technological and fundamental scientific importance.¹⁵ Specifically, high-quality

displays will require better low voltage efficiencies, chromaticity, saturation behavior, and maintenance of phosphors. Some possible routes to achieve the above improvements are discussed in the following section.

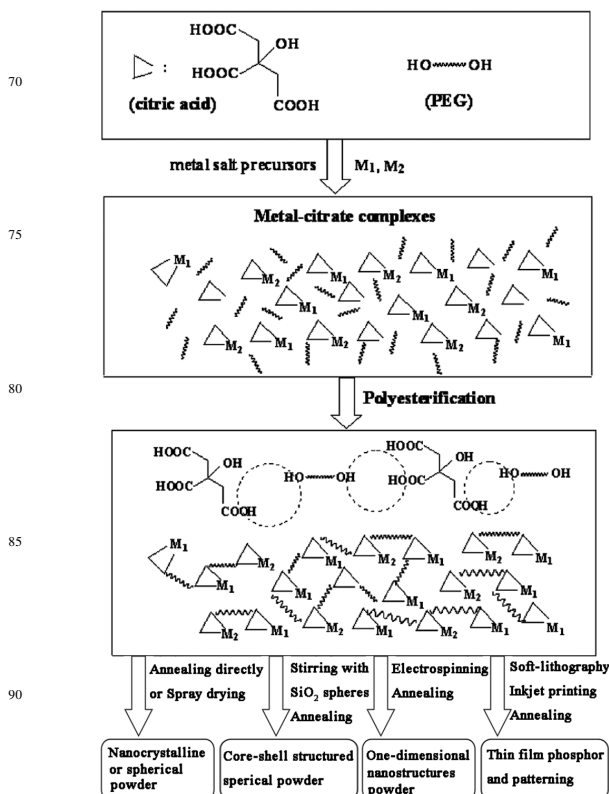
2.1.1. Modification of particle morphology, surface and size

Usually, soft chemistry processes are utilized to design and synthesize inorganic nano/microstructures with various kinds of shape, size, and chemical composition for application as advanced functional and engineering materials.^{99, 100} In recent years, a large number of synthetic methods have been developed for generating and improving inorganic cathodoluminescent materials.¹⁵ After reviewing recent phosphors being developed in FEDs devices, advances in soft chemistry synthesis (such as sol-gel, hydrothermal, spray pyrolysis, electrospinning, homogenous precipitation, high boiling solvent, combustion, and microwave) of low-voltage cathodoluminescent materials are summarized and discussed.^{15, 66, 86-97} In general, soft chemistry synthesis can produce future generation phosphors with better morphology and surface forms (more regular shape, spherical in some cases), and narrower size dispersions at moderate temperatures (<1000°C). These factors can decrease the light scattering and nonradiative transitions of phosphors, which is conducive to enhance the cathodoluminescent performance. On the other hand, for FED phosphor powders, the particle size is critical to loading on screens, which further influences their luminescent performance.^{27, 101} It is known that the cathodoluminescent emission intensities and brightness of FEDs phosphors increases with increasing the accelerating voltage and the filament current of anodes, which is attributed to the deeper penetration of the electrons into the phosphor body and the larger electron-beam current density. The electron penetration depth can be estimated using the empirical formula:

$$L[\text{Å}] = 250 \left(\frac{A}{\rho} \right) \left(\frac{E}{\sqrt{Z}} \right)^n, n = \frac{1.2}{1 - 0.29 \lg Z} \quad (1)$$

where $n = 1.2/(1 - 0.29 \lg Z)$, and A is the atomic or molecular weight of the material, ρ is the bulk density, Z is the atomic number or the number of electrons per molecule in the compounds, and E is the accelerating voltage (kV).⁸⁶ The deeper the electron penetration depth, the more plasma will be produced, which results in the CL intensity increases. However, according to the above empirical formula, the electron penetration depth into phosphors are general tens of nanometers in FED devices due to the low excitation voltage (1–7 kV), which makes activator ions in the inner of phosphor particles with big size (microsize) cannot be efficiently excited. So reasonable particle size is important for improving their cathodoluminescent efficiencies. In addition, the resolution is a pivotal index for display quality, which is also closely related to the particle size of the luminescent materials.¹⁰² Although, some theoretical and experimental considerations have suggested that the most efficient phosphors are submicron grain size of spherical shape,^{103, 104} nanoparticle phosphors might be more appropriate for low-voltage FED application in terms of the following aspects:^{15, 27, 101} 1) In some cases, the preparation of nanocrystalline phosphors requires much less temperature and time in comparison with conventional microsize grains, which low the synthesis cost; 2) The employment of such materials allowed for optimal packaging of grains, avoids cutting of the picture spot and decreases scattering of light-emitting layer, which enhance the efficiency of phosphor layer and the quality of images; 3) At present, many optoelectronic devices trend to micromation, phosphor powders with small grain size allowed a fabrication of thin light-emitting film that could extend the

display operating time and fundamentally decreased the total resistance of phosphor layer. Based on the above reasons, recently, some researchers pay more attention to optimize low-voltage cathodoluminescent materials in nano- or submicrosize via various soft chemical synthesis processes for improving their luminescence efficiency.



Scheme 2 Basic Principle of Pechini-Type Sol-Gel (PSG) Process and Multifunctional Optical Materials Derived from It. (reproduced with the permission from ref. 99, copyright 2007, American Chemical Society).

Sol-gel process. The sol-gel technique is one of the most well-known soft chemistry processes, which can be generally divided into three types judging by different use of precursors:⁹⁹ a) sol-gel process under hydrolysis and condensation of molecular precursors; b) gelation process under concentration of aqueous solutions into metal-chelates, namely, “chelate” route; c) polymerization and complex process (called Pechini-type sol-gel process, and abbreviate as PSG). Because most of the metal alkoxides suffer from high cost, unavailability, toxicity, and fast hydrolysis rate that result in difficult in controlling the homogeneity of different components during experimental processes, and thus the latter processes, especially PSG process are frequently employed in the preparation of multicomponent metal oxide materials. PSG process that commonly uses metal salts as precursors, citric acid (CA) as a chelating ligand of metal ions and polyhydroxy alcohol such as ethylene glycol (EG) or poly(ethylene glycol) (PEG) as a cross-linking agent to form a polymeric resin on the molecular level, which can ensure compositional homogeneity and enhance dispersion of particles. Since CA is a polybasic compound having three carboxylic acid groups and one alcoholic group in one molecule, rare earth ions

and other non-monovalent cations can form very stable chelate complexes with CA. The potential ability of CA to solubilize a wide range of metal ions in a mixed solvent of EG/PEG and H₂O is of prime importance, especially for systems involving cations that can be readily hydrolyzed to form insoluble precipitates in the presence of water. An advantage of the PSG process is that the viscosity and the molecular weight of the polymer can be tailored by varying the CA/EG(PEG) molar ratio. After a heat treatment at moderate temperature (500-1000 °C) followed by PSG process, the organic additives can be removed and a pure phase of multiple-components metal oxide are obtained. The final materials (including luminescent materials) can be made into powder and thin film forms and others (Scheme 2). It is pointed out that the PSG process may be far from a green chemistry due to the generation of the large amount of organic mass during the synthesis. So far, the PSG process has been extensively used for the synthesis of electric and magnetic materials.¹⁰⁵⁻¹⁰⁸ By PSG process, the physical properties of materials can be improved with respect to the other routes such as solid-state reaction process and amorphous citrate process, as suggested by Kakihana in a review article.¹⁰⁹ In the past decade, Lin's group has derived multifomed cathodoluminescent materials from the PSG process, including nanocrystalline luminescent materials, monodisperse and spherical core-shell structured phosphors, one-dimensional (1D) nanostructures (combined with the electrospinning process), thin film phosphors (via dip-coating), and their patterning (combined with the soft-lithography process). The basic principle is shown in Scheme 2. The purpose is to gain fine control of the material morphology, surface and size, and to find novel cathodoluminescent materials and optimize their cathodoluminescent performance. Typically, a series of oxide-based nanocrystalline phosphors from tens of nanometers to several hundred of nanometers have been prepared through the PSG process for FEDs, including La₂O₃/LaOCl/LaGaO₃/LaAlO₃:RE³⁺,^{14,86,92,110-113} Lu₃Ga₅O₁₂:RE³⁺,¹¹⁴ (Ca,Sr)In₂O₄:RE³⁺ (RE = Pr, Sm, Eu, Tb, Dy, Ho, Er, Tm),^{54, 71, 72} NaCaPO₄:Mn²⁺,⁹⁴ CaYAlO₄:Tb³⁺/Eu³⁺,⁹⁵ KNaCa₂(PO₄)₂:A (A = Ce³⁺, Eu²⁺, Tb³⁺, Mn²⁺, Sm³⁺),¹¹⁵ K(Sr,Ca)Gd(PO₄)₂:RE³⁺/Mn²⁺ (RE = Ce,Tb,Dy,Eu,Tm),^{96, 116} Ca₂Ba₃(PO₄)₃Cl:A,¹¹⁷ Ca₈(La,Gd)₂(PO₄)₆O₂:A (A = Eu²⁺, Ce³⁺, Dy³⁺, Tb³⁺, Mn²⁺),^{118, 119} and so on. It is found that the nanocrystalline phosphor layer could be much thinner compared to that consists of microsize phosphor grains, which can influence both total resistivity of the phosphor layer and amount of residual gasses bounded between the grains.^{27, 101} Then it further influences the efficiency of the light source, long time stability of the intensity of emitted light, and device lifetime. Psuja et al. investigated the effect of grain sizes on emission yield of RE doped nanophosphors in cases of Eu³⁺:Y₂O₃, Tb³⁺:Y₂O₃, Tb³⁺:Y₃Al₅O₁₂ (Tb:YAG), Ce³⁺:YAG, and Tb³⁺:YAG/Eu³⁺:YAG.²⁷ They found that the light-emitting efficiencies increase with grain size in the nanorange by a comparison of cathodoluminescent intensities of phosphor layer and powders, and Eu:Y₂O₃ nanopowder (900°C, 46 nm) was more efficient than commercially available microsize phosphor grains (3.5 μm). Moreover, the CIE chromatic coordinates did not change with phosphor grain sizes. Therefore, they suggested that the RE³⁺ doped nanocrystalline phosphors may effectively

replace the microsize phosphors in FED devices. Xu et al. also demonstrated that these as-prepared nanocrystalline phosphors (Lu₃Ga₅O₁₂:Tb³⁺) by PSG process can form a more compact phosphor screen, which exhibits an improved luminescent efficiency and stability under the bombardment of electron beam.⁶⁷ Wakefield et al. also confirmed that the nanocrystalline oxide based phosphors (Y₂O₃:Eu and Zn₂SiO₄:Mn) had better luminescence efficiency than that of commercial FED phosphors, which show promising properties for use in low voltage field emission displays.¹⁰¹

Homogenous precipitation process.

Homogenous precipitation process is a simple, effective solution-based method for a large-scale fabrication of novel inorganic nano/microstructured materials under template-free conditions. It is usually used to synthesize hydroxide materials under different precipitants using metal salts as precursors.⁸⁷ After an annealing process at moderate temperature, the obtained hydroxides can be transformed to oxide materials with maintaining morphology.

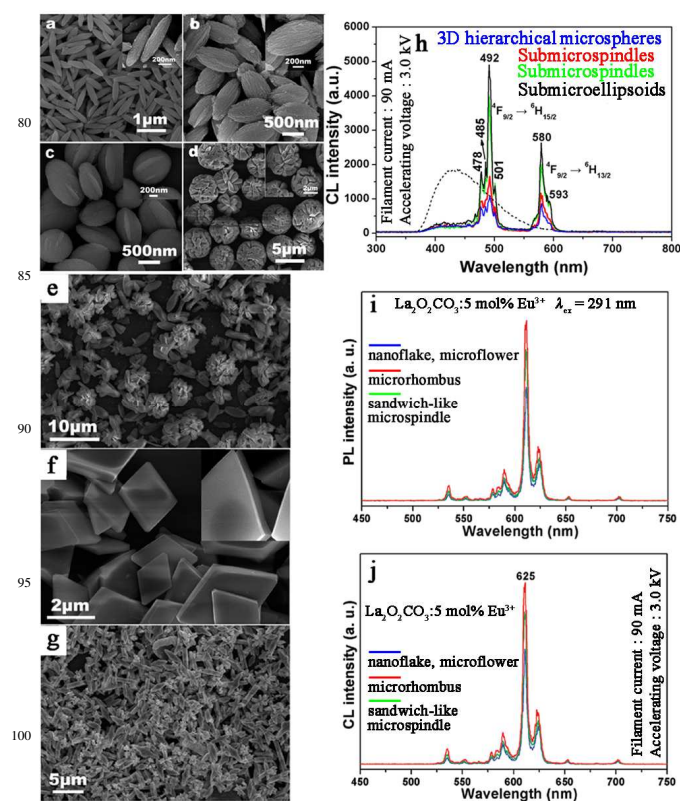


Fig. 1 (a-d) SEM micrographs of the GaOOH:Dy³⁺ prepared at different pH values: 4, 6, 7 and 9. (e-g) SEM images of LaCO₃OH:Eu³⁺ obtained at pH values are 2, 7 and 10, respectively. Following a heat treatment, the above samples are respectively transformed to β-Ga₂O₃:Dy³⁺ and La₂O₂CO₃/La₂O₃:Eu³⁺ phosphors without changing morphologies. (h) and (i, j) show the comparison of CL and photoluminescent (PL) emission intensity of β-Ga₂O₃:Dy³⁺ and La₂O₂CO₃:Eu³⁺. (reproduced with the permission from refs. 66 and 87, copyright 2009 and 2010, American Chemical Society).

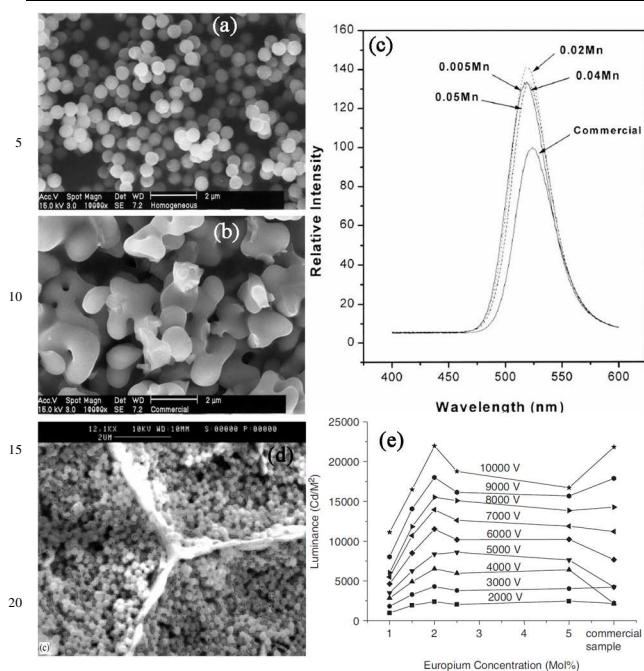


Fig. 2 SEM photographs of $\text{Zn}_2\text{SiO}_4:\text{Mn}$ phosphors by the homogeneous precipitation (a) and of the commercial phosphor (b). The emission spectra (c) of $\text{Zn}_2\text{SiO}_4:\text{Mn}$ phosphors synthesized as various Mn contents. (d) SEM image of cubic- $(\text{Y},\text{Gd})_2\text{O}_3:\text{Eu}^{3+}$ phosphor particles (270 nm). (e) CL luminance versus europium concentration plots of the spherical phosphor particles of cubic $\text{Y}_2\text{O}_3:\text{Eu}^{3+}$ (1–5mol% Eu) fired at 980 °C using a range of excitation energies from 1000–10000 V and 1mA emission current compared to a commercial sample. (reproduced with the permission from refs. 120 and 121, copyright 2007 and 2012, The Society for Information Display and Elsevier).

Over the past several years, monodisperse nano-/microstructures with controllable morphologies and sizes, which exhibit size-dependent luminescent properties, have been synthesized by the homogenous precipitation and investigated. Li et al. has reported the simple synthesis of monodisperse $\beta\text{-Ga}_2\text{O}_3:\text{Dy}^{3+}$, $\text{La}_2\text{O}_3/\text{La}_2\text{O}_2\text{CO}_3:\text{RE}^{3+}$ (RE = Eu, Tb, Yb, Ho, Er, Tm), etc. with defined morphologies and narrow size dispersion (Fig. 1a–1g) by optimizing the external experimental parameters. They demonstrated that the cathodoluminescent properties of phosphors can be improved by improving the morphologies and sizes of phosphors particles. As shown in Fig. 1h, the relative CL emission intensities of $\beta\text{-Ga}_2\text{O}_3:\text{Dy}^{3+}$ phosphors are different with different morphologies/sizes, which are attributed to the difference of surface defects. The more defects on phosphor particles surface, the lower luminescent efficiency are obtained due to the increase of nonradiative transitions. The similar situation appears in the as-prepared $\text{La}_2\text{O}_3/\text{La}_2\text{O}_2\text{CO}_3:\text{RE}^{3+}$ (RE = Eu, Tb) phosphors particles with different shapes and sizes (Fig. 1i and 1j). Jung et al. also improved the luminance of $\text{Zn}_2\text{SiO}_4:\text{Mn}$ phosphors by homogenous precipitation process.¹²⁰ The as-prepared $\text{Zn}_2\text{SiO}_4:\text{Mn}$ phosphor particles present uniform spherical shape and have an enhanced emission intensity than commercial $\text{Zn}_2\text{SiO}_4:\text{Mn}$ bulk phosphors, as shown in Fig. 2(a–c). In addition, spherical sub-micrometre $\text{Y}_2\text{O}_3:\text{Eu}^{3+}$ and cubic (Y,

$\text{Gd})_2\text{O}_3:\text{Eu}^{3+}$ phosphor particles have been synthesized through a novel homogeneous precipitation method by Silver et al.¹²¹ These cubic- $\text{Y}_2\text{O}_3:\text{Eu}^{3+}$ spherical phosphor particles (ca. 300 nm) will be ideal for FED devices as they can densely close-pack on screens (Fig. 2d) and they display high luminous efficiency under low-voltage electron beam excitation (Fig. 2e). It is also confirmed that these particles are useful in voltage ranges up to 5000V and perform well at such voltages compared to commercial phosphors. Therefore, it is concluded that the luminescent efficiencies of inorganic nano/microstructures are strongly related to their morphologies and sizes. Through the modification of morphology, size and surface, one can reduce surface defects and thus enhance the luminescent efficiencies of phosphors.

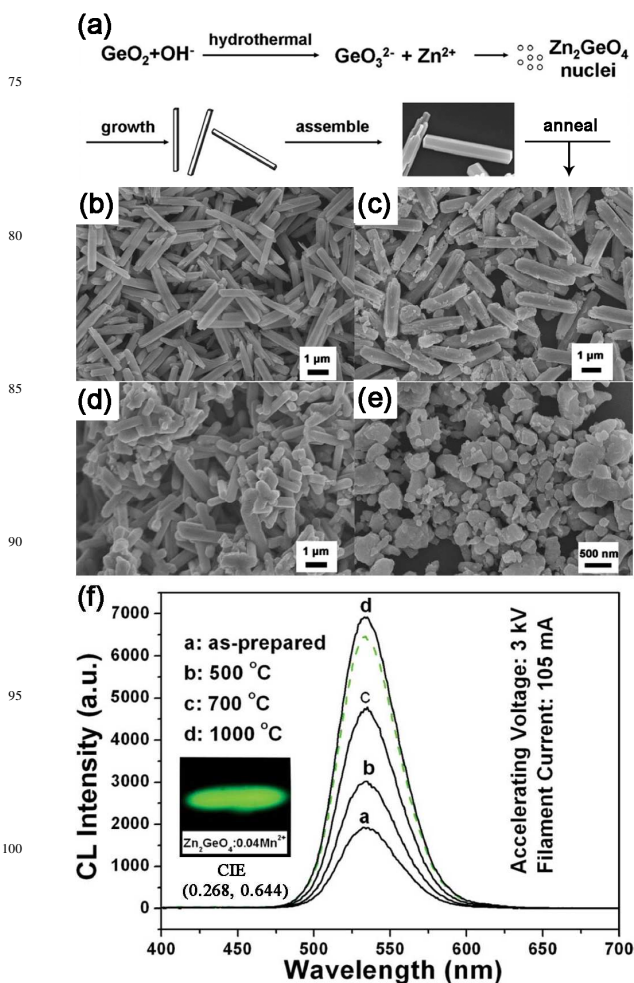


Fig. 3 (a) A possible formation mechanism of $\text{Zn}_2\text{GeO}_4:\text{Mn}^{2+}$ submicrorods. (b–e) SEM images and (f) CL spectra of $\text{Zn}_2\text{GeO}_4:\text{Mn}^{2+}$ submicrorods with different postcalcination temperatures: 500°C, 700°C, 1000°C and $\text{Zn}_2\text{GeO}_4:\text{Mn}^{2+}$ bulk material (solid state reaction process), respectively. The insets in (f) show the luminescent photographs of $\text{Zn}_2\text{GeO}_4:\text{Mn}^{2+}$ with highly pure green light emission. (reproduced with the permission from ref. 75, copyright 2011, Royal Society of Chemistry).

Hydro/solvothermal process. As a typical solution-based approach, hydro/solvothermal process generally employ water or organic solvents under certain temperatures and pressures for

synthesis of variously inorganic nano- and/or micro-crystals due to some acceptable advantages including relatively green synthesis, easily controllable reaction conditions, low reaction temperature (in general $< 250^\circ\text{C}$) and cost, high yield, specially, easily controlled size, structure and shapes of the products. Shang et al. developed a water-based hydrothermal system to prepare $\text{Zn}_2\text{GeO}_4:\text{Mn}^{2+}$ phosphors with irregular submicrorods shape.⁷⁵ Fig. 3a show a possible formation mechanism of $\text{Zn}_2\text{GeO}_4:\text{Mn}^{2+}$ submicrorods, as follows: Firstly, GeO_2 is hydrolyzed to form GeO_3^{2-} ions, and then Zn^{2+} , Mn^{2+} and GeO_3^{2-} ions combined to form Zn_2GeO_4 nuclei at the present of OH^- . These nuclei further grow along the *c*-axis to produce $\text{Zn}_2\text{GeO}_4:\text{Mn}^{2+}$ nanorods and finally aggregate together to form $\text{Zn}_2\text{GeO}_4:\text{Mn}^{2+}$ submicrorod-like bundle. Annealing at different temperatures can remove H_2O and organic components on surface, and then obtain $\text{Zn}_2\text{GeO}_4:\text{Mn}^{2+}$ submicrorods phosphors. As shown in Fig. 3b-3d, it is obviously seen that $\text{Zn}_2\text{GeO}_4:\text{Mn}^{2+}$ submicrorods phosphor has smooth surface, regular shape and narrow size distribution than bulk material prepared by solid state reaction method. Under the same excitation conditions, $\text{Zn}_2\text{GeO}_4:\text{Mn}^{2+}$ submicrorods phosphor has a higher CL emission intensity than that of bulk materials (Fig. 3f). Since the optimal shape, size and surface of particles, the cathodoluminescent efficiency of $\text{Zn}_2\text{GeO}_4:\text{Mn}^{2+}$ phosphor was enhanced.

During the process of hydro/solvothermal reaction, selecting an

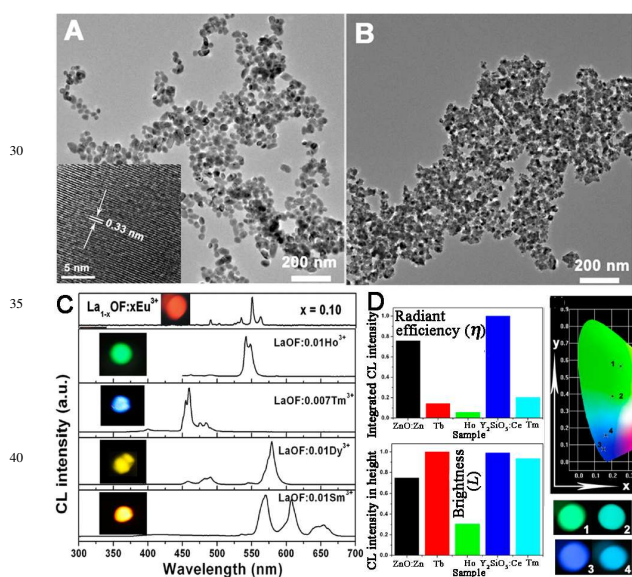


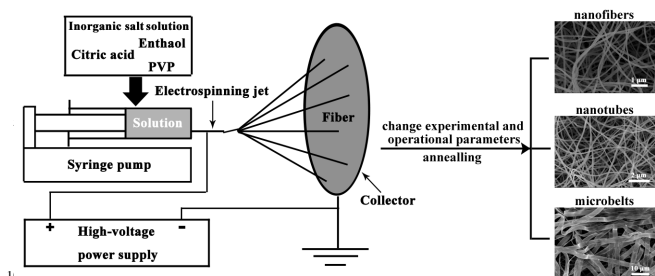
Fig. 4 Typical TEM images of the $\text{LaOF}:\text{RE}^{3+}$ ($\text{RE} = \text{Eu}^{3+}$, Ho^{3+} , Tm^{3+} , Dy^{3+} , Sm^{3+}) phosphors with (A) and without (B) oleic acid treatment. The inset in part A shows its HRTEM image. (C) The CL emission spectra and corresponding digital photographs of $\text{LaOF}:\text{RE}^{3+}$. (D) The CL emission intensities in height (Brightness) and integrated area (Radiant efficiency) of $\text{LaOF}:\text{RE}^{3+}$ ($\text{RE} = \text{Tm}^{3+}$, Tb^{3+}), $\text{ZnO}:\text{Zn}$ and $\text{Y}_2\text{SiO}_5:\text{Ce}$. The corresponding CIE chromaticity coordinates and digital photographs (1-4 represent $\text{LaOF}:\text{0.07Tb}^{3+}$ (0.2521, 0.5647), $\text{ZnO}:\text{Zn}$ (0.2053, 0.3879), $\text{LaOF}:\text{0.005Tm}^{3+}$ (0.1510, 0.0761) and $\text{Y}_2\text{SiO}_5:\text{Ce}$ (0.1651, 0.1568), respectively) are also shown. (reproduced with the permission from refs. 122 and 123, copyright 2012, American Chemical Society and Royal Society of Chemistry).

appropriate organic additive with functional groups is one of the promising and popular strategies to control shape and size.

The organic additive generally acts as complex agent or structure-directing agent. Through using oleic acid in reaction system, Shang et al. successfully prepared well-separated $\text{LaOF}:\text{RE}^{3+}$ ($\text{RE} = \text{Eu}^{3+}$, Ho^{3+} , Tm^{3+} , Dy^{3+} , Sm^{3+} , Tb^{3+}) nanoparticles with sizes of about 30–50 nm (Fig. 4A).^{122, 123} The HRTEM image (inset in Fig. 4A) shows lattice planes with perfect crystallinity. Due to the excellent dispersion and crystallinity, these as-prepared $\text{LaOF}:\text{RE}^{3+}$ phosphor nanoparticles can also be compactly coated on screen to improve the intensity of emitted light, and device lifetime. Doping RE^{3+} ions into LaOF host, emission colors from blue to red with high color purity ($4f-4f$ transition, Eu^{3+} , red; Ho^{3+} , green; Tm^{3+} , blue; Dy^{3+} , yellow; Sm^{3+} , orange in Fig. 4C) were obtained. Especially, green-emitting $\text{LaOF}:\text{Tb}^{3+}$ and blue-emitting $\text{LaOF}:\text{Tm}^{3+}$ with the CIE chromaticity coordinates $\text{LaOF}:\text{0.07Tb}^{3+}$ (0.2521, 0.5647) and $\text{LaOF}:\text{0.005Tm}^{3+}$ (0.1510, 0.0761) are more pure than those of $\text{ZnO}:\text{Zn}$ (0.2053, 0.3879) and $\text{Y}_2\text{SiO}_5:\text{Ce}$ (0.1651, 0.1568), respectively. For CL, the efficiency of a luminescent material includes the radiant efficiency (η) and the luminous efficiency (L , brightness),¹⁴ which can be compared roughly by their emission peak areas (integrated luminescence intensity) and the CL intensity (in height), respectively. It can be seen from Fig. 4D that under the same excitation condition, although the emission peak areas of the $\text{LaOF}:\text{0.07Tb}^{3+}$ and $\text{LaOF}:\text{0.005Tm}^{3+}$ are smaller than that of $\text{ZnO}:\text{Zn}$ and $\text{Y}_2\text{SiO}_5:\text{Ce}$; however, the CL intensity of the $\text{LaOF}:\text{0.07Tb}^{3+}$ is higher than that of the $\text{ZnO}:\text{Zn}$, and the $\text{LaOF}:\text{0.005Tm}^{3+}$ has the comparative CL intensity with the $\text{Y}_2\text{SiO}_5:\text{Ce}$ blue phosphor. According to these results, the as-prepared $\text{LaOF}:\text{RE}$ ($\text{RE} = \text{Eu}^{3+}$, Ho^{3+} , Tm^{3+} , Dy^{3+} , Sm^{3+} , Tb^{3+}) nanoparticles phosphors can be considered as potential full color FEDs phosphors. It is worth noting that the comparison of radiant efficiency and luminous efficiency between broad and narrow bands emission ions may be not reasonable and commonly have a big error. Therefore, the results are just considered as a reference.

In addition, the morphology and size of products can also be well controlled and modified by a combination of water and organic solvents in hydrothermal process. During these fabrication processes, organic solvents act as the “shape modifier” to either promote or inhibit crystal growth through modifying crystal growth dynamically and thus can adjust and control the morphology and size of the products. By the use of the above synthesis method, a series of cathodoluminescent materials such as $\beta\text{-Ga}_2\text{O}_3:\text{Dy}^{3+}$,^{66, 124} $\text{Gd}_2\text{O}_3:\text{Eu}^{3+}$,¹²⁵ $\text{Lu}_2\text{O}_3:\text{RE}^{3+}$ ($\text{RE} = \text{Eu}$, Tb , Dy , Pr , Sm , Er , Ho , Tm)¹²⁶ with regular prism, rod, sphere shapes in nano- to microscale were synthesized, which not only improve the cathodoluminescent performances of phosphors but also meet some requirements in micromatation of FEDs devices.

Electrospinning process. Since some specific and fascinating luminescence properties, for example, various emission lifetimes and increased luminescence efficiencies etc., there is growing interest on exploring new luminescent materials on one-dimensional (1D) nanostructures.¹²⁷⁻¹³⁴ These one-dimensional luminescence nanomaterials possess diverse potential applications in nanoscale electronics, photonics, display and advanced bioanalysis.³⁸ The electrospinning technique is an



Scheme 3 Schematic diagram of the electrospinning setup and the formation process of 1D luminescence nano-/microstructures. (reproduced with the permission from ref. 15, copyright 2010, Wiley)

effective and simple method for preparing one-dimensional (1D) nanomaterials. It is a process that uses the strong electrostatic force from a high static voltage act on a polymer solution placed into a container with a millimeter diameter nozzle. Under applied electrical force, the polymer solution is ejected from the nozzle.^{38, 133} After the solvents are evaporated during the course of jet spraying, the fibers are collected on a grounded collector. In the past few years, followed an annealing process to remove the organic additives, some researchers have extended the application of a sol-gel process combining with electrospinning technique to prepare a rich variety of 1D luminescence nanomaterials.^{38, 128-134} The electrospinning setup and formation process of 1D luminescent nano-/microstructures is shown in Scheme 3. 1D nanomaterials synthesized by this method usually have exceptional long length, uniform diameter and diverse composition.

Through the electrospinning process a variety of RE^{3+} ions doped 1D fiber, tube and belt-like cathodoluminescence materials including $LaOCl$,¹⁵ $CaTiO_3$,¹²⁹ YVO_4 ,¹³³ $GdVO_4$,¹³⁵ $LaPO_4$,¹³⁶ Y_2SiO_5 ,¹³⁷ $Ca_4Y_6(SiO_4)_6O$,¹³⁸ $Ca_2Gd_8(SiO_4)_6O_2$,¹³⁹ $La_{9.33}(SiO_4)_6O_2$,¹⁴⁰ $CaWO_4$,¹⁴¹ $Tb_2(WO_4)_3$,¹⁴² Gd_2MoO_6 ,¹⁴³ $CaMoO_4$ ¹⁴⁴ have been derived and/or optimized, especially morphology- and size-dependent luminescence performance were investigated and color tuning by doping different kinds of RE^{3+} ions, changing RE^{3+} ions concentrations, codoping and/or energy transfer were designed. For example, the as-prepared $LaOCl:Eu^{3+}$ 1D nanofiber, nanotube and microbelt phosphors are all composed of nanoparticles with perfect crystallinity, as shown in Fig. 5a-5c. The comparison of CL spectra of $LaOCl:Eu^{3+}$ 1D nanomaterials with three different morphologies/sizes (here all the experimental conditions were kept identical) is shown in Fig. 5d, it can be seen that the belt-like sample has a higher CL intensity than that of fiber-like and tube-like samples. That is because that the $LaOCl:Eu^{3+}$ nanofibers and nanotubes produce more surface defects than microbelts due to smaller nanoparticles and larger surface area. However, defects have serious drawback for luminescent intensity of phosphors as they provide nonradiative recombination routes for electrons and holes. The same morphology- and size-dependent luminescence performance appears in systems of $YVO_4:RE^{3+}$ ($RE = Eu, Tb, Dy, Sm$),¹³³ $LaPO_4:Ce^{3+}/Tb^{3+}$,¹³⁶ $CaWO_4:Tb^{3+}$ ¹⁴¹ and so on. Therefore, controllable modification of morphology and size of 1D luminescent materials can elevate their luminous efficiencies. Via the electrospinning process, RE^{3+} ($Eu^{3+}, Tb^{3+}, Tm^{3+}, Sm^{3+}$) can be homogeneously dispersed in $LaOCl$ systems and the CIE chromaticity coordinates of 1D $LaOCl:RE^{3+}$ nanomaterials phosphors can be tuned in a wide range through changing RE^{3+} concentrations and codoping RE^{3+} ions ($Eu^{3+}/Tb^{3+}, Eu^{3+}/Tm^{3+}$,

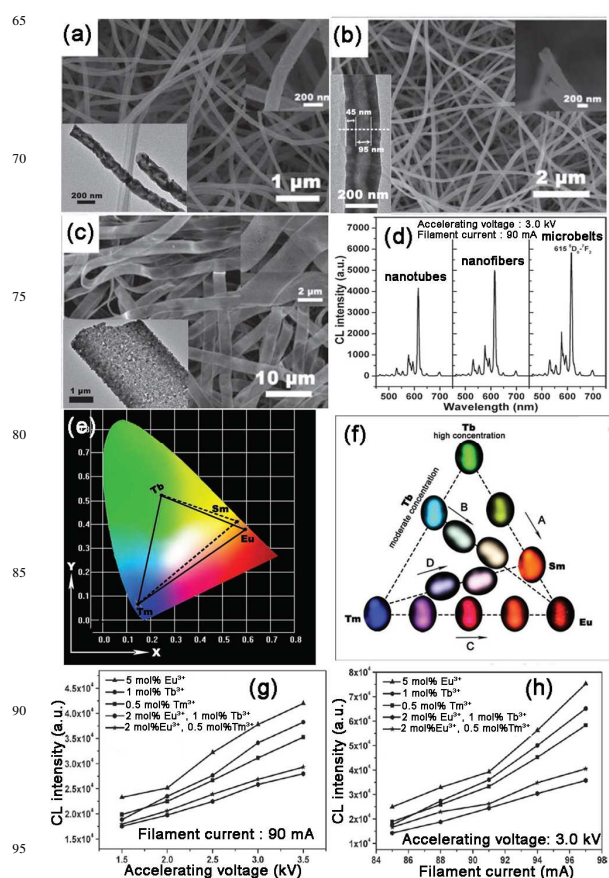
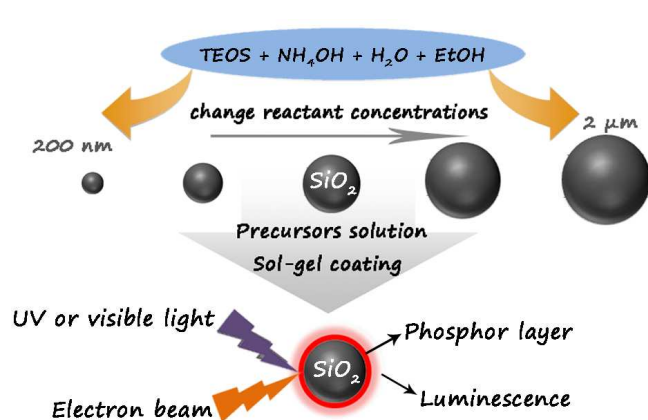


Fig. 5 (a-c) SEM, TEM images of the as-formed 1D $LaOCl:Eu^{3+}$ nanofiber, nanotube and microbelt phosphors. (d) The CL spectra of $LaOCl:Eu^{3+}$ phosphors with fiber, tube, and belt-like morphologies. (e) The range of CIE chromaticity coordinates of $LaOCl:RE^{3+}$ ($RE = Sm, Eu, Tb, Dy, Tm$) 1D nanomaterials, and corresponding CL photos are shown in (f). The dependence of CL intensities of $LaOCl:RE^{3+}$ 1D nanomaterials of (g) accelerating voltage (kV) and (h) filament current (mA), respectively. (reproduced with the permission from ref. 15, copyright 2010, Wiley)

$Eu^{3+}/Tb^{3+}/Tm^{3+}$) as shown in Fig. 5e. The corresponding CL digital photographs (Fig. 5f) also support the above results. Generally, the increase in CL intensity (brightness) with an increase in electron energy and filament current are attributed to the deeper penetration of the electrons into the phosphor body and the larger electron-beam current density. However, a larger current density may result in the accumulation of excess electrons on phosphor surface. If these electrons could not be promptly transferred, the cathodoluminescent efficiency will be reduced due to a saturation behavior. Under low-voltage electron beam excitation, the CL emission intensities of 1D $LaOCl:RE^{3+}$ nanophosphors gradually elevate with raising accelerating voltage and filament current without obvious saturation behavior (Fig. 5g and 5h), which is beneficial to apply in FEDs devices.

Hydrolysis-Sol/gel method. According to previous research, the emission performances can be improved in spherical phosphors with respect to the irregular ones, which are basically attributed to the high packing densities and low scattering of light.^{27, 101} Therefore, there is a growing interest in synthesizing inorganic phosphors with spherical morphologies in



Scheme 4 Hydrolysis-Sol/gel synthesis of spherical core-shell-structured phosphors.

recent years.¹⁴⁵ As one of the most well-known hydrolysis
 20 method, Stöber method¹⁴⁶ that based on hydrolysis of
 tetraethylorthosilicate (TEOS) in an alcohol medium in the
 presence of water and ammonia, has been extensively employed
 to prepare the monodisperse silica (SiO_2) spheres with different
 25 sizes from nano to micron meter by a modified procedure. Lin's
 group developed a combination of these monodisperse SiO_2
 spheres and the PSG process following suitable annealing
 temperatures to synthesize a series of monodisperse and spherical
 core-shell structured phosphors (Scheme 4). The size-dependent
 and/or tunable luminescence properties also have been
 30 extensively investigated.⁹⁹ The concrete experimental process is
 extremely simple as follow: first, stir the as-formed SiO_2 particles
 in corresponding PSG precursor solutions of the phosphors
 (composing of metal ions, citric acid, and PEG), then separate the
 SiO_2 particles by centrifugation following a heat treatment at
 35 certain temperature to obtain the final phosphor products. The
 size for the phosphor particles can be controlled by the ones of
 the silica cores and the number of coating cycles.¹⁴⁵ By the above
 method, a variety of precursor solutions of phosphors can be
 coated on the surface of SiO_2 spheres to form the desirable
 40 spherical phosphors. For example, the comparison of the TEM
 images of Fig. 6a and 6d clearly shows that the $\text{YVO}_4:\text{Eu}^{3+}$
 phosphor layer was formed on SiO_2 surface and the HRTEM and
 ED images also confirm the formation of $\text{YVO}_4:\text{Eu}^{3+}$ phase. The
 photoluminescence emission spectra of the as-formed
 45 $\text{SiO}_2@\text{YVO}_4:\text{Eu}^{3+}$ phosphor exhibits excellent red emission of
 Eu^{3+} (618 nm , ${}^5\text{D}_0 \rightarrow {}^7\text{F}_2$) in $\text{YVO}_4:\text{Eu}^{3+}$ system. More important,
 the luminescent properties of core-shell structured phosphor
 particles can be tuned and optimized by changing the size of SiO_2
 cores and thickness of phosphor shells (Fig. 6f).¹⁴⁷ Due to a low
 50 cost (silica is cheaper than most of pure phosphor materials that
 often employ the expensive rare earth elements as the activators
 and/or host components), and large scale synthesis, accordingly, a
 series of spherical core-shell structured cathodoluminescent
 materials were prepared and corresponding core-shell sizes and
 55 emission properties are collected in Table 1.^{145, 147-160}

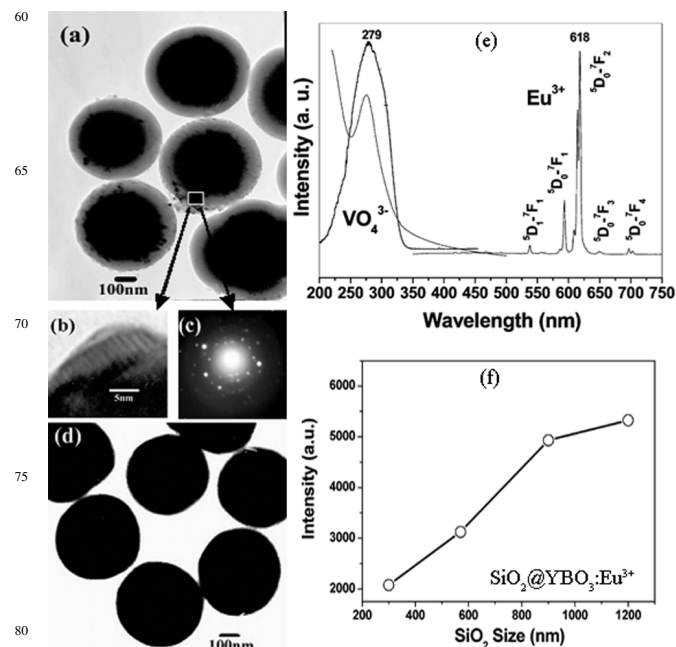


Fig. 6 (a-c) TEM, HRTEM and ED images of monodisperse and spherical $\text{SiO}_2@\text{YVO}_4:\text{Eu}^{3+}$ particles, respectively. (d) Typical TEM image of the as-formed SiO_2 spheres by Stöber method. (e) The PL spectra of representative spherical $\text{SiO}_2@\text{YVO}_4:\text{Eu}^{3+}$ phosphor. (f) The dependence of emission intensity with the sizes of SiO_2 spheres in $\text{SiO}_2@\text{YBO}_3:\text{Eu}^{3+}$ system. (reproduced with the permission from refs. 145 and 147, copyright 2005, American Chemical Society)

Table 1 Characteristics of some core-shell structured phosphor particles prepared by the PSG process.

| Sample | SiO_2 core/phosphor shell size (nm) | Emission colors | Refs |
|---|--|--|------------|
| $\text{SiO}_2@\text{Y}_2\text{O}_3:\text{Eu}^{3+}$ | 500/60 | red (Eu^{3+}) | 148 |
| $\text{SiO}_2@\text{YVO}_4:\text{Eu}^{3+}/\text{Dy}^{3+}/\text{Sm}^{3+}$ | 500/60 | red (Eu^{3+}); yellow (Dy^{3+}); orange (Sm^{3+}) | 145 149 |
| $\text{SiO}_2@\text{GdVO}_4:\text{Eu}^{3+}$ | 500/50 | red (Eu^{3+}) | 150 |
| $\text{SiO}_2@\text{Gd}_2(\text{WO}_4)_3:\text{Eu}^{3+}$ | 400, 500, 600, 700/50 | red (Eu^{3+}) | 151 |
| $\text{SiO}_2@\text{NaGd}(\text{WO}_4)_2:\text{Eu}^{3+}$ | 400/40 | red (Eu^{3+}) | 152 |
| $\text{SiO}_2@\text{CaWO}_4:\text{Eu}^{3+}/\text{Tb}^{3+}$ | 500/50 | red (Eu^{3+}); green (Tb^{3+}) | 153 |
| $\text{SiO}_2@\text{LaPO}_4:\text{Ce}^{3+}/\text{Tb}^{3+}$ | 1200/60 | purple (Ce^{3+}); green ($\text{Ce}^{3+}, \text{Tb}^{3+}$) | 154 |
| $\text{SiO}_2@\text{Y}_2\text{SiO}_5:\text{Eu}^{3+}/\text{Ce}^{3+}, \text{Tb}^{3+}$ | 385/50 | red (Eu^{3+}); green ($\text{Ce}^{3+}, \text{Tb}^{3+}$) | 155 |
| $\text{SiO}_2@\text{CaTiO}_3:\text{Pr}^{3+}$ | 500/70 | red (Pr^{3+}) | 156 |
| $\text{SiO}_2@\text{Gd}_2\text{MoO}_6:\text{Eu}^{3+}$ | 500/70 | red (Eu^{3+}) | 157 |
| $\text{SiO}_2@\text{CaMoO}_4:\text{Eu}^{3+}$ | 500/65 | Green (Tb^{3+}) | 158 |
| $\text{SiO}_2@\text{Gd}_2\text{Ti}_2\text{O}_7:\text{Eu}^{3+}$ | 500/60 | red (Eu^{3+}) | 159 |
| $\text{SiO}_2@\text{YBO}_3:\text{Eu}^{3+}$ | 300, 570, 950, 1200/100 | red (Eu^{3+}) | 147 |
| $\text{SiO}_2@\text{Y}_3\text{Al}_5\text{O}_{12}:\text{Ce}^{3+}/\text{Tb}^{3+}$ | 500/100 | green (Tb^{3+}) | 160 |

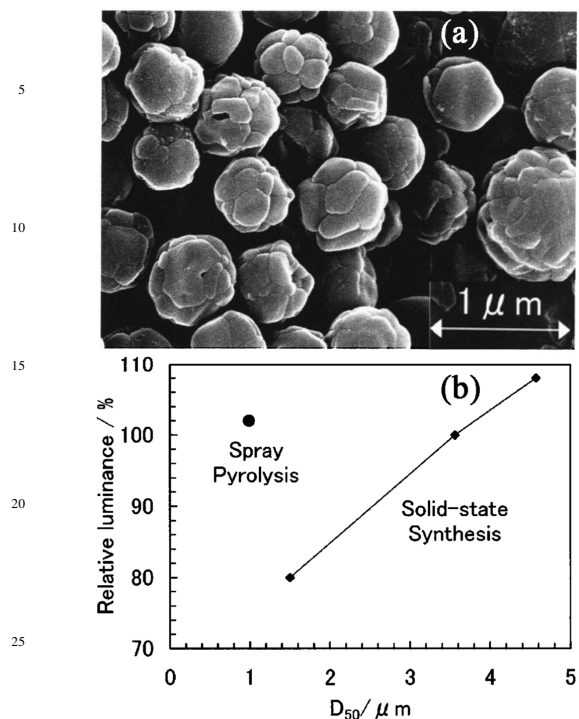


Fig. 7 (a) SEM images of $\text{Y}_2\text{O}_3:\text{Eu}^{3+}$ synthesized by alkali-salt-added spray pyrolysis process. (b) Relative luminance of $\text{Y}_2\text{O}_3:\text{Eu}^{3+}$ red phosphor as a function of particle size synthesized by (●) spray pyrolysis and (◆) solid-state reaction. (reproduced with the permission from ref. 57, copyright 2004, The Electrochemical Society)

Spray pyrolysis process. Except for hydrolysis-Sol/gel method, other better morphology of the spherical shape with a size around $0.5\text{--}3\ \mu\text{m}$ for phosphors can be obtained by the spray drying process.⁹⁰ It needs a combination of PSG precursor solutions and subsequent annealing process to obtain final phosphor products. Shimomura et al.⁵⁷ obtained high luminance and a small-sized $\text{Y}_2\text{O}_3:\text{Eu}^{3+}$ phosphor with little agglomeration by spray pyrolysis, as shown in Fig. 7a. Its maximum luminance in this study was better than that of commercial $\text{Y}_2\text{O}_3:\text{Eu}^{3+}$ phosphor synthesized by solid state reaction at the same median particle size (Fig. 7b). By loading the corresponding precursor solution on a spray drying apparatus and a following annealing process at high-temperature ($600\text{--}1200\ \text{°C}$), the representative red-emitting $\text{Y}_2\text{O}_3:\text{Eu}^{3+}$, red-emitting $\text{CaTiO}_3:\text{Pr}^{3+}$, green-emitting $\text{YBO}_3:\text{Tb}^{3+}$ and blue-emitting $\text{Sr}_2\text{CeO}_4:\text{Ce}^{3+}$ FEDs phosphors were also prepared to spherical particles with sizes ranging from 0.6 to $3.0\ \mu\text{m}$. It is demonstrated that the as-prepared spherical phosphors possess indeed improve their emission intensity over the other irregular ones, which is also due to high packing densities and low scattering of light.^{90, 99, 161} It is noticed that the disadvantages of phosphors prepared by spray pyrolysis is that the optimal heating temperature was generally higher than that for the solid-state reaction.⁵⁷ Moreover, it also has a bigger size distribution than that prepared by homogenous precipitation or hydrolysis-Sol/gel methods. Therefore, it will be further improved.

2.1.2 Modification of phosphor composition

For phosphors, it frequently involves in the substitution of cations in host lattice with activator ions to produce luminescence, which easily results in a mismatch of charge and

crystal lattice due to different valence state and ion radius. These mismatches will generate many defects (vacancy, gap, crystal lattice distortion and strain) to decrease the luminescent efficiency of phosphors, and as a result need to be avoided or reduced. By modifying phosphor composition, the luminescent performance of phosphors can be efficiently improved. Generally, composition modifications of phosphors mainly focus on two aspects: the one is to conduct charge compensations for relaxing charge mismatch; and the other one is to relieve crystal lattice

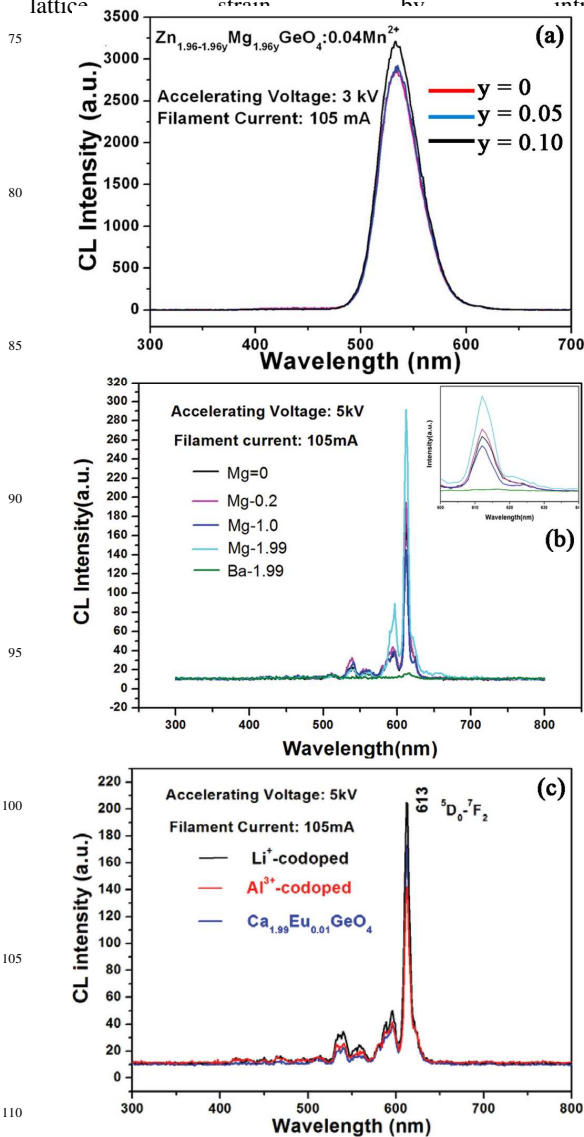
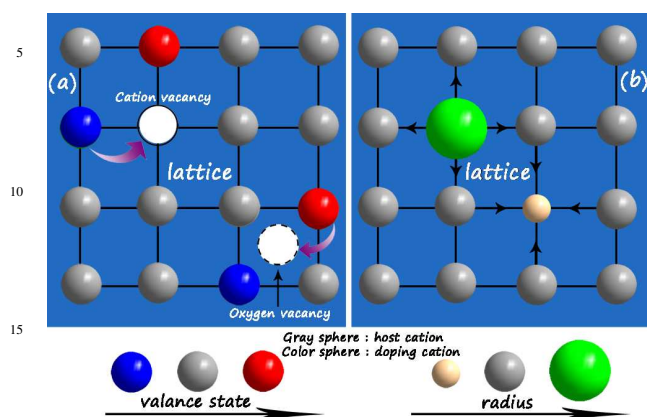


Fig. 8 (a) Comparison of CL intensities of $\text{Zn}_{1.96(1-y)}\text{Mg}_{1.96y}\text{GeO}_4:0.04\text{Mn}^{2+}$ samples at different Mg doping concentrations (0 red line, 0.05 blue line, 0.10 black line). (b) CL spectra of $\text{Ca}_{1.99-y}\text{M}_y\text{GeO}_4:0.01\text{Eu}^{3+}$ ($M = \text{Mg, Ba}$; $y = 0, 0.2, 1.0, 1.99$). Inset shows the magnified spectra from 600 to $640\ \text{nm}$. (c) CL spectra of $\text{Ca}_{1.99}\text{Eu}_{0.01}\text{GeO}_4$, $\text{Ca}_{1.98}\text{Li}_{0.01}\text{Eu}_{0.01}\text{GeO}_4$, and $\text{Ca}_{1.99}\text{Eu}_{0.01}\text{Al}_{0.01}\text{Ge}_{0.99}\text{O}_4$. (b) and (c) accelerating voltage = $5\ \text{kV}$, filament current = $105\ \text{mA}$. (reproduced with the permission from refs. 75 and 164, copyright 2011, Royal Society of Chemistry and The Electrochemical Society)



Scheme 5 A simple model to illustrate the possible increasing mechanism of luminescent efficiency by composition modification (charge compensations and crystal lattice strain relaxing).

other cations with complementary radius. Based on the above consideration, representative $\text{Ca}_2\text{GeO}_4:\text{Eu}^{3+}$ and $\text{Zn}_2\text{GeO}_4:\text{Mn}^{2+}$ phosphors have been optimized and the effect of composition modification on cathodoluminescent efficiencies of phosphors has been elaborately investigated. Fig. 8 shows the CL spectra of Mg-doped $\text{Zn}_{1.96}\text{GeO}_4:0.04\text{Mn}^{2+}$ and Li^+ , Al^{3+} , Mg^{2+} , Ba^{2+} -doped $\text{Ca}_{1.98}\text{GeO}_4:0.01\text{Eu}^{3+}$ systems. It can be seen that the CL spectra of $\text{Zn}_{1.96(1-y)}\text{Mg}_{1.96y}\text{GeO}_4:0.04\text{Mn}^{2+}$ samples show the maximum emission at 532 nm (green light with CIE chromaticity coordinates $x = 0.268$, $y = 0.644$) under the excitation of 3 kV accelerating voltage, which corresponds to the characteristic emission of Mn^{2+} from ${}^4\text{T}_1$ to ${}^6\text{A}_1$, as shown in Fig. 8a. Moreover, the CL intensity increases with the replacement of Mg^{2+} ions. The possible reason is the join of Mg^{2+} ions ($r = 0.57$ nm, Coordination Number (CN) = 4) decrease the crystal lattice strain due to mismatched ions radius with Zn^{2+} ($r = 0.60$ nm, CN = 4) and Mn^{2+} ($r = 0.66$ nm, CN = 4) ions. The relaxing of crystal lattice strain can efficiently suppress nonradiative processes and finally result in the improvement of cathodoluminescent efficiency. The similar situation appears in the Mg^{2+} , Ba^{2+} -doped $\text{Ca}_{1.99}\text{GeO}_4:0.01\text{Eu}^{3+}$ systems (Fig. 8b). The emission intensities of Mg-0.2 and Mg-1.0 doped $\text{Ca}_{1.99}\text{GeO}_4:0.01\text{Eu}^{3+}$ samples are comparable to or even higher than that of $\text{Ca}_{1.99}\text{GeO}_4:0.01\text{Eu}^{3+}$ sample, but the emission drastically decreases in the Ba-1.99 sample. This may be because the radius of Mg^{2+} ions is smaller than that of Ca^{2+} ions, which makes Mg^{2+} ions more easily enter into the host lattice, introducing the smaller lattice distortion. While the doping of Ba^{2+} ions increase the lattice distortion due to a larger ion radius than Ca^{2+} ions, and thus decrease the luminescent intensity. For $\text{Ca}_{1.99}\text{GeO}_4:0.01\text{Eu}^{3+}$ systems, there is a charge mismatch between Eu^{3+} and Ca^{2+} ions. According to the electroneutrality theory, two Eu^{3+} ions will replace three Ca^{2+} ions to obtain charge balance, and as a result two positive defects of $[\text{Eu}_{\text{Ca}}]^\bullet$ and one negative Ca^{2+} vacancy of $[\text{V}_{\text{Ca}}]^-$ would form. These defects and vacancies may capture excited electron to proceed to non-radiative transitions and damage the luminous efficiency. Therefore, Shang et al. introduced Li^+ ions or Al^{3+} ions to use as compensator for charge defects. Co-doping Li^+ ions can help to incorporate the Eu^{3+} ions into Ca^{2+} sites by compensating for the different charges between Eu^{3+} and Ca^{2+} ions and the red light emission intensity of $\text{Ca}_{1.98}\text{Li}_{0.01}\text{Eu}_{0.01}\text{GeO}_4$ is elevated with respect to $\text{Ca}_{1.99}\text{Eu}_{0.01}\text{GeO}_4$. In the Al^{3+} co-doped

$\text{Ca}_{1.99}\text{Eu}_{0.01}\text{GeO}_4$ sample, the Al^{3+} ions may replace the Ge^{4+} ions, which can also maintain the charge compensation and decrease the defect in the phosphor. Unexpectedly, it exhibits a decrease in luminescent intensity. This is attributed to the electronegativity difference between Ge and O ($\Delta X = 1.43$) is lower than that between Al and O ($\Delta X = 1.83$).^{163, 164} Because the compound composed of elements with small differences in electronegativity (X) should have a narrower band gap which leads to higher conductivity.^{164, 165} While the cathodoluminescence intensity is related to the conductivity of phosphors and a narrow gap can lead to higher conductivity which is beneficial to the cathodoluminescence.^{164, 166} So the CL emission intensity of the Al^{3+} -codoped sample is decreased compared with that of the undoped sample. An X-ray diffraction study by Shimomura et al.⁵⁷ indicated that the highest luminance $\text{Y}_2\text{O}_3:\text{Eu}^{3+}$ phosphor obtained by the addition of a lithium salt had little strain in the crystal and its crystal growth was promoted by the additive. Therefore, the luminance improvement by Li composition modification originated from the acceleration of crystal growth and reduction of its strain. The similar research was carried out on the $(\text{Gd}_{2-x-y}\text{M}_x)\text{O}_3:\text{Eu}_y^{3+}$ ($\text{M} = \text{Al}, \text{Ca}, \text{Mg}$) according to combinatorial Chemistry Method by Seo et al.⁵⁸ In order to reduce crystal lattice strain, three co-dopants (Al, Ca, Mg) were introduced into $\text{Gd}_2\text{O}_3:\text{Eu}^{3+}$. They developed a ternary material library of a triangle-type composition array to obtain the optimum composition of co-dopants. It was found that the cathodoluminescent efficiency of $\text{Gd}_2\text{O}_3:\text{Eu}^{3+}$ phosphor was obviously improved by introducing three co-dopants. Especially, the cathodoluminescent efficiency of Al co-doped phosphor, $(\text{Gd}_{1.83}\text{Al}_{0.05})\text{O}_3:\text{Eu}_{0.12}^{3+}$, was superior to that of the commercial red phosphor $\text{Y}_2\text{O}_3:\text{Eu}^{3+}$. Therefore, they suggested that these optimal $(\text{Gd}_{2-x-y}\text{M}_x)\text{O}_3:\text{Eu}_y^{3+}$ ($\text{M} = \text{Al}, \text{Ca}, \text{Mg}$) phosphors were excellent red FED phosphors at a low voltage excitation.

A simple model to illustrate the possible increasing mechanism of luminescent efficiency by composition modification is shown in Scheme 5. During the process of doping cations into host lattice, if its valance state is higher than that of host cations, cation vacancies will be produced, whereas oxygen vacancies will appear (Scheme 5a). These vacancies, namely, crystal lattice defects increase the probability of non-radiative transitions, and thus decrease luminescent efficiency. When introducing charge compensator ions into the host lattice, it will reduce charge defects and thus can improve luminescent performance. On the other hand, cationic replacements with different radius in one matrix will result in crystal expansion or shrinkage. This will generate strain or many defects due to the distorted crystal lattice, which also increases the possibility of non-radiative transitions. By doping other ions with complementary radius, it can relieve lattice strain and then decrease defects, which finally enhance luminescence efficiency of phosphor (Scheme 5b). In general, the cathodoluminescent efficiency of FED phosphors can be optimized by composition modification including charge compensations and crystal lattice strain relaxing, which promotes a potential application of phosphors in field emission display devices.

2.1.3 Improvement of conductivity

It is well known that electron beam is used as excitation source in field emission display technology. In order to realize highly efficient field emission display, phosphors should be efficiently excited by low voltage electrons. Although the accelerating voltage employed in FEDs is much less than that worked in CRTs, its energy is still much higher than UV or visible light radiation, which is around a few thousand to thousands of eV.¹⁴ If

could not be promptly transferred, these electrons very easily accumulate on the phosphor surface to recombine with holes/surface defects, which increase nonradiative transitions and thus decrease cathodoluminescent efficiency. In addition, excessive electrons staying on the phosphor surface also easily reach charge saturation. The tendency for the brightness to plateau even when the current is increased at a fixed electron voltage; this is a serious concern especially for FEDs since the voltage is normally low (<4 kV).⁵ Requiring high current for high power and brightness. Accordingly, an important question for FEDs is how to eliminate or weaken charging and surface recombination effects, and improve the saturation. One of the most promising and efficient approach is to improve the conductivity of FEDs phosphors. This approach can efficiently and opportunely release the accumulated charges on phosphors and thus improve the saturation of phosphors and enhance their cathodoluminescent efficiency. Generally, there are two main routes to increase the conductivity of FEDs phosphors: the one is the selection of semiconductor materials as host lattice and the other one is to mix transparent and conductive nanocrystalline powders with FEDs phosphors. For the selection of hosts, it is known that the compounds composed of elements with small differences in electronegativity should have a narrower band gap.¹⁶⁴

for stability comparison. Excited voltage = 2kv and Filament current = 16 mA (I_0 : initial intensity, I_t : intensity after continuous electron beams excitation for half an hour). (reproduced with the permission from ref. 71, copyright 2007, Elsevier)

Moreover, the bandgap of oxide-based phosphor systems is related to crystal structures of hosts.^{43, 75} Generally, reticular acid radical-coordinated polyhedrons in host easily result in a narrow bandgap of host. While the bandgap of host has great effects on the conductivity and luminescent efficiency of phosphors. A narrow gap can lead to higher conductivity which is beneficial to the cathodoluminescence. On the other hand, luminescence quenching will occur if the energy levels of excited states of activator ions located among the conduction band of host.⁴³ Only the excited states of activator ions locate below the conduction band of host, the phosphors present excellent luminescent performance.⁴³ Therefore, appropriate hosts with reasonable bandgap should be considered during the exploring and design of novel FED phosphors, which could merge the luminescence performance and conductivity of phosphors.^{43, 75} According to the first route, a series of RE³⁺ ions or Mn²⁺ ions activated Ga₂O₃,⁶⁶ (Ca,Sr)In₂O₄,^{54, 71} La(Ga,In)O₃,^{14, 112, 113, 167} Mg₂(Sn,Ti)O₄,³⁷ (Zn,Mg)₂GeO₄,⁷⁵ Li₂ZnGeO₄³⁹ etc. cathodoluminescent materials were derived, as summarized in Table 2. Except for the efficient transport of electrons, semiconductor hosts (emission from UV to bluish-green light region) generally have a sensitive enhancement for luminescent efficiency of RE³⁺ ions. A simple model illustrating luminescence mechanism of the representative phosphor example CaIn₂O₄:Dy³⁺, Pr³⁺, Tb³⁺ is shown in Fig. 9a. Under the excitation of electron beam, an electron (●) is excited from the VB to the CB. The electron (●) moves freely around the CB, finally relaxes to the donor band (oxygen vacancies). The recombination of the electron in the donor band with the acceptor (calcium vacancies or indium vacancies) yields a blue emission with a maximum wavelength at 450 nm. When Dy³⁺ (Pr³⁺ or Tb³⁺) is present in CaIn₂O₄ host lattices, the excitation energy can be nonradiatively transferred to Dy³⁺ (Pr³⁺ or Tb³⁺), resulting in an enhanced emission of Dy³⁺ (Pr³⁺ or Tb³⁺). Furthermore, after continuous electron beams excitation for half an hour, the CaIn₂O₄:0.015Dy³⁺, CaIn₂O₄:0.0016Pr³⁺ and CaIn₂O₄:0.0032Tb³⁺ still keep 88%, 92% and 90% of original intensity, but for commercial Y₂O₂S:0.05Eu³⁺ phosphor, it only keeps 80% the of original intensity value, as shown in Fig. 9a–9d, respectively. The results show that CaIn₂O₄-based phosphors have better stability than the Y₂O₂S based phosphors under the low-voltage excitation conditions. In general, the cathodoluminescent efficiency and electron beam-stimulated stability can be efficiently improved with the increase of conductivity of phosphor due to the decrease of charge accumulation and the reduction of surface chemical reaction, respectively.

Another route towards increasing phosphor conductivity is a mixing of conductive nanocrystalline powders like In₂O₃, SnO₂, ZnO, Au, Ag and so on.^{27, 67, 89, 168–170} Zhang et al. encapsulated In₂O₃ layer on Y₂O₃:Eu³⁺ phosphor particles to form Y₂O₃:Eu³⁺@In₂O₃ phosphor and concluded positive effect on their cathodoluminescent performance.⁸⁹ They found that the luminous efficiency of Y₂O₃:Eu³⁺@In₂O₃ phosphor screens was obviously improved with respect to uncoated Y₂O₃:Eu³⁺, as shown in Fig. 10a. Moreover, the luminous efficiency of the

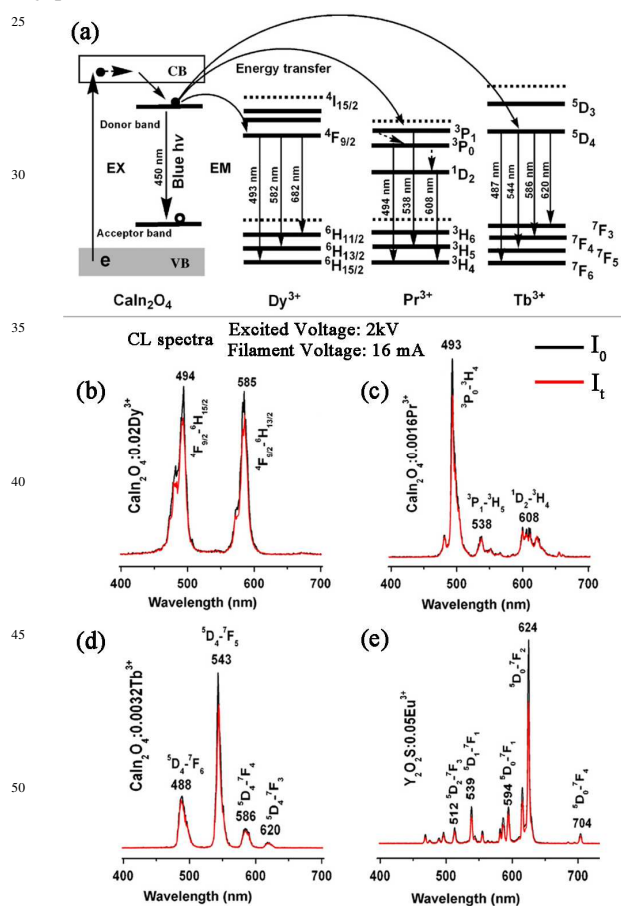


Fig. 9 (a) A simple model illustrating the blue emission process in CaIn₂O₄ and the energy transfer process from CaIn₂O₄ to Dy³⁺, Pr³⁺ and Tb³⁺. Typical CL spectra of (b) CaIn₂O₄:0.015Dy³⁺, (c) CaIn₂O₄:0.0016Pr³⁺, (d) CaIn₂O₄:0.0032Tb³⁺, and (e) Y₂O₂S:0.05Eu³⁺

former improves much more than the latter with an increase in the accelerating voltage. This is attributed to the increased electrical conductivity of $\text{Y}_2\text{O}_3:\text{Eu}^{3+}$ phosphors with increasing

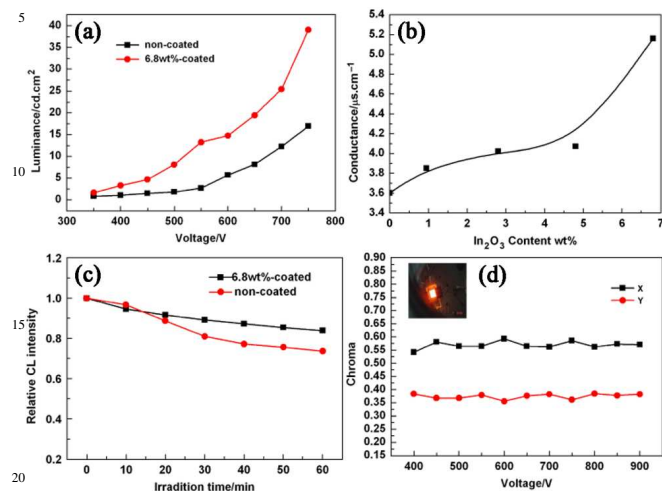


Fig. 10 (a) Dependence of luminous efficiency of $\text{Y}_2\text{O}_3:\text{Eu}^{3+}$ phosphor screens before and after In_2O_3 coating on the excitation voltage. (b) The electrical conductivity of $\text{Y}_2\text{O}_3:\text{Eu}^{3+}$ phosphors as a function of In_2O_3 coating at room temperature. (c) Comparison of the relative cathodoluminescence degradation behavior and of uncoated and In_2O_3 -coated $\text{Y}_2\text{O}_3:\text{Eu}^{3+}$ phosphor screens. (d) The variation of chromaticity of In_2O_3 -coated phosphor screen with an accelerating voltage. The inset shows a macrophotograph of the $\text{Y}_2\text{O}_3:\text{Eu}^{3+}$ phosphors coated with 6.8 wt% In_2O_3 on excitation at 700 V. (reproduced with the permission from ref. 89, copyright 2007, Wiley)

In_2O_3 coating (Fig. 10b), which is consistent with the previous reports.^{171, 172} Moreover, In_2O_3 -coated $\text{Y}_2\text{O}_3:\text{Eu}^{3+}$ phosphor screens have a better stability than uncoated one under 700 V accelerating voltage (Fig. 10c). This is because that the conductive In_2O_3 nanoparticles not only can reduce surface charge accumulation but also may serve as protective layer on phosphor surface to prevent chemical degradation caused by the direct electron beam bombardment. Finally, the aging rate of the low-voltage CL efficiency is suppressed and as a result the lifetime and stability of the phosphor screens are improved evidently.¹⁷¹ In addition, they also observed the Commission International de l'Eclairage (CIE) chromaticity coordinates stability of $\text{Y}_2\text{O}_3:\text{Eu}^{3+}@\text{In}_2\text{O}_3$ phosphors under electron beam radiation. Under the excitation of 700 V accelerating voltage, $\text{Y}_2\text{O}_3:\text{Eu}^{3+}@\text{In}_2\text{O}_3$ phosphors gives a bright red light, and its CIE values are nearly invariable (x and y keeps at about 0.575 and 0.375) with changing accelerating voltage (Fig. 10d), which is suitable for applying in field emission display. The similar improvement for cathodoluminescent efficiency and luminance appear in In_2O_3 -coated ZnGa_2O_4 and $\text{ZnGa}_2\text{O}_4:\text{Mn}^{2+}$ phosphors.^{168, 169} Therefore, employing some conductive materials on the surface of phosphor indeed can reduce the accumulated electrons on the surface of phosphor and improve the cathodoluminescent efficiency of phosphors. This may also act as a bridge to drain the coulomb charge to the ITO substrate efficiently, which decreases the excited voltage and improves the lifetime, stability, and efficiency of the phosphor screen.

2.2 The development of new phosphors for FEDs

Due to a relatively severe operation environment (low voltage and high current density) in FEDs, future generation phosphors should possess better low voltage efficiencies, chromaticity (high color purity and wide color gamut), saturation and degradation behavior, and maintenance. Possible routes to achieve these improvements include optimizing morphology, size, surface and crystallization of phosphor grains, enhancing electrical conductivity of phosphor particles, modifying composition of phosphors, enlarging color gamut, designing energy transfers and so on. On the basis of these approaches, in the past decade a series of novel FEDs phosphors has been developed, as collected in Table 2, which shows excellent low-voltage cathodoluminescent properties and has promising application in field emission display devices. Although most of the newly developed low-voltage cathodoluminescent materials commonly have the higher color purity and color stability than traditional FED phosphors, for examples, $\text{LaOCl}:\text{Tm}^{3+}$ and $\text{LaGaO}_3:\text{Tb}^{3+}$ than $\text{Y}_2\text{SiO}_5:\text{Ce}$ (blue),⁸⁶ $\text{LaOCl}:\text{Tb}^{3+}$ than $\text{ZnO}:\text{Zn}$ (green),⁹² $(\text{Zn},\text{Mg})_2\text{GeO}_4:\text{Mn}^{2+}$ and $\text{Mg}_2\text{SnO}_4:\text{Mn}^{2+}$ than $\text{Y}_2\text{SiO}_5:\text{Tb}^{3+}$ (green),^{37,75} $\text{NaCaPO}_4:\text{Mn}^{2+}$ than $(\text{Zn}, \text{CdS}):\text{Ag}^+$ (yellow),⁹⁴ the luminescent efficiencies of the formers are still lower than the latters. Fortunately, these luminescent disadvantages of the newly developed low-voltage cathodoluminescent materials can be reduced or eliminated to some extent through process optimization, including improves the morphology, size and crystallization of phosphors. Therefore, it is very necessary to explore appropriate preparation processes of these phosphors.

3. Phosphor thin films and patterning

Except for phosphor powders, phosphor thin films are the other important form to apply in display faceplates. Usually, the phosphor thin films are formed by depositing phosphor precursor on a substrate following a subsequent annealing. In the previous sections, the main discussions are focused on the cathodoluminescent materials in powder forms prepared by various soft chemical methods. While phosphor thin films appear more attractive for field emission displays (FEDs), because they could be operated at lower voltage and endure much higher power densities without degradation than those with powder phosphors.^{99, 173} In addition, phosphor thin films also offer advantages such as higher contrast and resolution, better thermal stability, superior thermal conductivity, a high degree of uniformity and better adhesion to the substrate, and reduced outgassing for FEDs compared with the conventional display screen prepared by the direct deposition of phosphor grains.¹⁷⁴⁻¹⁷⁸ In order to define a smaller pixel spot size and then to achieve a higher resolution, thin film phosphors should possess uniform thickness, smoother surface form and small grain size. To date, phosphor thin films have been prepared by a variety of deposition techniques, such as chemical vapor deposition (CVD),¹⁷⁸ physical vapor deposition (PVD),¹⁸⁰ Ion beam sputtering,¹⁸¹ filtered arc deposition,¹⁸² electrophoretic deposition (EPD),¹⁸³ spray pyrolysis,^{11, 12} and pulsed laser ablation.¹⁸⁴ These techniques are time-consuming or need expensive and complicated equipment setups. Therefore, a simple and economical method for making high quality phosphor thin films is desirable. Lin's group explored a facile preparation of oxide phosphor films by the PSG process and investigated their structure, morphology, and optical properties.¹⁸⁵⁻¹⁹⁸ The simple preparation process mainly involve in three steps: the first step is the preparation of the precursor solution with certain viscosity, including the dissolution of the starting materials, formation of metal chelates with citric acid (CA) and their polyesterification with PEG; the second step is the preparation of the amorphous precursor film by a dip-coating or spin-coating process on the desired substrates (silica glasses,

silicon wafers, ITO and quartz plates, some ceramics slides, etc.);

10

Table 2 Some newly developed rare earth ions or Mn²⁺ ions activated low voltage cathodoluminescent materials and their luminescent properties.

| Sample | Emission peaks (nm)/main transition | Color | CIE chromaticity coordinates (x, y) | Refs |
|---|--|---|--|------------|
| Ga ₂ O ₃ : Dy ³⁺ | 438/ ⁴ F ₁₋₂ A ₂ (GaO ₆) 492, 580/ ⁴ F _{9/2} to ⁶ H _{15/2} , ⁶ H _{13/2} (Dy ³⁺) | Blue White | (0.1837, 0.1602) (0.2994, 0.3331) | 66 |
| CaIn ₂ O ₄ : Eu ³⁺ | 431, 447, 467, 492, 512, 537, 588, 616/ ⁶ D _{0,1,2,3} - ⁷ F _{0,1,2,3} (Eu ³⁺); 588/ ⁶ D ₁₋₇ - ⁷ F ₂ ; 619/ ³ D ₀₋₇ - ⁷ F ₂ (Eu ³⁺) | White Red | (0.3237, 0.3232) (0.5646, 0.3481) | 54 |
| CaIn ₂ O ₄ : Dy ³⁺ , Pr ³⁺ , Tb ³⁺ | 493, 582/ ⁴ F _{9/2} to ⁶ H _{15/2} , ⁶ H _{13/2} (Dy ³⁺); 494/ ³ P ₀₋₃ H ₄ (Pr ³⁺); 487/ ⁶ D ₄₋₇ - ⁷ F ₆ , 544/ ⁶ D ₄₋₇ - ⁷ F ₅ (Tb ³⁺) | Yellowish white Cyan Green | (0.3456, 0.3758) _____ _____ | 71 |
| SrIn ₂ O ₄ : Dy ³⁺ , Pr ³⁺ , Tb ³⁺ | 493/ ⁴ F _{9/2} - ⁶ H _{15/2} , 582/ ⁴ F _{9/2} - ⁶ H _{13/2} (Dy ³⁺); 494/ ³ P ₀₋₃ H ₄ (Pr ³⁺); 487/ ⁶ D ₄₋₇ - ⁷ F ₆ , 544/ ⁶ D ₄₋₇ - ⁷ F ₅ (Tb ³⁺) | Bluish white Orange Green | (0.3019, 0.3291) (0.5447, 0.3482) (0.2496, 0.5564) | 72 |
| LaOCl: Tm ³⁺ , Dy ³⁺ , Sm ³⁺ , Tb ³⁺ , Eu ³⁺ | 458/ ⁴ D ₂₋₇ - ⁷ F ₄ (Tm ³⁺); 480, 571/ ⁴ F _{9/2} to ⁶ H _{15/2} , ⁶ H _{13/2} (Dy ³⁺); 565, 607, 650/ ⁶ G _{5/2} - ⁶ H _{5/2, 7/2, 9/2} (Sm ³⁺); 384, 416, 437, 486, 543/ ⁶ D _{3,4} - ⁷ F _j (j = 6-0) (Tb ³⁺); 615/ ⁶ D ₀₋₇ - ⁷ F ₅ (Eu ³⁺) | Blue Yellow Orange Blue Green Red | (0.1584, 0.0651) (0.3992, 0.4484) (0.5506, 0.4065) (0.1723, 0.1210) (0.2486, 0.5188) (0.6039, 0.3796) | 15, 86, 92 |
| LaGaO ₃ : Tm ³⁺ , Sm ³⁺ , Tb ³⁺ , Dy ³⁺ , Eu ³⁺ | 458/ ⁴ D ₂₋₇ - ⁷ F ₄ (Tm ³⁺); 561, 597, 642/ ⁶ G _{5/2} - ⁶ H _{5/2, 7/2, 9/2} (Sm ³⁺); 414, 437, 414, 437/ ⁶ D _{3,4} - ⁷ F _{5,4} (Tb ³⁺); 480, 572/ ⁴ F _{9/2} to ⁶ H _{15/2} , ⁶ H _{13/2} (Dy ³⁺); 590, 614/ ⁶ D ₀₋₇ - ⁷ F _{1,2} (Eu ³⁺) | Blue Yellow Blue Green Yellowish white Red | (0.1552, 0.0630) (0.4880, 0.4153) (0.2087, 0.1541) (0.2705, 0.5262) (0.3432, 0.3920) (0.5396, 0.3634) | 14 112 113 |
| LaInO ₃ : Eu ³⁺ | 465, 491, 512, 534, 588, 610 / ⁶ D _{0,1,2,3} - ⁷ F _{0,1,2,3} (Eu ³⁺); 588, 610/ ⁶ D ₀₋₇ - ⁷ F _{1,2} (Eu ³⁺) | Yellowish white Red | (0.3688, 0.4040) (0.5740, 0.3451) | 167 |
| Mg ₂ (Sn,Ti)O ₄ : Mn ²⁺ | 465/(SnO ₆); 456/(TiO ₆) 499/ ⁴ T ₁₋₆ A ₁ (Mn ²⁺) | Blue Blue Cyan Green | (0.1780, 0.2449) (0.1773, 0.2186) (0.1409, 0.3185) (0.0908, 0.5668) | 37 |
| Li ₂ ZnGeO ₄ : Mn ²⁺ | 530/ ⁴ T ₁₋₆ A ₁ (Mn ²⁺) | Green | (0.160, 0.108); (0.235, 0.702) | 39 |
| (Zn,Mg) ₂ GeO ₄ : Mn ²⁺ | 460/(GeO ₄); 531/ ⁴ T ₁₋₆ A ₁ (Mn ²⁺) | Blue; Green | (0.165, 0.209); (0.268, 0.644) | 75 |
| NaCaPO ₃ : Mn ²⁺ | 560/ ⁴ T ₁₋₆ A ₁ (Mn ²⁺) | Yellow | (0.428, 0.552) | 94 |
| Ca ₂ GeO ₄ : Eu ³⁺ | 613/ ⁶ D ₀₋₇ - ⁷ F ₅ (Eu ³⁺) | Red | (0.559, 0.341) | 164 |
| CaYAlO ₄ : Tb ³⁺ , Eu ³⁺ | 383, 416, 468, 537, 548/ ⁶ D _{3,4} - ⁷ F _j (j = 6-0) (Tb ³⁺); 593, 623/ ⁶ D ₀₋₇ - ⁷ F _{1,2} (Eu ³⁺) | Blue Green Red | (0.181, 0.123) (0.272, 0.480) (0.534, 0.347) | 95 |
| SrY ₂ O ₄ : Tb ³⁺ , Tm ³⁺ , Dy ³⁺ | 545/ ⁶ D ₄₋₇ - ⁷ F ₅ (Tb ³⁺); 455/ ⁴ D ₂₋₇ - ⁷ F ₄ (Tm ³⁺); 491, 581/ ⁴ F _{9/2} to ⁶ H _{15/2} , ⁶ H _{13/2} (Dy ³⁺) | Green Blue Yellowish white | (0.278, 0.531) (0.148, 0.059) (0.363, 0.395) | 97 |

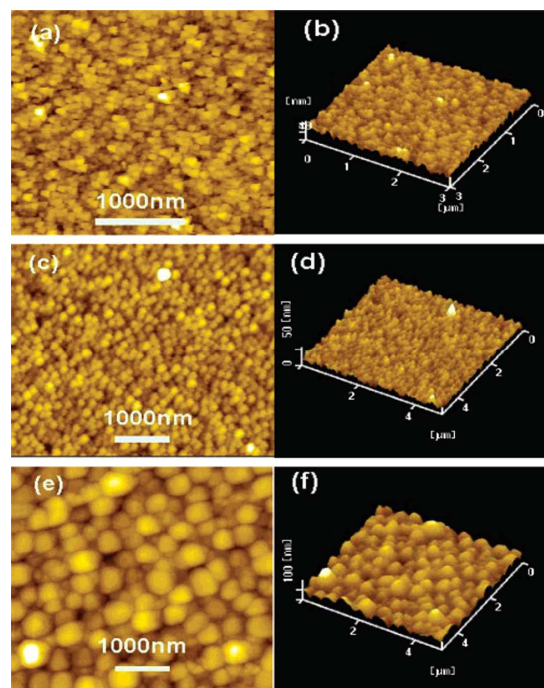


Fig. 11 Atomic force microscopy (AFM) images for YVO₄:Eu³⁺ (a and b), GdVO₄:Eu³⁺ (c and d), and LaVO₄:Eu³⁺ phosphor films prepared by the PSG dipcoating process. (reproduced with the permission from ref. 192, copyright 2005, American Institute of Physics)

finally, crystalline phosphor films are produced by the postannealing process at moderate temperature (500-1000°C) with a slow heating rate to avoid the cracking and peeling of the films. Generally, the phosphor thin films prepared via PSG process are smooth and consist of nanocrystalline grains ranging from 100 to 500 nm, as shown in Fig. 11.¹⁹² The as-prepared phosphor thin films via the PSG process have many advantages, as follow:¹⁸⁵⁻¹⁹⁸ a) simple process and equipment; b) low processing temperature, making it possible to prepare films on glass, semiconductor, and integrated photoelectronic devices; c) films can be coated on substrates with a large area, various shape and different material compositions; d) a easy control of homogeneity, constituents and microstructure; e) a controllable thickness by adjusting the viscosity of the coating solution or the repeating number of the coating process. It is noted that the thin film phosphors present similar luminescence properties to powder phosphors, but have lower emission intensity due to the light trapping inside the luminescent layer. Therefore, such films cannot presently compete with powder phosphors in applications phosphors in applications that require high brightness.¹⁸⁷⁻¹⁹³ On the other hand, full-color displays generally need to deposit the three color modules (red, green, blue) on the desired regions to form pixels.⁹⁹ Therefore, during the fabrication of display devices, patterning luminescent materials on screen to form pixel matrix is an essential and critical technique. An accurate patterning technology and screening process for phosphor screen has a vital effect on the resolution of display devices. For instance, pitches of phosphor lines for a supervideo graphics adapter with 800 × 600 lines, video graphics adapter with 640 × 480 lines, and quarter video graphics adapter with 320 × 240 lines in 6 in. color displays

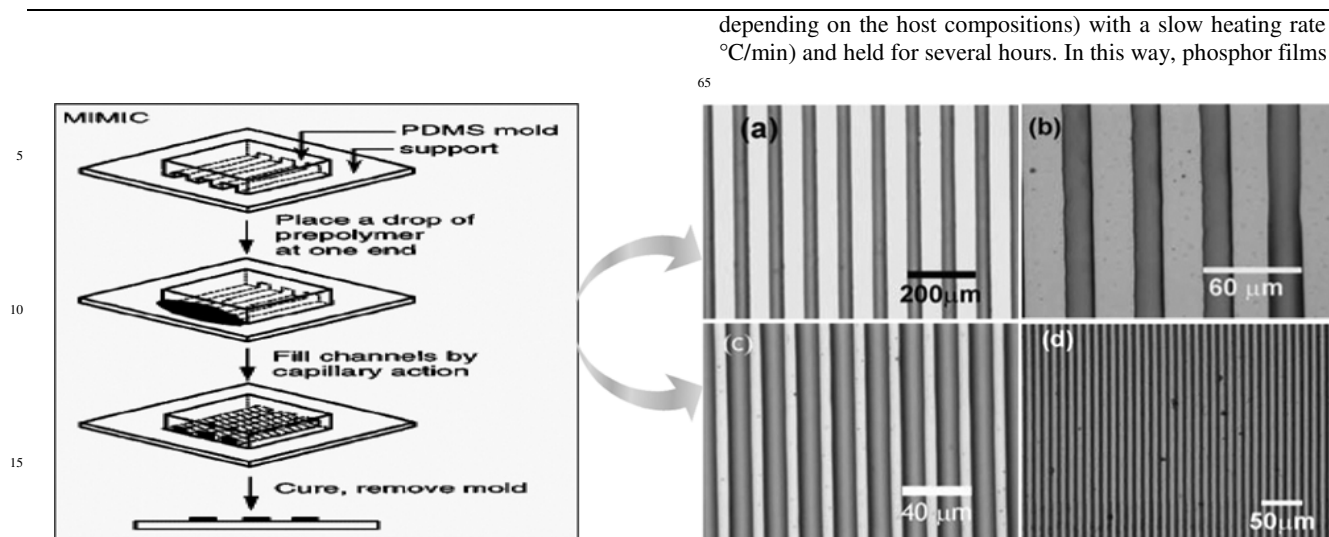


Fig. 12 Schematic procedures of MIMIC for patterning of phosphor films (Left) and the optical photographs for patterned $\text{LaPO}_4:\text{Ce}^{3+}$, Tb^{3+} phosphor films with different stripe width (Right, a-50 μm , b-20 μm , c-10 μm , d-5 μm). (reproduced with the permission from refs. 185 and 186, copyright 2002 and 2003, American Chemical Society and Royal Society of Chemistry)

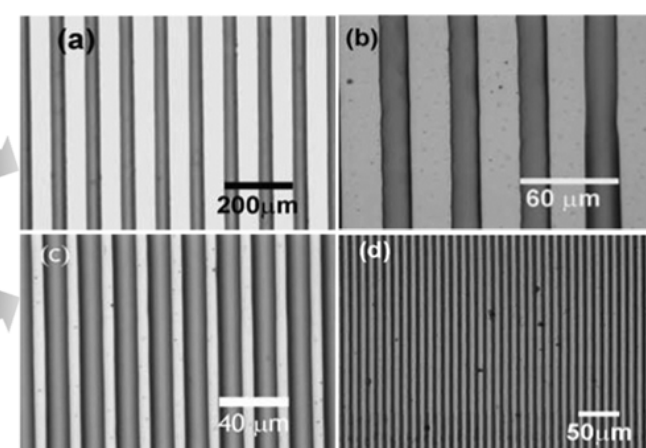
are defined as 50.8, 63.5, and 127 μm , respectively.^{99, 199} So far, electrophoretic deposition, screen printing, vacuum deposition, etc., based on photolithographic patterning technologies have been employed to fabricate flat panel displays (FPDs) devices.²⁰⁰ Unfortunately, these patterning techniques for a phosphor screen frequently require expensive photolithographic and etching equipment, complicated layout, and excessive loss of expensive phosphor materials during the fabrication process. Based on these considerations, a growing interest has been focused to soft lithography patterning techniques, which has the potential of becoming versatile and low cost methods for creating submicrometer and micrometer size structures.²⁰¹⁻²⁰³ Soft lithography technique uses a soft and flexible poly(dimethylsiloxane) (PDMS) elastomer that can exactly replicate the surface features of the master mold and transfer them in the patterning process instead of rigid materials as the stamp or mold and it is carried out by casting the prepolymer on a master with relief structure.²⁰¹ Recently, several soft lithography techniques including micromolding in capillaries (MIMIC), microtransfer molding (μTM), inkjet printing (IP) and microcontact printing (μCP) to realize the patterning of thin film phosphors have been well explored and developed. The detailed introductions are demonstrated in the following sections.

(1) Micromolding in capillaries (MIMIC)

As soft lithography technique, MIMIC can pattern a material based on a low-viscosity solution.²⁰¹⁻²⁰³ Phosphor thin films also can be patterned by the MIMIC technique. The basic principle of this process is shown in Fig. 12 (Left).⁹⁹ First, polydimethylsiloxane (PDMS) stamp modes (with different channel widths 5-50 μm) were fabricated by casting PDMS on masters having desired patterns.^{185, 186} Then the PDMS modes were placed in conformal contact with thoroughly cleaned silicon wafer substrates. The channels of the mode thus formed capillaries with the silicon wafer substrate. The phosphor precursor sol (via the PSG process) was then dropped at the open end with a transfer pipet. The capillary force made the sol flow into the mold. Then the modes and substrates were dried at 100°C overnight. After carefully removing the modes, the resulted patterned gel films were heated to high-temperature (500-1000 °C

depending on the host compositions) with a slow heating rate (1 °C/min) and held for several hours. In this way, phosphor films

65



with patterning were obtained. Fig. 12 (Right) shows optical micrographs of the as-prepared patterned $\text{LaPO}_4:\text{Ce}^{3+}$, Tb^{3+} gel films. The dark and white regions correspond to the film strips and spaces, respectively. It is clearly seen from Figure 13a-d that film strips have widths of 5, 10, 20, and 50 μm , respectively, with smooth and perfect surfaces. Patterned phosphor films were formed after a subsequent annealing of these patterned gel films.^{185, 186} According to the MIMIC technique, many other kinds of patterned phosphor films, such as $\text{Y}_2\text{O}_3:\text{Eu}^{3+}$, $\text{Gd}_2\text{O}_3:\text{Eu}^{3+}$, (Y, La, Gd) $\text{VO}_4:\text{Eu}^{3+}$ etc., can be prepared, which are promising for applications in the field emission display fields.^{197, 198}

100 (2) Microtransfer molding (μTM)

Microtransfer molding (μTM) is one of the most popular and typical soft-lithography techniques. This technique can directly replicate the feature of the stamp and form the pattern in accordance with the geometry of the stamp. Wang et al. introduce $\text{YVO}_4:\text{Eu}^{3+}$ as an example to illustrate the fabrication of light-emitting arrays via μTM technique, as shown in the left of Fig. 13a.²⁰⁴ First, the PDMS stamps were fabricated by casting the PDMS prepolymer, a mixture of Sylgard silicone elastomer, and its curing agent over a relief master prepared by photolithography. The elastomer was degassed for 30 min at room temperature and cured at 65°C for 4 h, then peeled gently from the master. In this way, PDMS stamps with microwells were obtained. Second, the quartz plates were transformed to hydrophilic properties by immersing them in a piranha solution of concentrated sulfuric acid and hydrogen peroxide. Next, the $\text{YVO}_4:\text{Eu}^{3+}$ precursor solution was cast on the patterned side of the PDMS mold and the excess solution was removed by scraping with a flat PDMS block. After spin-coating at 1500 rpm, the $\text{YVO}_4:\text{Eu}^{3+}$ precursor solution was deposited into the recessed square regions of the PDMS mold, and the mold was brought into contact with the quartz substrate. Then, the mold and substrate were dried at 100°C for 4 h. When the mold was peeled away carefully, patterned squares of the $\text{YVO}_4:\text{Eu}^{3+}$ precursor gels were left on the surface of the quartz substrate. Finally, the patterned substrate was calcined at 700°C for 3 h to pyrolyze the organic components and the precursor gel was transformed into

crystalline $\text{YVO}_4:\text{Eu}^{3+}$. The as-prepared $\text{YVO}_4:\text{Eu}^{3+}$ precursor gel pattern by the μTM technique (Fig. 13b) exhibits ordered square arrays without obvious swelling or

formation depends on the chemical heterogeneity of the substrate's surface, these techniques are continuously being

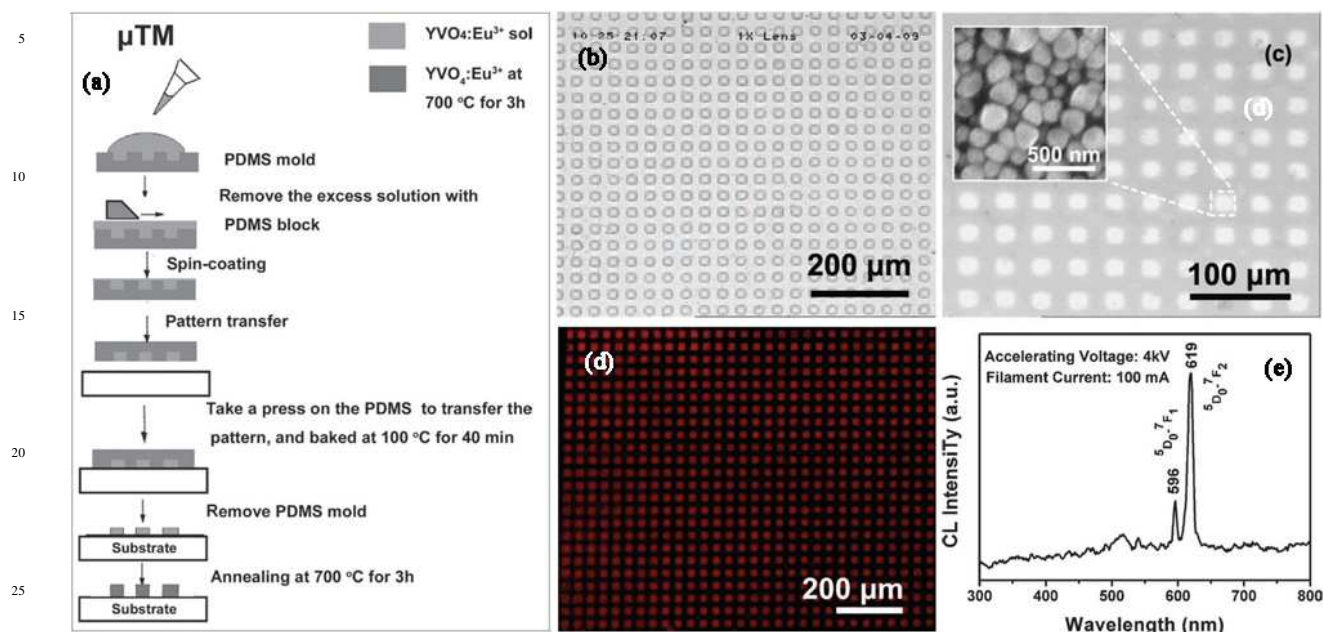


Fig. 13 (a) Schematic diagram of the experimental microtransfer molding (μTM) process used for patterning $\text{YVO}_4:\text{Eu}^{3+}$ films. Optical image of the patterned $\text{YVO}_4:\text{Eu}^{3+}$ precursor gel film fabricated by b) μTM , c) after calcination at 700 °C, and d) the corresponding luminescent image under 254-nm UV light excitation. The inset in (c) SEM image of the patterned $\text{YVO}_4:\text{Eu}^{3+}$ film, indicative of the morphology of the crystalline $\text{YVO}_4:\text{Eu}^{3+}$ particles after firing at 700 °C. (e) The CL spectra of the patterned $\text{YVO}_4:\text{Eu}^{3+}$ film (Accelerating Voltage: 4 kV; Filament Current: 100 mA). (reproduced with the permission from ref. 204, copyright 2011, Wiley)

deformation (a high fidelity to the initial PDMS stamp). The estimated side length of the precursor gel square is 22.56 ± 1.37 μm . After calcination at 700 °C in air, the patterned $\text{YVO}_4:\text{Eu}^{3+}$ crystalline film was formed on the quartz plate and the corresponding optical microscope image is shown in Fig. 13c. The white square is the final crystalline $\text{YVO}_4:\text{Eu}^{3+}$ and the black is the bare substrate. A size-shrinkage of the square gels was observed after firing, which is attributed to the pyrolysis and evaporation of the organic compounds in the gel. The estimated side length of the crystalline square is 19.17 ± 2.05 μm . As observed in Fig. 13b and 13c. The calcination procedure did not modify the morphology of the printed feature in principle, and the aspect ratio of the square pattern is 1:1 before and after heat treatment. However, the calcination reduces the size of the square gel spots owing to the pyrolysis and evaporation of the organic species, and the edges of the calcined square spots are not as clear as that of the uncalcined gel spots because of the shrinkage during the heat-treatment process. The red luminescent image (Fig. 13d) and CL spectrum (Fig. 13e) of $\text{YVO}_4:\text{Eu}^{3+}$ phosphor films indicated that the as-prepared $\text{YVO}_4:\text{Eu}^{3+}$ phosphor films can be efficiently excited by UV light and low voltage electron beam.

(3) Microcontact printing (μCP)

Microtransfer printing (μCP) is another one of the most popular and typical soft-lithography techniques.²⁰⁴ On the contrast to μTM , the μCP technique prints the self-assembled monolayer (SAM) pattern on the substrate in the first step, which makes the substrate change from being chemically homogeneous into chemically heterogeneous. Then, other functional materials can be grown or deposited on the desired patterned regions. Although μCP requires multiple steps and the final pattern

developed and improved. For example, a self-assembled monolayer can be firstly transferred onto a substrate and its end group can then be modified through organic synthesis to generate well-defined surfaces with a broad range of characteristics.²⁰⁵ Therefore, μCP is an improved technique based on μTM . Fig. 14a shows the process of fabricating a representative $\text{YVO}_4:\text{Eu}^{3+}$ arrays of dots via μCP . This technique is based on the modification of the substrate surface and the selective deposition on desired regions.²⁰⁶ First, the PDMS molds and the quartz plates were carried out the same treatment as μTM technique. The PDMS mold was subsequently flooded with 1H,1H,2H,2H-perfluorooctyltrichlorosilane (PFOTS) solution in n-octane (1 vol%) and blown dry with N_2 , then the PDMS mold was placed in contact with the as-cleaned quartz substrate to print the self-assembled PFOTS monolayer (SAM). Next, the patterned substrate was used as a template for the selective deposition of the metal salts solution by spin-coating. During this spin-coating process, the precursor solution was selectively deposited on the hydrophilic regions because of the poor adhesion between the solution and the SAM. Finally, the substrate with the patterned gel was calcined at 700 °C for 3 h to obtain the crystalline $\text{YVO}_4:\text{Eu}^{3+}$ film. Fig. 14b shows the optical microscopy image of a $\text{YVO}_4:\text{Eu}^{3+}$ precursor gel pattern (just spin-coating dried, without annealing) fabricated by the μCP technique. It can be seen that the ordered dot-patterned precursor gel arrays were transferred from the PDMS stamp to the quartz substrate. After calcination at 700 °C in air, the patterned $\text{YVO}_4:\text{Eu}^{3+}$ crystalline film was formed on the quartz plate and the corresponding optical microscope image is shown in Fig. 14c. Similarly, the calcination reduces the size of the dot gel spots owing to the pyrolysis and evaporation of the organic species, and the edges of the calcined square spots are not as clear as that of the uncalcined gel spots

because of the shrinkage during the heat-treatment process. Under 254 nm UV light excitation, the patterned $\text{YVO}_4:\text{Eu}^{3+}$ thin film phosphors show bright red light emission, as shown in Fig.

μTM and μCP methods, indicating that soft lithography (μTM and μCP) techniques could be used at all for the patterning of inorganic rare-earth salts.^{207,208} These results demonstrate that the Pechini-type sol-gel process has a good compatibility with soft-

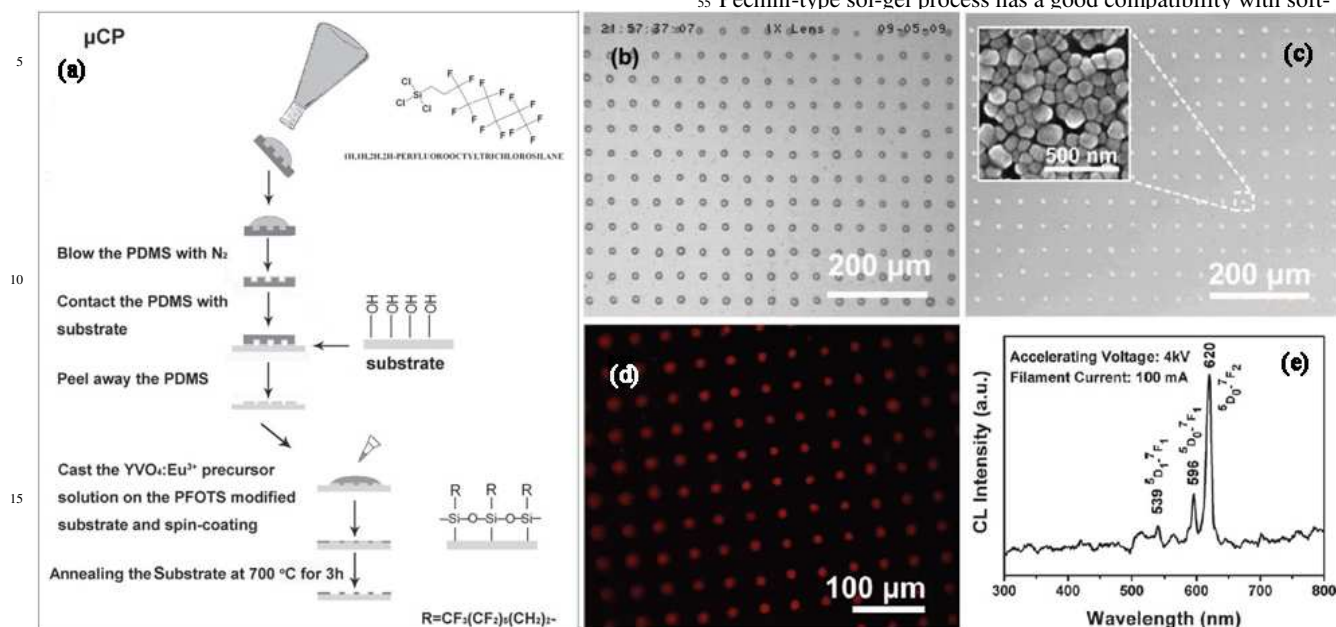


Fig. 14 (a) Schematic diagram of the experimental microcontact printing (μCP) process used for patterning $\text{YVO}_4:\text{Eu}^{3+}$ films. Optical image of the patterned $\text{YVO}_4:\text{Eu}^{3+}$ precursor gel film fabricated by b) μCP , c) after calcination at 700°C , and d) the corresponding luminescent image under 254-nm UV light excitation. The inset in (c) SEM image of the patterned $\text{YVO}_4:\text{Eu}^{3+}$ film, indicative of the morphology of the crystalline $\text{YVO}_4:\text{Eu}^{3+}$ particles after firing at 700°C . (e) The CL spectra of the patterned $\text{YVO}_4:\text{Eu}^{3+}$ film (Accelerating Voltage: 4 kV; Filament Current: 100 mA). (reproduced with the permission from ref. 204, copyright 2011, Wiley)

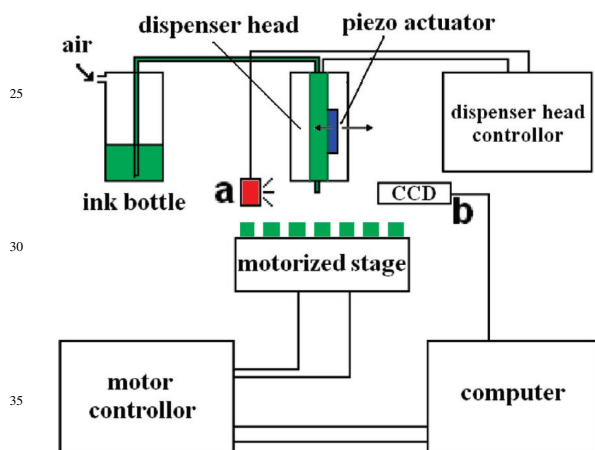


Fig. 15 Schematic Representation of the Inkjet Printing Setup. ^aThe inkjet printing system was manufactured by Microdrop Technique GmbH (Germany), which consists of a piezo-actuated inkjet dispenser head and its controller. A motorized stage under the inkjet printing head equipped with the computer and software provides the precise position of substrate. (reproduced with the permission from ref. 209, copyright 2010, American Chemical Society)

14d. The CL spectra of patterned $\text{YVO}_4:\text{Eu}^{3+}$ films in Fig. 14e also shows the characteristic Eu^{3+} emission at 596 nm and 619 nm, which correspond to the Eu^{3+} transitions of $^5\text{D}_0-^7\text{F}_1$ and $^5\text{D}_0-^7\text{F}_2$, respectively. Except for $\text{YVO}_4:\text{Eu}^{3+}$, many other kinds of patterned phosphor films, such as $\text{CaWO}_4:\text{Ln}^{3+}$ ($\text{Ln}=\text{Tb}, \text{Eu}$), $\text{Gd}_2(\text{WO}_4)_3:\text{Ln}^{3+}$ ($\text{Ln} = \text{Eu}, \text{Tb}$) were also prepared based on the

85 lithography techniques for patterning inorganic phosphor materials, which holds potential for fabricating new-generation field-emission display devices. Moreover, these results can guide us in future research, and be helpful to others who have interest in 90 these types of devices.

(4) Inkjet printing (IP)

Recently, inkjet printing has attracted substantial interest as a pathway to make display devices, in which the material deposition and patterning can be performed within a single step 95 by a fully digital driven process.²⁰⁹⁻²¹² This direct-writing technique has many advantages such as simple, fast, large area, and low material consumption. There are many reports for the applications of inkjet printing on the fabrication of polymer light-emitting diodes (PLED).²¹³⁻²²⁰ The deposition of light-emitting 100 polymers as pixels or conducting polymer PEDOT:PSS as the hole transportation layer can be carried out by inkjet printing in the PLED fabrication process. The bottleneck of the inkjet printing technique in organic electronics is being exceeded and some prototypes of full-color organic light-emitting televisions 105 have been demonstrated.^{217, 221} The quantum dots are also considered as excellent candidates for the inkjet printing route in fabricating a display device due to their good dispersibility in solvent and the size tunable light emission.²²²⁻²²⁵ Cheng et al. have made an attempt to pattern inorganic phosphor materials for 110 the applications of a field emission flat display by the inkjet printing technique. The principle of this process is shown in Fig. 15. Using $\text{YVO}_4:\text{Eu}^{3+}$ as a representative example, the patterning

of phosphor thin films through inkjet printing technique can be realized.²⁰⁹ The inkjet printing system consists of a piezoelectric type printing head with a nozzle diameter of 70 μm . The microdrops were squeezed out by applying a voltage to the glass capillary inside the dispenser head. A computer-controlled motorized translation stage can move in the X-Y directions relative to the dispenser head which provide the patterns on the substrate such as dots and lines. Prior to the inkjet printing process, the ITO glass plates were first immersed into the saturated NaOH/ethanol solution for 5 h and then ultrasonically cleaned for 10 min to remove the organic contamination. Then the ITO glass substrates were rinsed by copious amounts of deionized water and dried under nitrogen flow to form hydrophilic surface. Additionally, the hydrophobic ITO surface was obtained by putting the pre-cleaned ITO glass plates into a 3 mM perfluorooctyltrichlorosilane (PFOTS, Aldrich) solution in

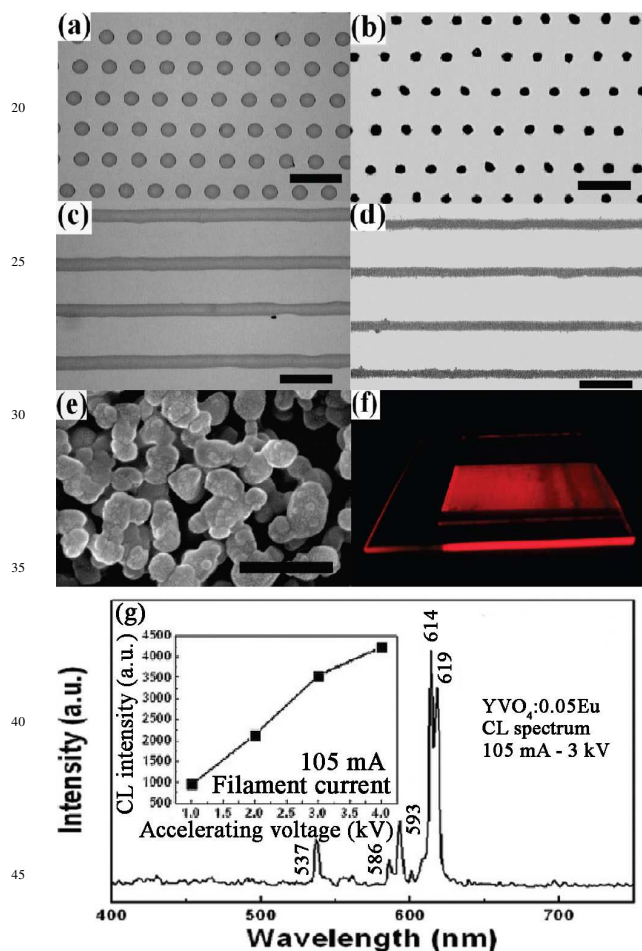


Fig. 16 Microscopy photographs of the as-inkjet-printed dots and lines of gel (a, c) and the corresponding phosphor pixels of crystalline $\text{YVO}_4:0.05\text{Eu}^{3+}$ (c, d); the SEM image showing the morphology of crystalline particles of $\text{YVO}_4:0.05\text{Eu}^{3+}$ after firing at 600°C (e); and digital photograph exhibiting the red-emission $\text{YVO}_4:0.05\text{Eu}^{3+}$ lines matrix (corresponding to Fig. 15d) with the size of $4\text{ cm} \times 6\text{ cm}$ prepared on ITO-coated glass and illuminated under 254 nm UV light (f) The scale bars represent 200 μm in panels a-d and 200 nm in panel e. (g) The CL spectrum of patterned $\text{YVO}_4:0.05\text{Eu}^{3+}$ on ITO-glass excited by electron beam. The inset shows the CL intensity of the

$\text{YVO}_4:0.05\text{Eu}^{3+}$ pattern as a function of electron beam voltage. (reproduced with the permission from ref. 209, copyright 2010, American Chemical Society)

hexane for 4 h to self-assemble the densely packed monolayer of PFOTS onto the ITO surface. After careful filtration with a polyvinylidene fluoride (PVDF) microporous filter, the ink solution was loaded on the inkjet printing system to produce the dots or lines pattern on the ITO glass. The driven voltage and pulse width are 20 V and 34 μs , respectively. The inkjetting frequency is 100 droplets per second. After being dried at 100°C for 20 min, the resulting pattern-formed substrates were baked at 600°C with an increasing rate of 1 deg/min and held there for 4 h in air in order to form the light-emitting $\text{YVO}_4:\text{Eu}^{3+}$ pixels. Fig. 16a, c and 16b, d shows the microscopy image of as-inkjet-printed dots array before and after annealing, respectively. Obviously, the as-inkjet-printed dots arrays are highly uniform before and after annealing. However, significant shrinking in the diameter of the dots due to the remove of organic components was observed after annealing at 600°C , although its shape was maintained. In addition, it can be seen from Fig. 16e that the crystalline $\text{YVO}_4:0.05\text{Eu}^{3+}$ are composed of fine particles with a size between 20 and 120 nm (measured on the long axis) after 600°C annealing. The patterned $\text{YVO}_4:0.05\text{Eu}^{3+}$ film shows the strong red emission under a hand-held UV light with 254 nm wavelength (Fig. 16f), which indicates the feasibility of printing inorganic nanophosphor material for high-resolution screen application through the Pechini-type sol-gel and inkjet printing route. Under the excitation of low voltage electron beam, the patterned $\text{YVO}_4:0.05\text{Eu}^{3+}$ film can also give good red light emission centered at 614 and 619 nm due to the $^5\text{D}_0\text{-}^7\text{F}_2$ transition, as shown in Fig. 16g. Moreover, the CL intensity increases quickly upon raising the accelerating voltage from 1 to 4 kV when the filament current is fixed on 105 mA, indicating the light-emitting intensity of $\text{YVO}_4:0.05\text{Eu}^{3+}$ is strongly dependent on the accelerating voltage, which is in line with FED working principle. In summary, the preparation of patterning $\text{YVO}_4:\text{Eu}^{3+}$ light-emitting pixels by a combination of inkjet printing and the PSG method show a feasible scheme for patterning inorganic thin film phosphors by the inkjet printing route. This facile and quick method has the potential to be used in the fabrication of FED devices by continuing efforts to further improving the properties of ink solution and prestructuring substrate, modifying the layout, and so forth.

4. Enlarge color-gamut and design white light emission

4.1 Enlarge color-gamut

The resolution is a vital parameter for display devices, which is strongly related to the color saturation, namely, the color gamut of phosphor.^{27, 76} Generally, the wider of color gamut of phosphor, the higher picture quality can be achieved.⁷⁶ The color gamut for phosphors is depicted by the location of their CIE chromaticity coordinates. The typical color gamut for FEDs is made up of a triangle region enclosed by three chromaticity coordinate points of trichromatic (Red, Green and Blue, RGB) FEDs phosphors, (0.647, 0.343) ($\text{Y}_2\text{O}_2\text{S}:\text{Eu}^{3+}$; red), (0.298, 0.619) ($\text{ZnS}:\text{Cu,Al}$; green) and (0.146, 0.056) ($\text{ZnS}:\text{Ag,Al}$; blue). In

order to realize high-quality full-color FEDs, it is necessary to enlarge the color gamut of these phosphors. There are two main strategies to reach this goal. The one is to develop FEDs phosphors with higher color purity with respect to current trichromatic FEDs phosphors. The other one is to explore some novel phosphors with their CIE chromaticity coordinates locating out of the above triangle area. According to the first strategy, Lin's group has developed a series of RGB phosphors with high color purity. For example, blue-emitting Tm^{3+} -doped La_2O_3 , LaOCl , LaOF , LaGaO_3 and so on were prepared and investigated.^{14, 86, 110, 155, 122} These phosphors all demonstrate more higher color purities than commercial FED blue phosphor $\text{Y}_2\text{SiO}_5:\text{Ce}$ due to main $^1\text{D}_2\text{-}^3\text{F}_4$ (around 458 nm) transition emission of Tm^{3+} ions (Table 2). In addition, some Tb^{3+} -activated phosphors such as Tb^{3+} -doped LaOCl , LaGaO_3 , $\text{KNaCa}_2(\text{PO}_4)_2$ etc., can also give highly pure blue emission through a low Tb^{3+} doping content due to the main $^5\text{D}_3\text{-}^7\text{F}_{6,0}$ transitions emission of Tb^{3+} ions.^{14, 92, 115} As mentioned in the previous section, rare earth (RE) ions have been playing an important role in display fields due to the abundant emission colors based on their $4f\text{-}4f$ or $5d\text{-}4f$ transitions. For $4f\text{-}4f$ transitions of RE ions, the emission spectra are narrow and the peak positions are basically stable in different hosts because the electrons in $4f$ orbitals are strongly shielded by the outside $5s$ and $5p$ electrons. As a result, their luminescent properties (peak width and position) are not strongly dependent on the crystal structure of host and can maintain a high color purity. For $5d\text{-}4f$ transitions of RE ions, the energy level of the excited state $4f^{n-1}5d$ is commonly lower than that of the lowest excited state in its $4f^n$ electron configuration, they generally presents broad band emission than $4f\text{-}4f$ transitions. The different coordination surroundings in a host that result in different crystal field strength have a prominent influence on its luminescence due to the $5d$ states of RE ions in outer orbitals.^{6, 8} Furthermore, the spectral position of $4f^{n-1}5d \rightarrow 4f^n$ transition is closely related to the nephelauxetic effect.²²⁶ The higher charge and the smaller radius of ligand ion, the stronger the nephelauxetic effect appears, which will result in the lower the position of $5d$ energy level. So, the $4f \rightarrow 5d$ transitions of RE ions depends deeply on the host lattice, and the emission color from the $4f^{n-1}5d \rightarrow 4f^n$ transition can be adjusted from ultraviolet to red light region.⁹ Hirosaki et al.¹³ realized a highly pure blue emission of Eu^{2+} in AlN host with CIE coordinate (0.139, 0.106). Under electron beam excitation, it showed better saturation behavior, brightness and degradation behavior than that of $\text{Y}_2\text{SiO}_5:\text{Ce}$. So it is an excellent blue-emitting FEDs phosphor. For green-emitting phosphors, Mn^{2+} -activated Mg_2SnO_4 , $(\text{Zn},\text{Mg})_2\text{GeO}_4$ and $\text{Li}_2\text{ZnGeO}_4$ systems have promising properties for use in FEDs.^{37, 39, 75} Because the Mn^{2+} is a transition metal ion with $3d^5$ electronic configuration, its emission, corresponding to $^4\text{T}_1 \rightarrow ^6\text{A}_1$ transition, consists of a broad band whose position depends strongly on the host lattices.^{227, 228} If the crystal field around Mn^{2+} ion is weak, the splitting of the excited energy levels in d orbitals will be small resulting in Mn^{2+} emission with higher energy, whereas it will give lower energy emission.^{32, 33} Due to the weak crystal field surroundings, the as-prepared Mn^{2+} -activated Mg_2SnO_4 , $(\text{Zn},\text{Mg})_2\text{GeO}_4$ and $\text{Li}_2\text{ZnGeO}_4$ phosphors give brilliant green emission from 500 nm to 530 nm with narrow band width, which makes them have higher green purity than commercial green

$\text{ZnO}:\text{Zn}$ phosphors (Table 2). While $\text{Mg}_2\text{Y}_8(\text{SiO}_4)_6\text{O}_2:\text{Ce}^{3+}/\text{Mn}^{2+}$ and $\text{Ca}_4\text{Y}_6(\text{SiO}_4)_6\text{O}:\text{Ce}^{3+}/\text{Mn}^{2+}$ show excellent red emission of Mn^{2+} due to the strong crystal field surroundings, which can be used for highly efficient red-emitting FED phosphors. In addition,

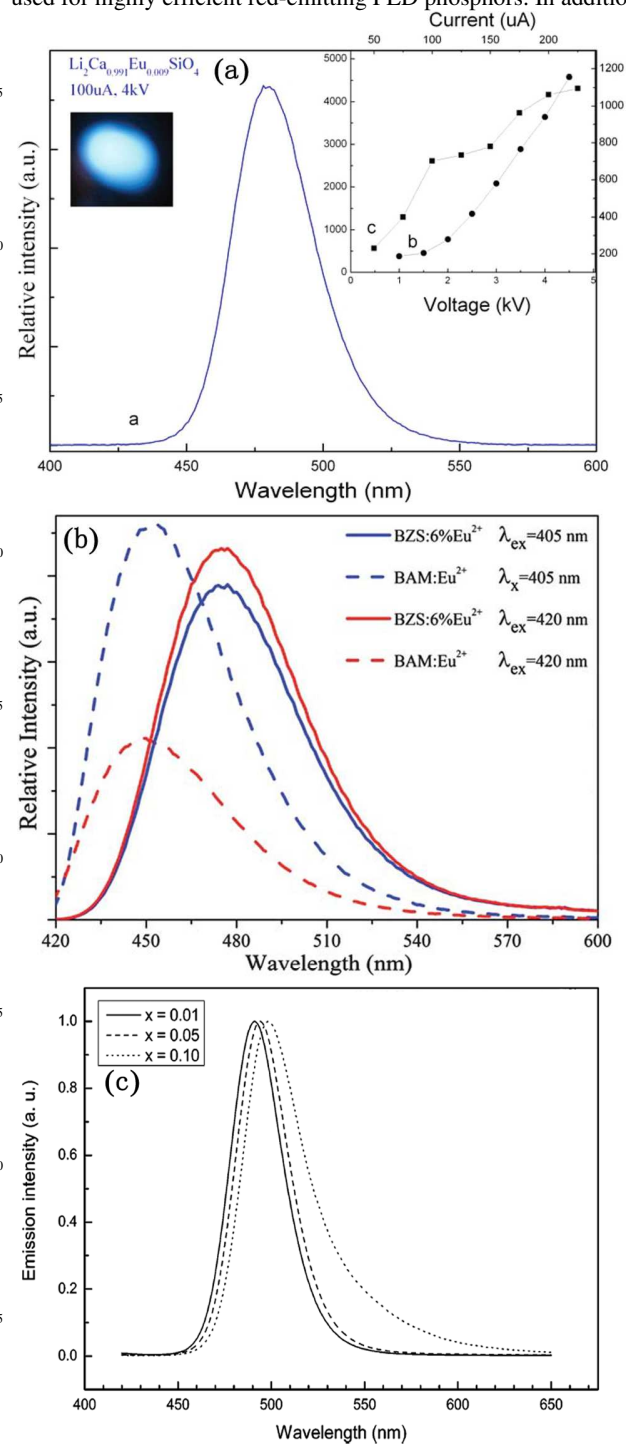


Fig. 17 (a) CL emission spectrum of $\text{Li}_2\text{CaSiO}_4:\text{Eu}^{2+}$. Left inset is the relevant luminescent photograph. Right inset is CL intensity as a function of accelerating voltages and filament currents. (b) PL spectra of $\text{BaZrSi}_3\text{O}_9:\text{Eu}^{2+}$ with that of $\text{BAM}:\text{Eu}^{2+}$ under 405 nm and 420 nm excitations. (c) Emission spectra of $\text{Ba}_{1-x}\text{Eu}_x\text{Si}_2\text{O}_2\text{N}_2$ with varying Eu^{2+} concentration ($\lambda_{\text{ex}} = 440$ nm).

(reproduced with the permission from refs. 232-234, copyright 2005 and 2011, American Chemical Society, Royal Society of Chemistry and The Electrochemical Society)

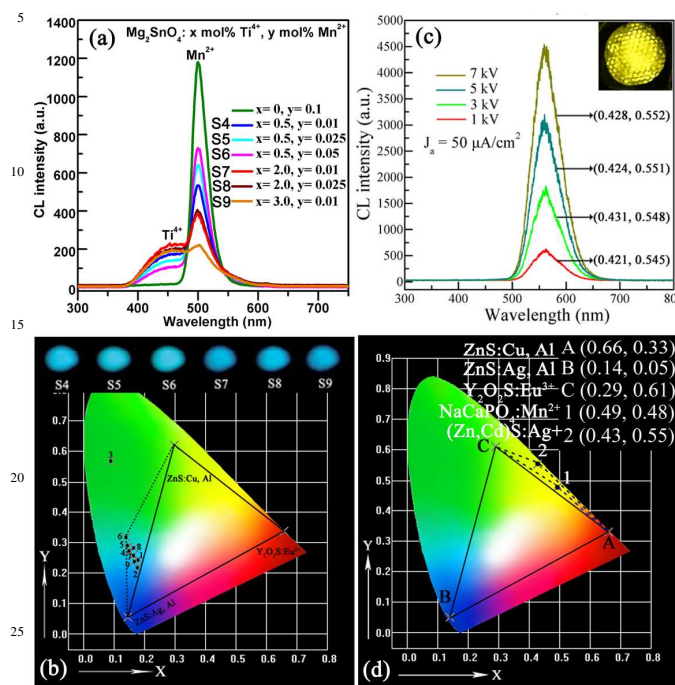


Fig. 18 The CL spectra of (a) $\text{Mg}_2\text{SnO}_4:x \text{ mol\% Ti}^{4+}, y \text{ mol\% Mn}^{2+}$ ($x = 0-3.0, y = 0.01-0.1$) and (c) $\text{NaCaPO}_4:3 \text{ mol\% Mn}^{2+}$ samples. The CIE chromaticity coordinates of (b) $\text{Mg}_2\text{SnO}_4:x \text{ mol\% Ti}^{4+}, y \text{ mol\% Mn}^{2+}$ ($x = 0-3.0, y = 0-0.1$) and (d) $\text{NaCaPO}_4:3 \text{ mol\% Mn}^{2+}$ samples. The triangle and quadrangle in (b) and (d) show the typical and enlarged color gamut for FED phosphors, respectively. The insets in (b) and (c) are cathodoluminescent photographs of $\text{Mg}_2\text{SnO}_4:x \text{ mol\% Ti}^{4+}, y \text{ mol\% Mn}^{2+}$ ($x = 0-3.0, y = 0-0.1$) and $\text{NaCaPO}_4:3 \text{ mol\% Mn}^{2+}$ samples, respectively. (reproduced with the permission from ref. 37 and 94, copyright 2011, Optical Society of America and Royal Society of Chemistry)

another promising red-emitting phosphors like $\text{Ca}_2\text{GeO}_4:\text{Eu}^{3+}$ and $\text{CaTiO}_3:\text{Pr}^{3+}$ also have potential application in FEDs due to high color purity (Table 2).^{156, 164, 229, 230} In general, these trichromatic phosphors have higher color purity than those of commercial RGB phosphors, resulting in potential applications in full-color FEDs. Developing phosphors with higher color purity than commercial RGB FED phosphors is also a feasible strategy to improve display quality.

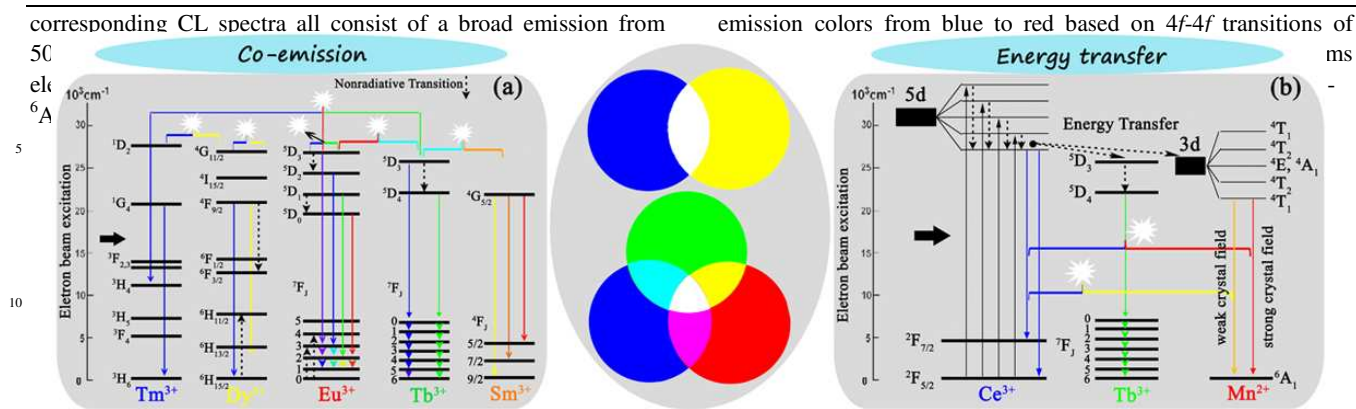
On the other hand, the colors observed by the human eye are those depicted in the whole 1931 Commission International de l'Eclairage (CIE) chromaticity diagram according to the colorimetry theory. At a four-color system, if four points are selected as red, yellow, green and blue (RYGB) or red, green, cyan and blue (RGCB), they would surround a larger color gamut than the three-color system.^{14, 17, 94} Therefore, these four-color systems will display more natural color than RGB system, and thus better meet people's individual requirements. Moreover, four-color system, has a higher "information density" (namely,

the pixels per unit area) compared with three-color system. Accordingly, the second strategy to enhance the display quality is to explore suitable four-color (RYGB) or (RGCB) systems phosphors such as cyan- or yellow-emitting phosphors. As

Table 3 The CIE chromaticity coordinates, emission colors of color-gamut enlarged phosphors under low voltage electron beam excitation.

| Sample | Color coordinates | Color | Refs |
|--|-------------------|--------|------|
| $\text{Mg}_{2(1-y)}\text{Sn}_{(1-x)}\text{O}_4: x\% \text{Ti}^{4+}, y\% \text{Mn}^{2+}$ | | | |
| $x = 0.5, y = 0.05$ | (0.1409, 0.3185) | | 37 |
| $x = 2.0, y = 0.01$ | (0.1637, 0.2574) | cyan | |
| $x = 2.0, y = 0.025$ | (0.1647, 0.2819) | | |
| $\text{Li}_2\text{CaSiO}_4:\text{Eu}^{2+}$ | (0.119, 0.203) | cyan | 232 |
| $\text{BaZrSi}_3\text{O}_9:\text{Eu}^{2+}$ | | cyan | 233 |
| $\text{BaSi}_2\text{O}_2\text{N}_2:\text{Eu}^{2+}$ | | cyan | 234 |
| $\text{NaCaPO}_4:\text{Mn}^{2+}$ | (0.428, 0.552) | yellow | 94 |
| $\text{LaGaO}_3:0.5\%\text{Sm}^{3+}$ | (0.4880, 0.4153) | yellow | 14 |
| ZnGeN_2 | | yellow | 17 |
| $\text{LaAlO}_3:0.25\%\text{Sm}^{3+}$ | (0.5133, 0.4625) | yellow | 111 |
| $\text{Ca}_2\text{Gd}_8(\text{SiO}_4)_6\text{O}_2:5\%\text{Ce}^{3+}, 10\%\text{Mn}^{2+}$ | (0.497, 0.401) | | |
| $\text{Ca}_2\text{Gd}_8(\text{SiO}_4)_6\text{O}_2:5\%\text{Ce}^{3+}, 18\%\text{Mn}^{2+}$ | (0.519, 0.414) | yellow | 231 |
| $\text{Ca}_2\text{Gd}_8(\text{SiO}_4)_6\text{O}_2:5\%\text{Ce}^{3+}, 25\%\text{Mn}^{2+}$ | (0.545, 0.415) | | |

mentioned in the previous section, the emission of Eu^{2+} ion can vary from ultraviolet to red light depends on the host lattice. Therefore, Eu^{2+} ion can obtain cyan emission by selecting suitable host. Xie and Wang et al. realized cyan emission of Eu^{2+} ions in $\text{Li}_2\text{CaSiO}_4:\text{Eu}^{2+}$ and $\text{BaZrSi}_3\text{O}_9:\text{Eu}^{2+}$ systems, respectively, as shown in Fig. 17 and Table 3. We can obviously observe that the CL emission intensities increase in direct proportion to voltage and current of anodes without saturation. The as-prepared $\text{BaZrSi}_3\text{O}_9:\text{Eu}^{2+}$ has comparable emission intensity than that of commercial blue phosphor (BAM) under the same excitation condition. Eu^{2+} -activated $\text{BaSi}_2\text{O}_2\text{N}_2$ can also be developed as cyan-emitting FED phosphor due to its excellent stability and high color purity (Fig. 17c and Table 3).^{234, 235} In addition, Li et al. designed a highly pure cyan light emission by mixing blue light (Ti^{4+}) and green light (Mn^{2+}) in $\text{Ti}^{4+}, \text{Mn}^{2+}$ -codoped Mg_2SnO_4 system, as shown in Fig. 18a and 18b. The as-prepared cyan-emitting phosphors have good stability under low voltage electron beam excitation. After continuous electron beam excitation for an hour, it still keeps 92% of its original intensity, with little change of their CIE chromaticity coordinates.³⁷ Therefore, it is promising phosphor for use in FED. Based on the second strategy, $\text{NaCaPO}_4:\text{Mn}^{2+}$ shows bright yellow emission under electron beam excitation with the CIE chromaticity coordinate (0.428, 0.552), which has a higher color purity than commercial yellow-emitting FED phosphor ($\text{Zn}, \text{CdS}:\text{Ag}^+$), as shown in the inset of Fig. 18c and 18d. The



Scheme 6 The schematic mechanisms of generation of white light via (a) co-emission (mono-/codoing RE³⁺ ions) and (b) energy transfer (from hosts or RE ions to RE ions or Mn²⁺ ions) in single-phase host. (c) A generation of white light through the complex of different colors, Blue-Yellow (BY) or Red-Green-Blue (RGB). Colored straight lines with arrows represent different luminescence. The horizontal braces with different colors represent different light emission and white stars represent white light by the complex of different light emission.

15

70

electron beam bombardment, its CIE chromaticity coordinates present a good stability. The luminance of NaCaPO₄: 3 mol% Mn²⁺ phosphor screen increase with increasing the accelerating voltage (V_a) and current density (J_a) and the luminance of 1510 cd/m² can be achieved when $V_a = 7$ kV and $J_a = 130$ $\mu\text{A}/\text{cm}^2$ (Fig. 17c). Moreover, there is no obvious saturation effect for the CL intensity of these phosphors with the increase of V_a and J_a . So the as-prepared NaCaPO₄: Mn²⁺ phosphors have potential to be used as yellow-emitting phosphor in four-color system (RGBY) FEDs due to its good color purity and stability. Other yellow-emitting LaGaO₃:Sm³⁺,¹⁴ ZnGeN₂,¹⁷ LaAlO₃:Sm³⁺,¹¹¹ and Ca₂Gd₃(SiO₄)₆O₂:Ce³⁺/Mn²⁺²³¹ also demonstrate excellent chromaticity coordinates and stability (Table 3), which are also potential RYGB system phosphors in FEDs devices. In general, the development of highly pure RGB phosphors and appropriate four-color system (cyan or yellow emitting phosphors) phosphors can efficiently enlarge color gamut and improve color saturation, and further to realize high-quality field emission display.

4.2 Design of white light emission

It is well known that excellent white light emission can supply excellent backlights in the display fields like LED, LCD, PDP and FED, which has a positive effect on display quality.^{7, 8} In recent years, there is an increasing focus on obtaining white light emission in single-phase host due to some potential advantages in luminous efficacy, chromatic stability, color-rendering index and cost against the mixing of two or three different phosphors.²³⁶⁻²³⁹ Many excellent and tunable white light emitting materials for FEDs can be obtained via designing co-emission (mono- or co-doping RE³⁺ ions) and energy transfer (from hosts or RE ions to RE ions or Mn²⁺ ions) in single-phase hosts. The basic guiding principle mainly involves in a complex of complementary luminescence such as blue and yellow light, red, green and blue light to obtain white light emission. A schematic illustration of generation of white light via co-emission and energy transfer in single-phase host is shown in Scheme 6. Due to abundant

doping Tm³⁺/Dy³⁺, Tb³⁺/Sm³⁺, Tb³⁺/Eu³⁺, Tm³⁺/Tb³⁺/Eu³⁺ ions etc., into single matrix (Scheme 6a). While white light emission in energy transfer systems mainly result from the Ce³⁺→Mn²⁺ (Blue-Yellow light complex) and Ce³⁺→Tb³⁺, Mn²⁺ (Red-Green-Blue light complex) energy transfers, as shown in Scheme 6b. The summary of luminescent properties for single-phase white-emitting phosphors via co-emission and energy transfer under low voltage electron beam excitation is shown in Table 4. It is noticed that the energy can also be transferred to the lower energy excited state among the RE ions, depending on the RE concentration, energy transfers rates and phonon energy. Moreover, the more energy transfer occur among the RE ions, the lower the luminescence efficiency. Therefore, it is important to optimize RE ions doping concentrations and select suitable hosts. The elaborate discussions are shown as follow.

(1) Singly doping RE³⁺ ions like Eu³⁺ or Dy³⁺ into appropriate single host.

The trivalent Eu³⁺ ion is well-known as a red-emitting activator due to its ⁵D₀₋₇F_J transitions (J = 0, 1, 2, 3, 4, usually ranging from 578 nm to 700 nm) based on 4f⁶ configuration with the most prominent ⁵D₀₋₇F₂ emission group around 610-625 nm.^{54, 70} Except for the main red emission, some other emission lines located in blue-green region from higher ⁵D levels, such as ⁵D₁ (green), ⁵D₂ (green, blue), and ⁵D₃ (blue) can also appear at the low phonon frequencies of the host lattices and the low doping concentration of Eu³⁺ (Scheme 6a). That is attributed to the avoidance of the multiphonon relaxation and cross relaxation occurring among the energy levels of Eu³⁺, respectively. If the phonon energy (highest vibration frequency, ν_{max}) of the host lattice is high enough to cause multiphonon relaxation, it will quench the higher-level ⁵D_{1,2,3} emission of Eu³⁺. Moreover, if the doping concentration of Eu³⁺ is high, the ⁵D_{1,2,3} emission might be quenched by cross-relaxation between two neighboring Eu³⁺ ions, such as Eu³⁺ (⁵D₁) + Eu³⁺ (⁷F₀) → Eu³⁺ (⁵D₀) + Eu³⁺ (⁷F₃) and Eu³⁺ (⁵D₃) + Eu³⁺ (⁷F₀) → Eu³⁺ (⁵D₂) + Eu³⁺ (⁷F₄) (Scheme 5a). So whether the emission can occur from higher excited states ⁵D₁, ⁵D₂, and ⁵D₃ or not for Eu³⁺ ion depends critically upon the

highest vibration frequencies (ν_{\max}) available in the host lattice and the doping concentration of Eu^{3+} . In other words, an appropriate selection of the host lattice and doping concentration of Eu^{3+} is possible to yield simultaneously the red emission from ${}^5\text{D}_0$ energy level and the blue and green emissions from the higher ${}^5\text{D}_{1,2,3}$ energy levels of Eu^{3+} with comparable intensity, thus generating a white light emission from Eu^{3+} -monodoped materials. It has been proposed by Blasse and Grabmaier that the radiative rate is approximately equal to the nonradiative rate if the energy gap in the nonradiative transition amounts to 4–5 times the maximum phonon frequency of the host lattices.³¹ For Eu^{3+} -doped CaIn_2O_4 , the ν_{\max} of CaIn_2O_4 is determined to be 475 cm^{-1} , whereas the energy gaps for ${}^5\text{D}_1 \rightarrow {}^5\text{D}_0$, ${}^5\text{D}_2 \rightarrow {}^5\text{D}_1$, and ${}^5\text{D}_3 \rightarrow {}^5\text{D}_2$ of Eu^{3+} are 1571, 2563, and 2948 cm^{-1} , respectively.⁵⁴ Thus, the ν_{\max} of CaIn_2O_4 is low enough and the numbers of phonons

chromaticity coordinates $x = 0.3019$ and $y = 0.3291$. (reproduced with the permission from refs. 54, 70, 72, copyright 2007, The Electrochemical Society, American Institute of Physics and American Chemical Society)

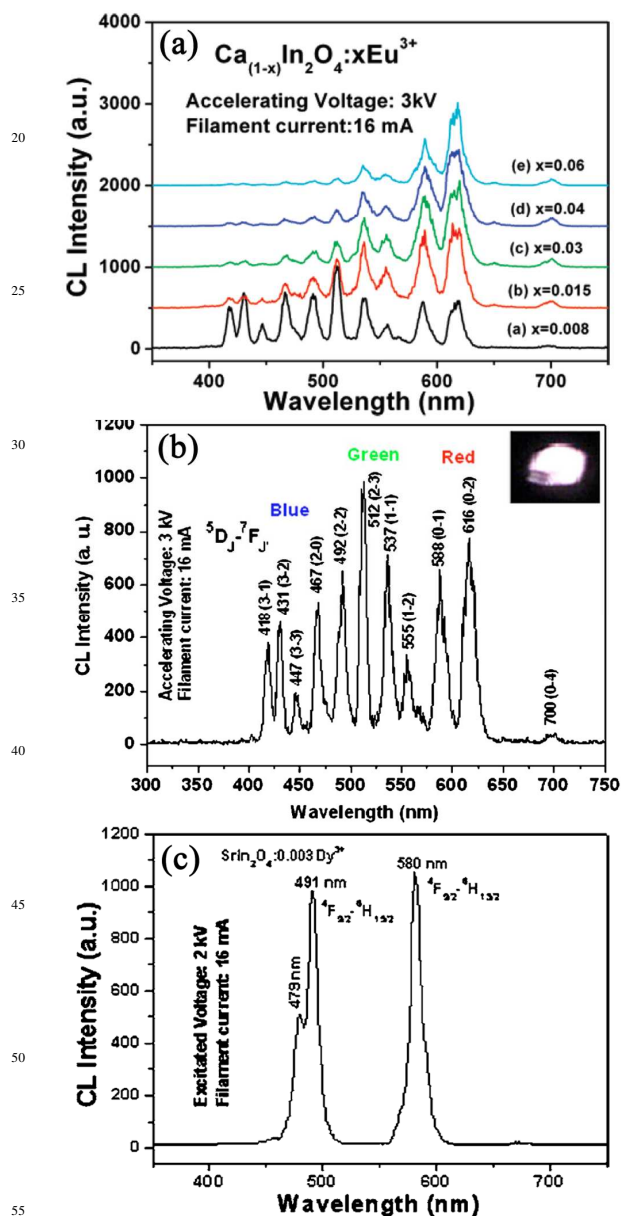


Fig. 19 Emission spectrum of (a) $\text{CaIn}_2\text{O}_4:\text{xEu}^{3+}$ ($x = 0.008-0.06$) and (b) $\text{CaIn}_2\text{O}_4:0.01\text{Eu}^{3+}$ under the excitation of electron beam. The inset shows luminescent photograph with white light emission. (c) Typical cathodoluminescence spectra of $\text{SrIn}_2\text{O}_4:0.003\text{Dy}^{3+}$ with CIE

needed to bridge these neighboring excited levels are 4 (${}^5\text{D}_1 \rightarrow {}^5\text{D}_0$), 5 (${}^5\text{D}_2 \rightarrow {}^5\text{D}_1$), and 6 (${}^5\text{D}_3 \rightarrow {}^5\text{D}_2$), respectively. So it is reasonable that all of the emissions from higher energy levels ${}^5\text{D}_{1-3}$ of Eu^{3+} are present, apart from the lowest ${}^5\text{D}_0$ excited state in CaIn_2O_4 host lattice. Under low voltage electron beam excitation, the emission spectra of $\text{CaIn}_2\text{O}_4:\text{xEu}^{3+}$ consists of all the emission lines from the ${}^5\text{D}_{0,1,2,3}$ excited states to the ${}^7\text{F}_j$ ground states of Eu^{3+} , i.e., ${}^5\text{D}_3-{}^7\text{F}_1$ (418 nm), ${}^5\text{D}_3-{}^7\text{F}_2$ (431 nm), ${}^5\text{D}_3-{}^7\text{F}_3$ (447 nm), ${}^5\text{D}_2-{}^7\text{F}_0$ (467 nm), ${}^5\text{D}_2-{}^7\text{F}_2$ (492 nm), ${}^5\text{D}_2-{}^7\text{F}_3$ (512 nm), ${}^5\text{D}_1-{}^7\text{F}_1$ (537 nm), ${}^5\text{D}_1-{}^7\text{F}_2$ (555 nm), ${}^5\text{D}_0-{}^7\text{F}_1$ (588 nm), ${}^5\text{D}_0-{}^7\text{F}_2$ (616 nm), and ${}^5\text{D}_0-{}^7\text{F}_4$ (700 nm), as shown in Fig. 19a. These emission lines of Eu^{3+} cover the whole visible spectral region and the relative intensities vary with the doping concentration of Eu^{3+} based on the cross relaxation effects. At appropriate Eu^{3+} -doping concentration at $x = 0.01$, the above emission lines of $\text{CaIn}_2\text{O}_4:\text{xEu}^{3+}$ have comparable intensities and give a brilliant white light emission (Fig. 19b). Moreover, tunable white light emission can be obtained by precisely controlling the doping concentration of Eu^{3+} ions, as shown in Table 4. According to the same approach, $\text{LaInO}_3:\text{Eu}^{3+}$, $\text{LaOF}:\text{Eu}^{3+}$ and $\beta\text{-NaYF}_4:\text{Eu}^{3+}$ have been developed as single-phase white light emitting cathodoluminescent materials (Table 4).^{122, 167, 240}

It is known that the emission spectrum of Dy^{3+} can be mainly separated into two groups, the blue emission from 460 to 505 nm and the yellow emission from 570 to 600 nm accompanied by a group of weak lines in the red region from 650 to 700 nm based in its $4f^9$ configuration. These emissions correspond to the transitions from ${}^4\text{F}_{9/2}$ to ${}^6\text{H}_{15/2}$, ${}^6\text{H}_{13/2}$ and ${}^6\text{H}_{11/2}$ of Dy^{3+} (Scheme 6a), respectively.⁸⁶ The yellow-emitting ${}^4\text{F}_{9/2}-{}^6\text{H}_{13/2}$ transition is hypersensitive transition, which is susceptible to the crystal environment. However, the blue emission is basically invariant with the surrounding environment. In composite oxides, the covalency between Dy^{3+} and O^{2-} has an important effect on the ratio of yellow to blue emission. Generally, the bigger covalency, the stronger yellow emission of Dy^{3+} ion will be achieved. Moreover, the covalency of $\text{Dy}^{3+}-\text{O}^{2-}$ is different in different host matrix due to the local variation of the symmetry and coordination environment of crystal structure. Therefore, the ratio of yellow to blue emission can be adjusted by doping into different host lattice, resulting in a possible to obtain white-light emission in Dy^{3+} -monodoped luminescence material. For example, for $\text{SrIn}_2\text{O}_4:0.015\text{Dy}^{3+}$ phosphor, its CL spectrum (Fig. 19c) is made up of the characteristic emission lines of Dy^{3+} , i.e., ${}^4\text{F}_{9/2}-{}^6\text{H}_{15/2}$, 491 nm and ${}^4\text{F}_{9/2}-{}^6\text{H}_{15/2}$, 580 nm. It has a suitable yellow-to-blue intensity ratio, and thus appear a white emission of Dy^{3+} in SrIn_2O_4 with CIE chromaticity coordinates $x = 0.3019$ and $y = 0.3291$. The Dy^{3+} -doped CaIn_2O_4 , LaGaO_3 and Ga_2O_3 are also considered as excellent single-phase white emitting FEDs phosphors with tunable chromaticity coordinates in white light region, as shown in Table 4. Moreover, an enhanced cathodoluminescent performance is observed by host sensitization effect in the above mentioned Dy^{3+} -doped phosphors.

(2) Co-doping different RE³⁺ ions such as Tm³⁺/Dy³⁺, Tb³⁺/Sm³⁺, Tb³⁺/Eu³⁺, Tm³⁺/Tb³⁺/Eu³⁺ etc., into single matrix. such as Tm³⁺, Dy³⁺, Tb³⁺, Sm³⁺, Eu³⁺ ions, they produce various luminescence colors covering the whole visible light region.³¹

Due to the abundant energy levels in 4f orbits of RE³⁺ ions

Table 4 Summary of luminescent properties for single-phase white-emitting phosphors via co-emission and energy transfer systems under low voltage electron beam excitation.

| Phosphor | Emission peaks (nm)/Transitions/Colors | CIE (x, y) | Refs. |
|---|---|----------------|-------|
| Monodoping Eu ³⁺ or Dy ³⁺ systems | | | |
| CaIn ₂ O ₄ : 0.5%Eu ³⁺ | all the emissions from Eu ³⁺ : ⁵ D _J – ⁷ F _J : | (0.290, 0.310) | 54 |
| CaIn ₂ O ₄ : 1%Eu ³⁺ | ⁵ D ₀ – ⁷ F _J , orange-red; ⁵ D ₁ – ⁷ F _J , green | (0.324, 0.323) | |
| CaIn ₂ O ₄ : 1.5%Eu ³⁺ | ⁵ D ₂ – ⁷ F _J , green-blue; ⁵ D ₃ – ⁷ F _J , blue | (0.358, 0.345) | |
| LaInO ₃ : 0.5%Eu ³⁺ | (J = 0, 1, 2, 3; J' = 0, 1, 2, 3, 4) | (0.369, 0.404) | 167 |
| LaOF: 0.2%Eu ³⁺ | | (0.291, 0.340) | 123 |
| CaIn ₂ O ₄ : 1.5%Dy ³⁺ | 493, 582/ ⁴ F _{9/2} to ⁶ H _{15/2} , blue; ⁶ H _{13/2} , yellow | (0.226, 0.250) | 71 |
| SrIn ₂ O ₄ : 1.5%Dy ³⁺ | 491, 580/ ⁴ F _{9/2} to ⁶ H _{15/2} , blue; ⁶ H _{13/2} , yellow | (0.302, 0.329) | 72 |
| LaGaO ₃ : 1.5%Dy ³⁺ | 480, 572/ ⁴ F _{9/2} to ⁶ H _{15/2} , blue; ⁶ H _{13/2} , yellow | (0.343, 0.392) | 113 |
| Ga ₂ O ₃ : 3%Dy ³⁺ | 492, 580/ ⁴ F _{9/2} to ⁶ H _{15/2} , blue; ⁶ H _{13/2} , yellow | (0.299, 0.333) | 66 |
| Co-doping Tm ³⁺ /Dy ³⁺ , Tb ³⁺ /Sm ³⁺ , Tb ³⁺ /Eu ³⁺ , Tm ³⁺ /Tb ³⁺ /Eu ³⁺ systems | | | |
| LaOCl: Tm ³⁺ , Dy ³⁺ | 458/ ¹ D ₂ – ³ F ₄ (Tm ³⁺), blue; | (0.318, 0.329) | 86 |
| | 480, 571/ ⁴ F _{9/2} to ⁶ H _{15/2} , ⁶ H _{13/2} (Dy ³⁺), yellow | | |
| LaOCl: Tb ³⁺ , Sm ³⁺ | 384, 417, 438, 486, 543/ ³ D _{3,4} – ⁷ F _{6,2} (Tb ³⁺), bluish green; | (0.341, 0.321) | 92 |
| | 565, 607, 650/ ⁶ G _{5/2} – ⁶ H _{5/2, 7/2, 9/2} (Sm ³⁺), orange | | |
| LaGaO ₃ : Tb ³⁺ , Sm ³⁺ | 414, 437/ ³ D _{3,4} – ⁷ F _{5,4} ; 414, 437/ ³ D ₄ – ⁷ F ₅ (Tb ³⁺), bluish green | (0.341, 0.334) | 14 |
| | 561, 597, 642/ ⁶ G _{5/2} – ⁶ H _{5/2} , ⁶ H _{7/2} , ⁶ H _{9/2} (Sm ³⁺), yellow | | |
| LaOCl: Tb ³⁺ , Eu ³⁺ | 416, 438, 543, 486/ ³ D _{3,4} – ⁷ F _{6,4} (Tb ³⁺), bluish green; | (0.354, 0.344) | 15 |
| | 577, 594, 615/ ⁵ D ₀ – ⁷ F _{0,1,2} (Eu ³⁺), red; | | |
| LaOCl: Tb ³⁺ , Eu ³⁺ , Tm ³⁺ | 416, 438, 543, 486/ ³ D _{3,4} – ⁷ F _{6,4} (Tb ³⁺), bluish green; | (0.291, 0.312) | 15 |
| | 577, 594, 615/ ⁵ D ₀ – ⁷ F _{0,1,2} (Eu ³⁺), red; | | |
| | 458/ ¹ D ₂ – ³ F ₄ (Tm ³⁺), blue | | |
| Ce ³⁺ → Mn ²⁺ , Eu ²⁺ → Mn ²⁺ and Ce ³⁺ → Tb ³⁺ , Mn ²⁺ energy transfer systems | | | |
| Mg ₂ Y ₈ (SiO ₄) ₆ O ₂ :Ce ³⁺ , Mn ²⁺ , Tb ³⁺ | 425, 455/ ⁵ d ¹ – ⁴ f ¹ (Ce ³⁺) blue; 613/ ⁴ T ₁ – ⁶ A ₁ (Mn ²⁺) red; 544/ ⁵ D ₄ – ⁷ F ₅ (Tb ³⁺), green | (0.332, 0.337) | 229 |
| Ca ₄ Y ₆ (SiO ₄) ₆ O:Ce ³⁺ , Mn ²⁺ , Tb ³⁺ | 423/ ⁵ d ¹ – ⁴ f ¹ (Ce ³⁺) blue; 614/ ⁴ T ₁ – ⁶ A ₁ (Mn ²⁺) red; 543/ ⁵ D ₄ – ⁷ F ₅ (Tb ³⁺), green | (0.328, 0.331) | 230 |
| Ca ₅ (PO ₄) ₂ SiO ₄ :Ce ³⁺ , Mn ²⁺ , Tb ³⁺ | 416/ ⁵ d ¹ – ⁴ f ¹ (Ce ³⁺) blue; 618/ ⁴ T ₁ – ⁶ A ₁ (Mn ²⁺) red; 544/ ⁵ D ₄ – ⁷ F ₅ (Tb ³⁺), green | (0.331, 0.343) | 259 |
| Ca ₉ MgNa(PO ₄) ₇ :Ce ³⁺ , Mn ²⁺ , Tb ³⁺ | 376/ ⁵ d ¹ – ⁴ f ¹ (Ce ³⁺) blue; 625/ ⁴ T ₁ – ⁶ A ₁ (Mn ²⁺) red; 547/ ⁵ D ₄ – ⁷ F ₅ (Tb ³⁺), green | (0.319, 0.327) | 260 |
| Ca ₂ Ca ₈ (SiO ₄) ₆ O ₂ :Ce ³⁺ , Mn ²⁺ | 403, 428/ ⁵ d ¹ – ⁴ f ¹ (Ce ³⁺) blue; 590/ ⁴ T ₁ – ⁶ A ₁ (Mn ²⁺) yellow | (0.342, 0.318) | 231 |
| Ca ₃ Gd ₇ (PO ₄) ₃ (SiO ₄) ₂ O ₂ :Ce ³⁺ , Mn ²⁺ | 400/ ⁵ d ¹ – ⁴ f ¹ (Ce ³⁺) blue; 575/ ⁴ T ₁ – ⁶ A ₁ (Mn ²⁺) red | (0.322, 0.326) | 261 |
| Sr ₃ In(PO ₄) ₃ :Ce ³⁺ , Mn ²⁺ | 375/ ⁵ d ¹ – ⁴ f ¹ (Ce ³⁺) blue; 568/ ⁴ T ₁ – ⁶ A ₁ (Mn ²⁺) yellow | (0.331, 0.319) | 262 |
| Ca ₃ Sc ₂ Si ₃ O ₁₂ :Ce ³⁺ , Mn ²⁺ | 450, 505/ ⁵ d ¹ – ⁴ f ¹ (Ce ³⁺) blue to green; 574, 680/ ⁴ T ₁ – ⁶ A ₁ (Mn ²⁺) red | | 263 |
| Ca ₄ Si ₂ O ₇ F ₂ :Eu ²⁺ , Mn ²⁺ | 463/ ⁵ d ¹ – ⁴ f ¹ (Eu ²⁺) blue to green; 576/ ⁴ T ₁ – ⁶ A ₁ (Mn ²⁺) orange-red | (0.351, 0.332) | 264 |
| Ca ₉ Y(PO ₄) ₇ :Eu ²⁺ , Mn ²⁺ | 486/ ⁵ d ¹ – ⁴ f ¹ (Eu ²⁺) blue to green; 638/ ⁴ T ₁ – ⁶ A ₁ (Mn ²⁺) red | (0.310, 0.330) | 265 |
| Ca ₉ Gd(PO ₄) ₇ :Eu ²⁺ , Mn ²⁺ | 494/ ⁵ d ¹ – ⁴ f ¹ (Eu ²⁺) blue to green; 652/ ⁴ T ₁ – ⁶ A ₁ (Mn ²⁺) red | (0.326, 0.328) | 266 |
| Na _{0.34} Ca _{0.66} Al _{1.66} Si _{2.34} O ₈ :Eu ²⁺ , Mn ²⁺ | 440/ ⁵ d ¹ – ⁴ f ¹ (Eu ²⁺) blue to green; 570/ ⁴ T ₁ – ⁶ A ₁ (Mn ²⁺) yellow | (0.333, 0.317) | 267 |
| BaMg ₂ Al ₆ Si ₉ O ₃₀ :Eu ²⁺ , Mn ²⁺ , Tb ³⁺ | 376, 450/ ⁵ d ¹ – ⁴ f ¹ (Eu ²⁺) blue to green; 610/ ⁴ T ₁ – ⁶ A ₁ (Mn ²⁺) red; 545/ ⁵ D ₄ – ⁷ F ₅ (Tb ³⁺) green | (0.310, 0.330) | 268 |

Tm³⁺ ion mainly emits blue light around 458 nm due to ¹D₂ – ³F₄ transition. Dy³⁺ ion usually exhibits two main emissions in the visible region: one in the blue region (470–500 nm) and one in the yellow region (570–600 nm), which originate from ⁴F_{9/2} → ⁶H_{13/2} and ⁴F_{9/2} → ⁶H_{15/2} transitions of Dy³⁺ ions, respectively. The emission of Eu³⁺ ion mainly appears in red region with the maximum between 610 nm and 625 nm due to ⁵D₀ – ⁷F₂ emission. The emission of Sm³⁺ is situated in the orange spectral region and consists of transitions from the excited ⁴G_{5/2} level to the ground state ⁶H_{5/2} and higher levels ⁶H_J (J > 5/2). Tb³⁺ ion has a low-energy ground state ⁷F_J (J = 6, ...0) and excited states ⁵D₃ and ⁵D₄. Generally, with a low doping concentration of Tb³⁺ in host matrix, the transitions of ⁵D₃ to ⁷F_J dominate and produce the blue emissions. As Tb³⁺ concentration increases, the cross relaxation from ⁵D₃ to ⁵D₄ occurs owing to the interaction

between Tb³⁺ ions, which enhances the transitions of ⁵D₄ to ⁷F_J with a green emission. Although these RE³⁺ ions generally are used as single activator in single host, they also generate highly

efficient luminescence when coexisting in single matrix. Accordingly, many RE³⁺ ions co-doped single-phase phosphor systems were designed to realize white light emission, for examples, Tm³⁺/Dy³⁺, Tb³⁺/Sm³⁺, Tb³⁺/Eu³⁺, Tm³⁺/Tb³⁺/Eu³⁺ systems, as shown in Table 4. Fig. 20 exhibits the CL spectra and corresponding luminescent photographs of codoping phosphor systems. Under electron beam excitation, LaOCl:Tm³⁺ and LaOCl:Dy³⁺ emit blue light (458 nm, ¹D₂ – ³F₄) and yellow light (571 nm, ⁴F_{9/2} – ⁶H_{13/2}), respectively. When codoping Tm³⁺ and Dy³⁺ ions into LaOCl host, it simultaneously gives blue and yellow emission with comparable, which results in a white light emission (CIE coordinates, x = 0.318, y = 0.329) by the complex

of blue and yellow lights (Fig. 20a and Table 4). For Tb³⁺/Sm³⁺-codoped LaGaO₃, the white emission is realized by the complex of red, green and blue components. The red component comes from the characteristic transitions of Sm³⁺ (561, 597, 642 nm⁴G_{5/2}-⁶H_{5/2}, ⁶H_{7/2}, ⁶H_{9/2}), while the green and blue components result from the mixing emissions of 414, 437 nm⁵D₃-⁷F_{5,4}; 414,

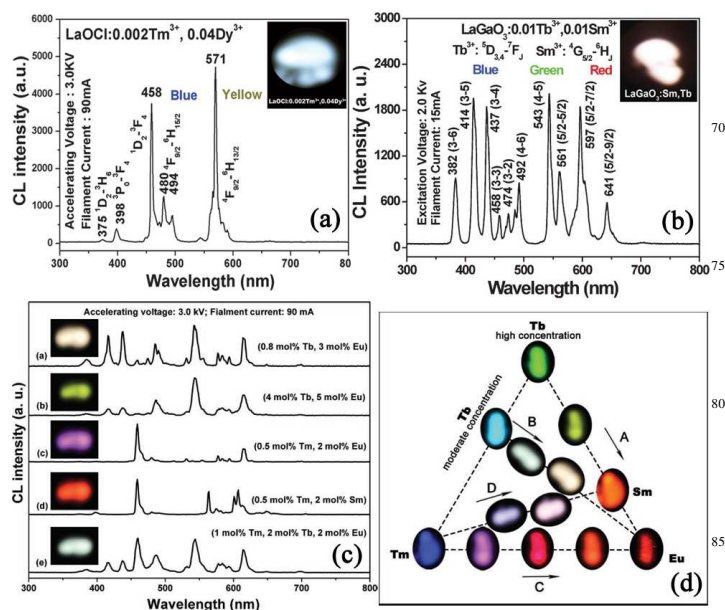


Fig. 20 The CL spectra and corresponding luminescence photographs of RE³⁺ co-doped phosphor systems. (a) LaOCl: Tm³⁺, Dy³⁺, (b) LaGaO₃: Tb³⁺, Sm³⁺, (c) LaOCl: Tb³⁺, Eu³⁺ and LaOCl: Tb³⁺, Eu³⁺, Tm³⁺. (d) The cathodoluminescent colors of LaOCl: Tb³⁺, Eu³⁺, Tm³⁺ phosphor systems. Arrow A, B, C and D represent the co-doping of Eu/Tb (high Tb³⁺ concentration), Eu/Tb (moderate Tb³⁺ concentration), Eu/Tm and Tm/Sm in the LaOCl host, respectively. (reproduced with the permission from refs. 14, 15 and 86, copyright 2008, 2009, 2010, Wiley and Royal Society of Chemistry)

437 nm⁵D₄-⁷F₅ at a moderate Tb³⁺ doping concentration (Fig. 20b and Table 4). Based on the same complex method, LaOCl:Tb³⁺/Eu³⁺, LaOCl:Tb³⁺/Sm³⁺, LaOCl:Tb³⁺/Eu³⁺/Tm³⁺ phosphor system also obtained excellent white light emission (Fig. 20c and Table 4). Fig. 20d intuitively shows the adjustment of emission colors in LaOCl:Tb³⁺/Eu³⁺/Tm³⁺ systems via precisely controlling the doping contents of RE³⁺ ions. Consequently, the CIE chromaticity coordinates and luminescent efficiencies of white light emission in co-doped systems can be optimized through appropriate selection of various RE³⁺-doping contents. These advantages make RE³⁺-codoped single-phase white light emission have potential application as backlights in FEDs devices.

(3) Designing energy transfers from host or RE ions to RE ions or Mn²⁺ ions to in single host.

It is well-known that energy transfer plays an important role in the optical properties of luminescent materials both from theoretical and practical points of view, because it can not only enhance the luminescent efficiency but also tune the luminescent color in the single-phase host.²⁴¹ The Ce³⁺ with the 4f¹

configuration in solids shows efficient broad band luminescence due to the 4f-5d parity allowed electric dipole transition.²⁴² The Ce³⁺ ion has a larger Stokes shift than those of the other rare earth ions, because of the extended radial wave functions of the 5d state. Furthermore, the Ce³⁺ ion can also act as an efficient sensitizer by transferring a better part of its excitation energy to 65 coactivators.²⁴³ The transition metal ion Mn²⁺ can give a broad

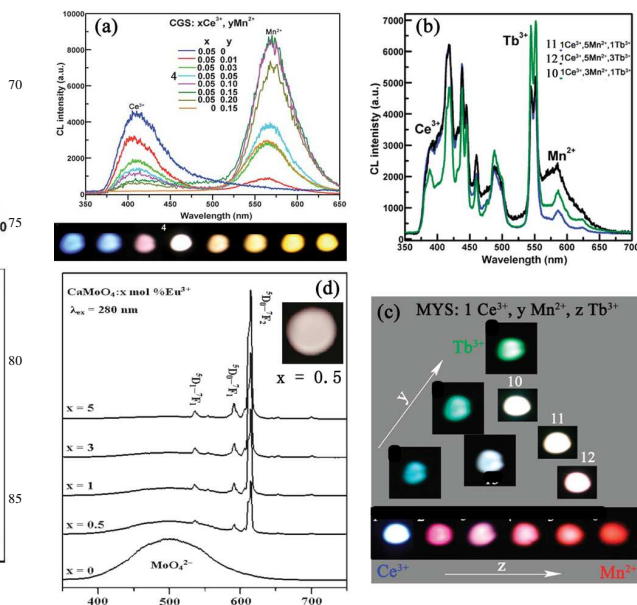


Fig. 21 The CL spectra and corresponding luminescence photographs of energy transfer phosphor systems: (a) Ca₂Ca₈(SiO₄)₆O₂:Ce³⁺, Mn²⁺ (b) Mg₂Y₈(SiO₄)₆O₂:Ce³⁺, Mn²⁺, Tb³⁺. (c) The cathodoluminescent photographs of Mg₂Y₈(SiO₄)₆O₂:Ce³⁺, Mn²⁺, Tb³⁺ with different Ce³⁺, Mn²⁺, Tb³⁺-doping concentrations. (d) The emission spectra of CaMoO₄: x mol% Eu³⁺ with the x values. Arrow A, B, C and D represent the co-doping of Eu/Tb (high Tb³⁺ concentration), Eu/Tb (moderate Tb³⁺ concentration), Eu/Tm and Tm/Sm in the LaOCl host, respectively. (reproduced with the permission from refs. 144, 229 and 231, copyright 2009, 2011, American Chemical Society and Royal Society of Chemistry)

band emission in the visible range owing to the d-d transition, and the emission color of Mn²⁺ can vary from green to red depending on the crystal field.³² Because the d-d transition of Mn²⁺ is forbidden and difficult to pump, the emission of Mn²⁺ ions is generally excited by energy transfer from the host or the sensitizer. Caldiño et al. reported the spectral overlap between 5d¹→4f¹ Ce³⁺ emission and ⁶A₁→⁴T₂ Mn²⁺ absorption.²⁴⁴ So far, the Ce³⁺→Mn²⁺ energy transfers have been reported in many inorganic hosts, such as fluorides,^{245, 246} phosphates,²⁴⁷ and borates,²⁴⁸ and the corresponding mechanisms have been extensively investigated. In these systems, there is a common feature that Ce³⁺ and Mn²⁺ ions simultaneously substitute one or two lattice sites and the Ce³⁺ ions serve as effective sensitizer ions for Mn²⁺, transferring the energy from the 5D level of the Ce³⁺ to the 4G level of the Mn²⁺ by a process of resonance transfer via a spin exchange mechanism, which not only help Mn²⁺ ions to emit efficiently but also tune their emission colors from blue to yellow or orange/red, acrossing the whole white light region, as shown Scheme 5b and Table 4. Generally, there are main two aspects responsible for the resonant energy-transfer mechanism: one is exchange interaction and the other is

multipolar interaction.²⁴⁹ It is known that if energy transfer results from the exchange interaction, the critical distance between the sensitizer and activator should be shorter than 4 Å.²⁵⁰ The critical distance R_C for energy transfer from the Ce^{3+} to Mn^{2+} ions can firstly be calculated using the concentration quenching method. According to Blasse,²⁵¹ the critical distance R_C can be expressed by

$$R_C \approx 2 \left[\frac{3V}{4\pi X_C N} \right]^{1/3} \quad (2)$$

where N is the number of available sites for the dopant in the unit cell, X is the total concentration of Ce^{3+} and Mn^{2+} , and V is the volume of the unit cell. The radiative emission from Ce^{3+} prevails when $R_{Ce-Mn} > R_C$ and energy transfer from Ce^{3+} to Mn^{2+} dominates when $R_{Ce-Mn} < R_C$. If the R_C value is much longer than 4 Å, it indicates little possibility of energy transfer via the exchange interaction mechanism. Thus, the energy transfer between the Ce^{3+} and Mn^{2+} ions mainly takes place via electric multipolar interactions. On the basis of Dexter's energy-transfer expressions of multipolar interaction and Reisfeld's approximation, the following relation can be given:^{247, 249, 252}

$$\frac{\eta_{S0}}{\eta_S} \propto C^{n/3} \quad (3)$$

where η_{S0} and η_S are the luminescence quantum efficiency of Ce^{3+} in the absence and presence of Mn^{2+} ; C is the sum of the content of Ce^{3+} and Mn^{2+} . The η_0/η can be approximately calculated by the ratio of related luminescence intensities as^{253, 254}

$$\frac{I_{S0}}{I_S} \propto C^{n/3} \quad (4)$$

The n value can be obtained by observing the linear relationship of $I_{S0}/I_S - C^{n/3}$ plots and $n = 6, 8,$ and 10 corresponds to dipole-dipole, dipole-quadrupole, and quadrupole-quadrupole interactions, respectively. Under normal conditions, energy transfer from Ce^{3+} to Mn^{2+} is through the dipole-quadrupole interaction in most of the host materials.²³⁶ The energy transfer probability P_{SA} (in s^{-1}) from Ce^{3+} to Mn^{2+} for dipole-quadrupole interaction is given by the following formula:²⁵⁵

$$P_{Eu-Mn}^{DQ} = 3.024 \times 10^{12} \frac{\lambda_s^2 f_q}{R^8 \tau_s} \int \frac{F_S(E) F_A(E) dE}{E^4} \quad (5)$$

where f_q is the oscillator strength of the involved absorption transition of the acceptor (Mn^{2+}), λ_s (in Å) is the wavelength position of the sensitizer's (Ce^{3+}) emission, τ_s is the radiative decay time of the sensitizer (in seconds), R is the sensitizer-acceptor average distance (in Å), E is the energy involved in the transfer (in eV), and $\int F_S(E) F_A(E) / E^4 dE$ represents the spectral overlap between the normalized shapes of the Ce^{3+} emission $F_S(E)$ and the Mn^{2+} excitation $F_A(E)$. The critical distance (R_C) of energy transfer from the Ce^{3+} to Mn^{2+} is further defined as the distance for which the probability of transfer equals the probability of radiative emission of donor, the distance for which $P^{DQ} \tau_s = 1$. Hence, R_C can be obtained from eqn 1 as²⁵⁶

$$R_C^8 = 3.024 \times 10^{12} \lambda_s^2 f_q \int \frac{F_S(E) F_A(E) dE}{E^4} \quad (6)$$

The oscillator strength of the Mn^{2+} electric quadrupole transition (f_q) is about 10^{-10} . So the critical distance R_C of energy transfer can be calculated by the spectra overlap method. If this result is in good agreement with that obtained using the concentration quenching method, which further reveals that the mechanism of

energy transfer from the Ce^{3+} to Mn^{2+} ions is mainly due to a dipole-quadrupole interaction. On the other hand, the trivalent Tb^{3+} are generally used as an green emitting activator, whose emission is mainly due to transitions of ${}^5D_3 \rightarrow {}^7F_J$ in the blue region and ${}^5D_4 \rightarrow {}^7F_J$ in the green region ($J = 6, 5, 4, 3, 2$) depending on its doping concentration.^{19, 20} Ce^{3+} ion can also efficiently transfer energy to Tb^{3+} ions in single host, and the $Ce^{3+} \rightarrow Tb^{3+}$ energy transfer has been extensively reported.^{257, 258} Furthermore, a single-phase white-light-emitting phosphor utilizing energy transfer can avoid the reabsorption for blue or UV light by the red-/green emitting phosphors and the mixing of RGB phosphors. Consequently, it can enhance the luminescence efficiency and color reproducibility of the white light source and reduce manufacturing costs. Some research groups have demonstrated the above situation in many Ce^{3+} - Mn^{2+} (blue-yellow) or Ce^{3+} - Mn^{2+} - Tb^{3+} (blue-red-green) codoped systems such as $Mg_2Y_8(SiO_4)_6O_2$,²²⁹ $Ca_4Y_6(SiO_4)_6O$,²³⁰ $Ca_2Ca_8(SiO_4)_6O_2$,²³¹ $Ca_5(PO_4)_2SiO_4$,²⁵⁹ $Ca_9MgNa(PO_4)_7$,²⁶⁰ $Ca_3Gd_7(PO_4)(SiO_4)_5O_2$,²⁶¹ $Sr_3In(PO_4)_3$,²⁶² $Ca_3Sc_2Si_3O_{12}:Ce^{3+}, Mn^{2+}$ ²⁶³ and so on (Table 4). For example, there is an efficient energy transfer from Ce^{3+} to Mn^{2+} in $Ca_2Ca_8(SiO_4)_6O_2:Ce^{3+}, Mn^{2+}$ phosphor, and the energy transfer mechanism of $Ce^{3+} \rightarrow Mn^{2+}$ pair is dominated by an electric dipole-dipole interaction. This phosphor simultaneously emits blue light of Ce^{3+} ions (428 nm) and yellow light of Mn^{2+} ions (490 nm) (Fig. 21a), respectively. By changing the relative doping concentration of Ce^{3+} and Mn^{2+} , the ratio of blue to yellow is controllable and thus obtains an excellent white light emission (Fig. 21a) with CIE coordinates (0.342, 0.318). For Ce^{3+} - Mn^{2+} - Tb^{3+} -codoped systems, there simultaneously exist two energy transfer processes of $Ce^{3+} \rightarrow Mn^{2+}$ and $Ce^{3+} \rightarrow Tb^{3+}$, which emit red light and green light, respectively (Fig. 21b). Because these energy transfer processes can be controlled via tuning the relative doping concentrations of Ce^{3+} , Tb^{3+} and Mn^{2+} ions. Therefore, the relative emission intensities of blue, green and red light can be adjusted in single-phase phosphor, resulting in the controllable white light emission (Fig. 21c). In summary, by designing efficient energy transfer process $Ce^{3+} \rightarrow Mn^{2+}$ or $Ce^{3+} \rightarrow Mn^{2+}, Tb^{3+}$ in single host lattices, excellent white light emission with tunable chromaticity coordinates and high efficiency can be obtained, which is promising in field emission display backlights. Except for the above energy transfer processes, other energy transfer routes like from Eu^{2+} to Mn^{2+}/Tb^{3+} such as $Ca_4Si_2O_7F_2:Eu^{2+}, Mn^{2+}, Tb^{3+}$,²⁶⁴ $Ca_9Y(PO_4)_7:Eu^{2+}, Mn^{2+}, Tb^{3+}$,²⁶⁵ $Ca_9Gd(PO_4)_7:Eu^{2+}, Mn^{2+}, Tb^{3+}$,²⁶⁶ $Na_{0.34}Ca_{0.66}Al_{1.66}Si_{2.34}O_8:Eu^{2+}, Mn^{2+}, Tb^{3+}$ ²⁶⁷ and $BaMg_2A_{16}Si_9O_{30}:Eu^{2+}, Mn^{2+}, Tb^{3+}$ ²⁶⁸ from host or self-activated luminescent center to RE^{3+} ions such as $Ga_2O_3:Dy^{3+}$ ²⁶⁹ and $CaMoO_4:Eu^{3+}$ ¹⁴⁴ (Fig. 21d) also can gain excellent white light emission, as shown in Table 4.

5. Improvement of electron-stimulated degradation behavior

It is known that most phosphors will degrade upon exposure to large doses of electrons (>50 C/cm²). The luminescent degradation property of phosphors under electron beam bombardment is very important for their FED application. The origin of this degradation is now becoming clear, which is generally considered to be related to the stability of crystal structures and electron stimulated surface chemical reaction of phosphor grains.^{77, 269, 270} Because prolonged electron beam

irradiation commonly can decompose phosphors into volatile atomic species through the surface chemical reaction and then a possible formation of new layers on the surface. While the decomposition and hence the formation of the new layers has negative effects on both the chemical stability and luminescent intensity of the FED phosphors. To prevent the phosphors from decomposition, two strategies can be employed: first, selecting

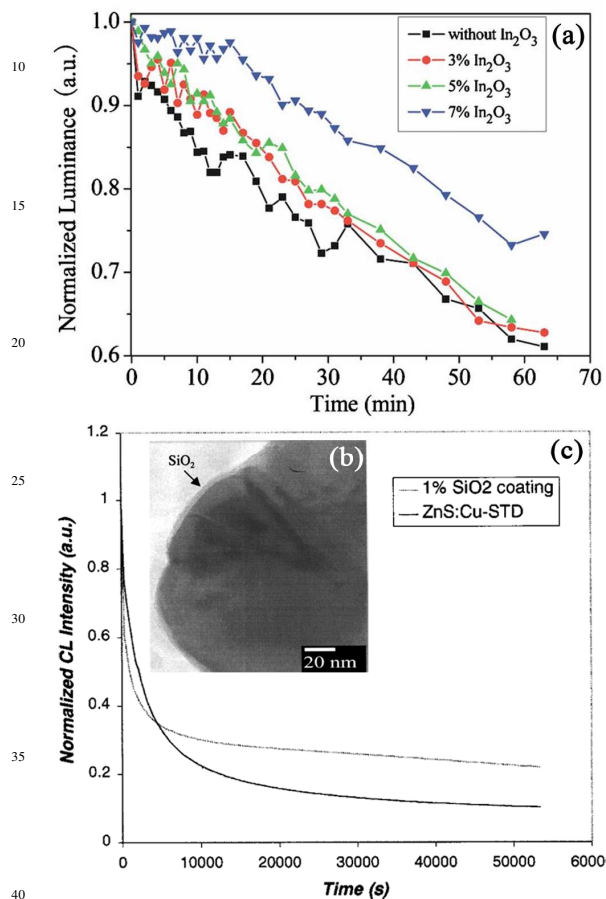


Fig. 22 (a) Normalized luminescence decay of Lu₃Ga₅O₁₂:Tb³⁺ phosphor mixed with and without In₂O₃ nanoparticles as a function of bombardment time. (b) TEM cross-sectional micrographs of 1.0 wt % SiO₂-coated ZnS:Cu phosphors. (c) Normalized CL intensity at 2 kV of 1.0 wt % SiO₂-coated and uncoated ZnS:Cu phosphors as a function of time. (reproduced with the permission from refs. 67 and 276, copyright 2010, American Vacuum Society and The Electrochemical Society)

hosts with excellent chemical stability under electron beam irradiation; second, coating Al₂O₃, In₂O₃, Y₂O₃, ZnO, SiO₂, MgO, and organic polymers on phosphor surface.²⁷¹ The formers require stable crystal phases and crystal structures for phosphors, which can endure continuous electron beam irradiation. For example, the rare earth ions activated semiconductor materials and (oxo)nitrilosilicates are possible selections.^{5, 13, 43, 272} The use of coatings can also yield excellent stability to the phosphors when exposed to moisture and other atmospheric components, and to protect phosphors from irradiation damage. For example, Xu et al.⁶⁷ investigated the degradation properties after mixing the representative Lu₃Ga₅O₁₂:Tb³⁺ phosphor with In₂O₃ nanoparticles. Fig. 22a shows that the degradation of the phosphor film becomes slow after being mixed with In₂O₃. Moreover, is become slower with increasing In₂O₃ contents. The

decay is partially due to the charge-up of the phosphor. The improvement of the conductivity of Lu₃Ga₅O₁₂:Tb³⁺ phosphor film by mixing with In₂O₃ eases the charge-up effect and thus the slower decay can be observed. After stopping bombardment for a while, however, the luminance could not restore to the initial value, indicating besides the charge-up effect, permanent damage to the phosphor occurs. According to the X-ray photoelectron spectroscopy analyses, they found that

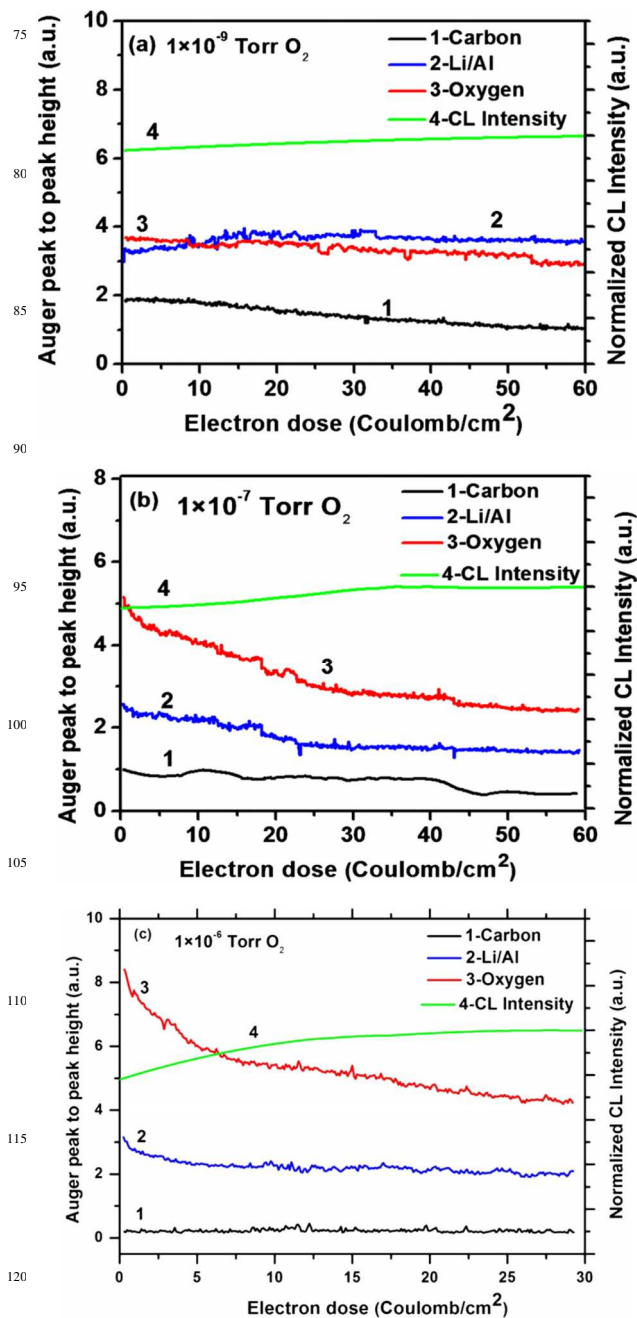


Fig. 23 (Color online) Auger peak to peak heights (APPH) and CL intensity (right scale) as a function of electron beam exposure for the LiAl₅O₈:Tb phosphor at (a) 1 × 10⁻⁹ Torr, (b) 1 × 10⁻⁷ Torr, and (c) 1 × 10⁻⁶ Torr O₂ pressure. (reproduced with the permission from ref. 269, copyright 2011, American Institute of Physics)

no obvious change was observed for Lu 3d, Ga 2p, and Tb 3d peaks. However the intensity of carbon 1s peak increased

significantly after bombardment. Therefore, the degradation of luminescence may be due to the accumulation of carbon at the surface during electron bombardment. Accretion of graphitic carbon during electron-beam exposure at high current densities is a well-known effect.^{273, 274} This carbon contamination will prevent low-energy electrons from reaching the phosphor grains and also exacerbate surface charging, and thus lower the luminescence.²⁷⁵ Although the short time experiment indicates that the stability of the phosphor is good, further experiments are needed to verify the long term stability of In_2O_3 -coated $\text{Lu}_3\text{Ga}_5\text{O}_{12}:\text{Tb}^{3+}$ phosphor. Other In_2O_3 -coated FEDs phosphors also confront the same problem and need to be overcome. In addition to the mixing with semiconductive materials, Do et al. confirmed that coating SiO_2 on phosphor surface can also efficiently improve their electron-stimulated stability.²⁷⁶ Fig. 22b shown the formation of thin and uniform coatings on $\text{ZnS}:\text{Cu}$ powders with a thickness of 5 nm. They found that the SiO_2 -coated phosphors were far more resistant to the loss of S species and to the formation of oxide dead layer. The CL aging study (Fig. 22c) showed much improved CL efficiency curves for the coated phosphors, confirming that the encapsulation of thin and uniform SiO_2 coatings on $\text{ZnS}:\text{Cu}$ served as protective layers retarding the surface-related degradation, which is critically important for the development of commercial FEDs. On the other hand, the surface protective species need not necessarily be always externally applied, they can also originate from electron stimulated surface chemical reaction.²⁶⁹ This is attributed to surface disassociates partially of a phosphor compound. Pitale et al. found that a thermodynamically stable Al_2O_3 layer could be formed on the surface of lithium aluminate family like $\text{LiAl}_5\text{O}_8:\text{Tb}$ as a result of the electron stimulated surface chemical reactions.^{269, 277} Moreover, it generates a positive contribution to the CL stability of the $\text{LiAl}_5\text{O}_8:\text{Tb}$ phosphor, as shown in Fig. 23.²⁶⁹ The time stability of the $\text{LiAl}_5\text{O}_8:\text{Tb}$ phosphor under prolonged electron beam exposure suggests that it can be used in information displays.²⁶⁹ Therefore, it is necessary to develop phosphors from this family whose partial decomposition can form a protective layer such as Al_2O_3 during electron beam exposure to enhance the chemical stability without affecting the original properties of the phosphor itself. In general, the stable crystal structures and the surface protective species indeed can enhance the time stability of phosphors under electron beam irradiation to some extent. It is noticed that although the improvement can simply attributed to electron stimulated surface chemical reaction, the more exact degradation mechanism is not clear and need to be further studied.

6. Summary and Outlook

Field emission displays (FEDs) is a promising newcomer to the world of panel technologies due to their advantages in high-quality display performances and low energy consumption with respect to other display devices. Phosphors are irreplaceable components in FEDs devices and thus the development of FEDs inevitably requires the appearance of highly efficient low voltage cathodoluminescent materials. In the past decade, the exploring of highly efficient FEDs phosphors has been becoming the focus of realizing high-quality field emission display. In this review, we have discussed the importance of FEDs phosphors and the recent progress in chemical synthesis and improvement of existing and new phosphors including rare-earth and transition metal ions activated inorganic solid-state luminescent materials, semiconductor-based luminescence materials, self-activated luminescent materials etc. We have also outlined the common strategies for the modifications and optimizations in morphology,

size, composition, conductivity of phosphors and corresponding effects on their cathodoluminescent properties. Special emphases are mainly focused on the studies of selection of hosts and luminescent centers, enhancement of efficiency through energy transfer, adjustment and design of emission colors, improvement of color index and color gamut as well as color stability and degradation behavior of phosphors. Based on the above modifications and optimizations, the cathodoluminescent performances like emission intensity, brightness, color purity and saturation behavior can be obviously improved. Simultaneously, conductivity and degradation behaviors of phosphors are also optimized. Therefore, the improved low-voltage cathodoluminescent materials have potential application in full-color FEDs. In addition, single-phase white light emitting FEDs phosphors with excellent emission properties and tunable CIE chromaticity coordinates have also been developed through designing co-emission and energy transfer between hosts or RE ions and RE ions or Mn^{2+} ions, which are promising backlights in FEDs devices.

Although substantial and rapid progress has been made in the synthesis, properties, and applications of FEDs phosphors in the recent years, developing better synthetic routes to further improve their luminescent performances and more detailed fundamental studies of luminescent properties and mechanisms have a level of urgency, thus there still remains much room for improvement in the future. First, despite the fact that the cathodoluminescent performances of FEDs phosphors can be improved by optimizing their morphology, size, surface state and crystallization, further and detailed investigations are still required to exactly explore how the effect happen, and to develop better synthesis routes for highly efficient cathodoluminescent material. Secondly, as the cathodoluminescent properties of phosphors are strongly related to the electrical conductivity of their matrix, how to make the matrix maintain a proper electrical conductivity is also a difficult issue to be addressed. Thirdly, although some possible degradation processes under electron beam bombardment have been depicted by many researchers, exact degradation mechanism should be further investigated in order to develop highly efficient FEDs phosphors with better stability. Fourthly, to move forward, researchers with various backgrounds like electronic technology and process optimization may be needed to develop multicolor-system display units and color-gamut enlarged phosphors to improve the color saturation of FEDs devices. Finally, the methods through solely doping or multi-doping to obtain white light in a single-phase host material have a good controllability of emission colors, while the luminous efficiency and intensity are lower. Therefore, numerous efforts need be made to further develop the single-phase white-emitting luminescence materials based on the energy transfer from sensitizer to activator to contain the advantages of a controllability of emission colors and high luminous efficiency. In addition, processes and methods for preparing phosphor thin films and screen should be optimized to further enhance their cathodoluminescent performances in FEDs device. From a long-term point of view, some emerging phosphors like defect-related environment-friendly phosphors that have high luminous efficiency should be actively explored to open the door to novel display applications. From the point of view of devices, the development of highly efficient low voltage cathodoluminescent materials might not only promote their application in daily display fields but also offer possibilities for FEDs devices incorporation in exploration, expedition, aviation, marine and military fields due to the perfect adaptation of some extremely harsh environment such as very cold or hot conditions. In summary, a large amount of newer improvement methods and novel low voltage cathodoluminescent materials are still in the

research stage. There is a long way in achieving the high-quality field emission display, and thus need more efforts to pay attention to it.

Acknowledgement

This project is financially supported by National Basic Research Program of China (Grants No. 2010CB327704), the National Natural Science Foundation of China (Grants Nos. NSFC 60977013, 51172227, 21221061, 21301162) and the Fundamental Research Funds for the Central Universities (Grant Nos. CUG 130402).

Notes and references

- 1 H. A. Höpfe, *Angew. Chem. Int. Ed.*, 2009, **48**, 3572–3582.
- 2 I. Shah, *Physics World*, 1997, **10**, 45–48.
- 3 B. Chalamala, Y. Wei and B. Gnade, *IEEE Spectr.*, 1998, **35**, 42–51.
- 4 R. Waser, *Nanoelectronics and Information Technology*, chapter 39, Wiley-Vch, Weinheim, Germany, 2003.
- 5 P. H. Holloway, T. A. Trottier, B. Abrams, C. Kondoleon, S. L. Jones, J. S. Sebastian, W. J. Thomes and H. Swart, *J. Vac. Sci. Technol. B*, 1999, **17**, 758–764.
- 6 T. Jüstel, H. Nikol and C. Ronda, *Angew. Chem., Int. Ed.*, 1998, **37**, 3084–3103.
- 7 C. C. Lin and R. S. Liu, *J. Phys. Chem. Lett.*, 2011, **2**, 1268–1277.
- 8 R. J. Xie and N. Hirosaki, *Sci. Technol. Adv. Mater.*, 2007, **8**, 588–600.
- 9 M. Zeuner, S. Pagano and W. Schnick, *Angew. Chem. Int. Ed.*, 2011, **50**, 7754–7775.
- 10 M. Yokoyama and S. H. Yang, *J. Vac. Sci. Technol. A*, 2000, **18**, 2472–2476.
- 11 J. H. Hao, J. Gao and M. Cocivera, *Appl. Phys. Lett.*, 2003, **82**, 2224–2226.
- 12 J. H. Hao, J. Gao, and M. Cocivera, *Appl. Phys. Lett.*, 2003, **82**, 2778–2780.
- 13 N. Hirosaki, R. J. Xie, K. Inoue, T. Sekiguchi, B. Dierre and K. Tamura, *Appl. Phys. Lett.*, 2007, **91**, 061101.
- 14 X. M. Liu and J. Lin, *J. Mater. Chem.*, 2008, **18**, 221–228.
- 15 G. G. Li, Z. Y. Hou, C. Peng, W. X. Wang, Z. Y. Cheng, C. X. Li, H. Z. Lian and J. Lin, *Adv. Funct. Mater.*, 2010, **20**, 3446–3456.
- 16 T. C. Liu, H. Kominami, H. F. Greer, W. Zhou, Y. Nakanishi and R. S. Liu, *Chem. Mater.*, 2012, **24**, 3486–3492.
- 17 Q. H. Zhang, J. Wang, C. W. Yeh, W. C. Ke, R. S. Liu, J. K. Tang, M. B. Xie, H. B. Liang and Q. Su, *Acta Mater.*, 2010, **58**, 6728–6735.
- 18 S. Zhang, H. B. Liang, C. M. Liu, Z. M. Qi, T. Shao and Y. Y. Wang, *Opt. Lett.*, 2013, **38**, 612–614.
- 19 K. S. Sohn, Y. G. Choi, Y. Y. Choi and H. D. Park, *J. Electrochem. Soc.*, 2000, **147**, 3552–3558.
- 20 K. S. Sohn, Y. Y. Choi, H. D. Park and Y. G. Choi, *J. Electrochem. Soc.*, 2000, **147**, 2375–2379.
- 21 Y. D. Jing, F. Zhang, C. J. Summers and Z. L. Wang, *Appl. Phys. Lett.*, 1999, **74**, 1677–1679.
- 22 A. K. Sharma and K. S. Sohn, *J. Soc. Inf. Display*, 2009, **17**, 1073–1080.
- 23 S. Itoh, T. Niiyama and M. Yokoyama, *J. Vac. Sci. Technol. B*, 1993, **11**, 647–650.
- 24 P. H. Holloway, J. Sebastian, T. Trottier, H. Swart and R. O. Petersen, *Solid State Tech.*, 1995, **38**, 47–54.
- 25 J. I. Han, M. G. Kwak, Y. K. Park, S. C. Lim, I. K. Lee, K. I. Cho H. J. Yoo, *J. Vac. Sci. Technol. B*, 1998, **16**, 1236–1238.
- 26 S. Tominetti and M. Amiotti, *Proc. IEEE.*, 2002, **90**, 540–558.
- 27 P. Psuja, D. Hreniak and W. Strek, *J. Nanomater.*, 2007, **2007**, 81350.
- 28 E. Coetsee, H. C. Swart and J. J. Terblans, *J. Vac. Sci. Technol. A*, 2007, **25**, 1226–1230.
- 29 Z. L. Wang, H. L. W. Chan, H. L. Li and J. H. Hao, *Appl. Phys. Lett.*, 2008, **93**, 141106.
- 30 A. K. Sharma, K. H. Son, B. Y. Han, K. S. Sohn, *Adv. Funct. Mater.*, 2010, **20**, 1750–1755.
- 31 G. Blasse and B. C. Grabmaier, *Luminescence Materials* (Springer-Verlag, Berlin and Heideberg, 1994), ch. 4–5.
- 32 L. Shi, Y. L. Huang and H. J. Seo, *J. Phys. Chem. A*, 2010, **114**, 6927–6934.
- 33 S. Zhang, Y. Huang, W. Kai, L. Shi and H. J. Seo, *Electrochem. Solid-State Lett.*, 2010, **13**, J11–J14.
- 34 X. M. Liu and J. Liu, *J. Lumin.*, 2007, **122–123**, 700–703.
- 35 S. Yang, C. Stoffers, F. Zhang, S. M. Jacobsen, B. K. Wagner and C. J. Summers, *Appl. Phys. Lett.*, 1998, **72**, 158–160.
- 36 T. Yamashita and K. Ueda, *J. Solid State Chem.*, 2007, **180**, 1410–1413.
- 37 G. G. Li, X. Zhang, C. Peng, M. M. Shang, D. L. Geng, Z. Y. Cheng and J. Lin, *J. Mater. Chem.*, 2011, **21**, 6477–6479.
- 38 Z. Y. Hou, G. G. Li, H. Z. Lian and J. Lin, *J. Mater. Chem.*, 2012, **22**, 5254–5276.
- 39 M. M. Shang, G. G. Li, D. M. Yang, X. J. Kang, C. Peng and J. Lin, *Dalton Trans.*, 2012, **41**, 8861–8868.
- 40 F. L. Zhang, S. Yang, C. Stoffers, J. Penczek, P. N. Yocom, D. Zaremba, B. K. Wagner and C. J. Summers, *Appl. Phys. Lett.*, 1998, **72**, 2226–2228.
- 41 A. Vecht, C. Gibbons, D. Davies, X. Jing, P. Marsh, T. reland, J. Silver, A. Nowport and D. Barber, *J. Vac. Sci. Technol. B*, 1999, **17**, 750–757.
- 42 K. Tanaka, S. Okamoto, H. Kominami, Y. Nakanishi, X. L. Du and A. Yoshikawa, *J. Appl. Phys.*, 2002, **92**, 834–837.
- 43 P. Guo, F. Zhao, G. Li, F. Liao, S. Tian and X. Jing, *J. Lumin.*, 2003, **105**, 61–67.
- 44 Y. C. Li, Y. H. Chang, Y. F. Lin, Y. J. Lin and Y. S. Chang, *Appl. Phys. Lett.*, 2006, **89**, 081110.
- 45 V. A. Bolchouchine, E. T. Goldburt, B. N. Levonovitch, V. N. Litchmanova and N. P. Sochtine, *J. Lumin.*, 2000, **87–89**, 1277–1279.
- 46 Y. R. Do, D. H. Park, Y. C. Kim and Y. D. Huh, *J. Electrochem. Soc.*, 2003, **150**, H260–H265.
- 47 S. H. Shin, Y. C. You and S. H. Lee, *J. Electrochem. Soc.*, 2004, **151**, H40–H30.
- 48 J. Rodriguez-Viejo, K. F. Jensen, H. Mattoussi, J. Michel, B. O. Dabbousi and M. G. Bawendi, *Appl. Phys. Lett.*, 1997, **70**, 2132–2134.
- 49 S. Shionoya and W. M. Yen, *Phosphors Handbook*, CRC Press, New York, NY, USA, 1998.
- 50 B. H. Lee, H. G. Jeong and K. S. Sohn, *J. Electrochem. Soc.*, 2010, **157**, J227–J232.
- 51 I. M. Nagpure, Shreyas S. Pitale, E. Coetsee, O. M. Ntwaeaborwa, J. J. Terblans and H. C. Swart, *Appl. Surf. Sci.*, 2011, **257**, 10147–10155.
- 52 A. M. Srivastava and C. R. Ronda, *Electrochem. Soc. Interface*, 2003, **12**, 48–51.
- 53 C. E. Hunt and A. G. Chakhovskoi, *J. Vac. Sci. Technol. B*, 1997, **15**, 516–519.
- 54 X. Liu, C. Lin and J. Lin, *Appl. Phys. Lett.*, 2007, **90**, 081904.

- 55 A. V. Murugan, A. K. Viswanath, V. Ravi, B. A. Kakade and V. Saaminathan, *Appl. Phys. Lett.*, 2006, **89**, 123120.
- 56 G. Wakefield, E. Holland, P. J. Dobson and J. L. Hutchison, *Adv. Mater.*, 2000, **13**, 1557–1560.
- 57 Y. Shimomura and N. Kijima, *J. Electrochem. Soc.*, 2004, **151**, H86–H92.
- 58 S. Y. Seo, K. S. Sohn, H. D. Park and S. Lee, *J. Electrochem. Soc.*, 2002, **149**, H12–H18.
- 59 S. S. Yi, J. S. Bae, B. K. Moon, J. H. Jeong and J. H. Kim, *Appl. Phys. Lett.*, 2005, **86**, 071921.
- 60 J. Y. Cho, Y. R. Do and Y. D. Huh, *Appl. Phys. Lett.*, 2006, **89**, 131915.
- 61 S. H. Yang, T. J. Hsueh and S. J. Chang, *J. Electrochem. Soc.*, 2005, **152**, H191–H195.
- 62 H. S. Jang, J. H. Kang, Y. H. Won, S. Lee and D. Y. Jeon, *Appl. Phys. Lett.*, 2007, **90**, 071908.
- 63 C. H. Lin, B. S. Chiou, C. H. Chang and J. D. Lin, *Mater. Chem. Phys.*, 2003, **77**, 647–654.
- 64 H. Hayashi, A. Ishizaka, M. Haemori and H. Koinuma, *Appl. Phys. Lett.*, 2003, **82**, 1365–1367.
- 65 Q. R. Ou, T. Matsuda, M. Mesko, A. Ogino and M. Nagatsu, *Jpn. J. Appl. Phys.*, 2008, **47**, 389–393.
- 66 G. G. Li, C. Peng, C. X. Li, P. P. Yang, Z. Y. Hou, Y. Fan and J. Lin, *Inorg. Chem.*, 2009, **49**, 1449–1457.
- 67 X. G. Xu, J. Chen, S. Z. Deng, N. S. Xu and J. Lin, *J. Vac. Sci. Technol. B*, 2010, **28**, 490–494.
- 68 M. Lei, Q. R. Hu, X. Wang, S. L. Wang and W. H. Tang, *J. Alloys Compds.*, 2010, **489**, 663–666.
- 69 B. D. Liu, Y. Bando, B. Dierre, T. Sekiguchi, C. C. Tang, M. Mitome, A. M. Wu, X. Jiang and D. Golberg, *Nanotechnology*, 2009, **20**, 365705–365711.
- 70 X. M. Liu, C. X. Li, Z. W. Quan, Z. Y. Cheng and J. Lin, *J. Phys. Chem. C*, 2007, **111**, 16601–16607.
- 71 X. M. Liu, R. Pang, Q. Li and J. Lin, *J. Solid State Chem.*, 2007, **180**, 1421–1430.
- 72 X. M. Liu, C. K. Lin, Y. Luo and J. Lin, *J. Electrochem. Soc.*, 2007, **154**, J21–J27.
- 73 H. Jiao, J. G. Wang, F. H. Liao, S. J. Tian and X. P. Jing, *J. Electrochem. Soc.*, 2004, **151**, H49–H51.
- 74 Q. H. Zhang and J. Wang, *Appl. Phys. A*, 2012, **108**, 943–948.
- 75 M. M. Shang, G. G. Li, D. M. Yang, X. J. Kang, C. Peng, Z. Y. Cheng and J. Lin, *Dalton Trans.*, 2011, **40**, 9379–9387.
- 76 Y. R. Jung, Y. W. Jung and K. S. Sohn, *J. Electrochem. Soc.*, 2009, **156**, J321–J325.
- 77 I. M. Nagpure, S. S. Pitale, E. Coetsee, O. M. Ntwaeaborwa, J. J. Terblans and H. C. Swart, *Opt. Mater.*, 2012, **34**, 1398–1405.
- 78 J. Henzie, M. Grünwald, A. Widmer-Cooper, P. L. Geissler and P. Yang, *Nature Mater.*, 2011, **11**, 131–137.
- 79 Y. Yin, C. K. Erdonmez, A. Cabot, S. Hughes and A. P. Alivisatos, *Adv. Funct. Mater.*, 2006, **16**, 1389–1399.
- 80 Z. G. Yan and C. H. Yan, *J. Mater. Chem.*, 2008, **18**, 5046–5059.
- 81 A. L. Pénard, T. Gacoin and J. P. Boilot, *Acc. Chem. Res.*, 2007, **40**, 895–902.
- 82 C. X. Li, J. Yang, P. P. Yang, H. Z. Lian and J. Lin, *Chem. Mater.*, 2008, **20**, 4317–4326.
- 83 P. A. Tanner, *J. Nanosci. Nanotechnol.*, 2005, **5**, 1455–1464.
- 84 Y. N. Xia, Y. J. Xiong, B. Lim and S. E. Skrabalak, *Angew. Chem. Int. Ed.*, 2008, **47**, 2–46.
- 85 C. X. Li and J. Lin, *J. Mater. Chem.*, 2010, **20**, 6831–6847.
- 86 G. G. Li, C. X. Li, C. M. Zhang, Z. Y. Cheng, Z. W. Quan, C. Peng and J. Lin, *J. Mater. Chem.*, 2009, **19**, 8936–8943.
- 87 G. G. Li, C. Peng, C. M. Zhang, Z. H. Xu, M. M. Shang, D. M. Yang, X. J. Kang, W. X. Wang, C. X. Li, Z. Y. Cheng and J. Lin, *Inorg. Chem.*, 2010, **49**, 10522–10535.
- 88 G. G. Li, M. M. Shang, D. L. Geng, D. M. Yang, C. Peng, Z. Y. Cheng and J. Lin, *CrysEngComm*, 2012, **14**, 2100–2111.
- 89 M. C. Zhang, X. J. Wang, H. Ding, H. L. Li, L. K. Pan and Z. Sun, *Int. J. Appl. Ceram. Technol.*, 2011, **8**, 752–758.
- 90 X. M. Liu, Y. Luo and J. Lin, *J. Crystal Growth.*, 2006, **290**, 266–271.
- 91 Y. Zhang, X. J. Kang, D. L. Geng, M. M. Shang, Y. Wu, X. J. Li, H. Z. Lian, Z. Y. Cheng and J. Lin, *Dalton Trans.*, 2013, **42**, 14140–14148.
- 92 G. G. Li, C. X. Li, Z. Y. Hou, C. Peng and J. Lin, *Opt. Lett.*, 2009, **34**, 3833–3835.
- 93 G. G. Li, C. X. Li, Z. H. Xu, Z. Y. Cheng and J. Lin, *CrysEngComm*, 2010, **12**, 4208–4216.
- 94 G. G. Li, X. G. Xu, C. Peng, M. M. Shang, D. L. Geng, Z. Y. Cheng, J. Chen and J. Lin, *Opt. Exp.*, 2011, **19**, 16423–16431.
- 95 D. L. Geng, G. G. Li, M. M. Shang, C. Peng, Y. Zhang, Z. Y. Cheng and J. Lin, *Dalton Trans.*, 2012, **41**, 3078–3086.
- 96 D. L. Geng, M. M. Shang, D. M. Yang, Y. Zhang, Z. Y. Cheng and J. Lin, *Dalton Trans.*, 2012, **41**, 14042–14045.
- 97 Y. Zhang, D. L. Geng, M. M. Shang, X. Zhang, X. J. Li, Z. Y. Cheng, H. Z. Lian and J. Lin, *Dalton Trans.*, 2013, **42**, 4799–4808.
- 98 X. R. Xu and M. Z. Su, *Luminescence Science and Luminescent Materials* (in Chinese); Chemical Industry Publisher: Beijing, 2004.
- 99 J. Lin, M. Yu, C. K. Lin and X. M. Liu, *J. Phys. Chem. C*, 2007, **111**, 5835–5845.
- 100 B. L. Cushing, V. L. Kolesnichenko and C. J. O'Connor, *Chem. Rev.*, 2004, **104**, 3893–3946.
- 101 G. Wakefield, D. M. Williams, C. G. Harris and P. J. Dobson, *SID Symposium Digest of Technical Papers*, 2000, **31**, 691–693.
- 102 Y. B. Mao, T. Tran, X. Guo, J. Y. Huang, K. Shih, K. L. Wang and J. P. Chang, *Adv. Funct. Mater.*, 2009, **19**, 748–754.
- 103 C. Y. Xu, B. A. Watkins, R. E. Sievers, X. P. Jing, P. Trowga, C. S. Gibbons and A. Vecht, *Appl. Phys. Lett.*, 1997, **71**, 1643–1645.
- 104 E. Zych, J. Trojan-Piegza, L. Kepinski, D. Herniak and W. Strek, *Acta Universitatis Wratislaviensis*, pp.277–291, 2004 (Polish).
- 105 M. Kakihana and K. Domen, *MRS Bull.*, 2000, **25**, 27–31.
- 106 B. Zhou, Y. W. Zhang, C. S. Liao, Y. J. Yu and C. H. Yan, *Appl. Phys. Lett.*, 2003, **82**, 1188–1190.
- 107 M. Yoshino and M. Kakihana, *Chem. Mater.*, 2002, **14**, 3369–3376.
- 108 C. M. Zhang and J. Lin, *Chem. Soc. Rev.*, 2012, **41**, 7938–7961.
- 109 M. Kakihana and M. Yoshimura, *Bull. Chem. Soc. Jpn.*, 1999, **72**, 1427–1443.
- 110 X. M. Liu and J. Lin, *Electrochem. Solid-State Lett.*, 2008, **11**, J96–J99.
- 111 X. M. Liu, J. P. Zou, and J. Lin, *J. Electrochem. Soc.*, 2009, **156**, P43–P47.
- 112 X. M. Liu and J. Lin, *Appl. Phys. Lett.*, 2007, **90**, 184108.
- 113 X. M. Liu and J. Lin, *J. Appl. Phys.*, 2006, **100**, 124306.
- 114 X. M. Liu, L. Zhu, L. L. Wang, C. C. Yu and J. Lin, *J. Electrochem. Soc.*, 2008, **155**, P21–P27.
- 115 D. L. Geng, M. M. Shang, Y. Zhang, H. Z. Lian and J. Lin, *Inorg. Chem.*, 2013, **52**, 13708–13718.
- 116 D. L. Geng, M. M. Shang, D. M. Yang, Y. Zhang, Z. Y. Cheng and J. Lin, *J. Mater. Chem.*, 2012, **22**, 23789–23798.

- 117 M. M. Shang, D. L. Geng, D. M. Yang, X. J. Kang, Y. Zhang and J. Lin, *Inorg. Chem.*, 2013, **52**, 3102–3112.
- 118 M. M. Shang, D. L. Geng, Y. Zhang, G. G. Li, D. M. Yang, X. J. Kang and J. Lin, *J. Mater. Chem.*, 2012, **22**, 19094–19104.
- 119 M. M. Shang, G. G. Li, D. L. Geng, D. M. Yang, X. J. Kang, Y. Zhang, H. Z. Lian and J. Lin, *J. Phys. Chem. C*, 2012, **116**, 10222–10231.
- 120 H. K. Jung, K. S. Sohn, B. Y. Sung and H. B. Park, *J. Inf. Display*, 2000, **1**, 35–41.
- 121 J. Silver, R. Withnall, A. Lipman, T. G. Ireland, G. R. Fern, *J. Lumin.*, 2007, **122**, 562–566.
- 122 M. M. Shang, G. G. Li, X. J. Kang, D. M. Yang, D. L. Geng, C. Peng, Z. Y. Cheng, H. Z. Lian and J. Lin, *Dalton Trans.*, 2012, **41**, 5571–5580.
- 123 M. M. Shang, D. L. Geng, X. J. Kang, D. M. Yang, Y. Zhang and J. Lin, *Inorg. Chem.*, 2012, **51**, 11106–11116.
- 124 J. Zhang, Z. G. Liu, C. K. Lin and J. Lin, *J. Cryst. Growth*, 2005, **280**, 99–106.
- 125 J. Yang, C. X. Li, Z. Y. Cheng, X. M. Zhang, Z. W. Quan, C. M. Zhang and J. Lin, *J. Phys. Chem. C*, 2007, **111**, 18148–18154.
- 126 J. Yang, C. M. Zhang, L. L. Wang, Z. Y. Hou, S. S. Huang, H. Z. Lian and J. Lin, *J. Phys. Chem. C*, 2008, **112**, 12777–12785.
- 127 F. Vetrone, J. C. Boyer, J. A. Capobianco, in *Encyclopedia of Nanoscience and Nanotechnology*, Vol. **10** (Ed: H. S. Nalwa), American Scientific Publishers, Stevenson Ranch CA 2004, p.725.
- 128 G. P. Dong, X. D. Xiao, X. F. Liu, B. Qian, Z. J. Ma, D. P. Chen and J. R. Qiu, *J. Electrochem. Soc.*, 2009, **156**, J356–J360.
- 129 C. Peng, Z. Y. Hou, C. M. Zhang, G. G. Li, H. Z. Lian, Z. Y. Cheng and J. Lin, *Opt. Exp.*, 2010, **18**, 7543–7553.
- 130 H. W. Song, L. X. Yu and S. Z. Lu, *Opt. Lett.*, 2005, **30**, 483–485.
- 131 H. Zhang, H. W. Song and H. Q. Yu, *J. Phys. Chem. C*, 2007, **111**, 6524–6527.
- 132 H. Zhang, H. W. Song and H. Q. Yu, *Appl. Phys. Lett.*, 2007, **90**, 103103.
- 133 Z. Y. Hou, P. P. Yang, C. X. Li, L. L. Wang, H. Z. Lian, Z. W. Quan and J. Lin, *Chem. Mater.*, 2008, **20**, 6686–6696.
- 134 X. Y. Chen, L. Q. Liu, G. K. Liu, *J. Nanoscience Nanotechnology*, 2008, **8**, 1126–1137.
- 135 X. Li, M. Yu, Z. Y. Hou, G. G. Li, P. A. Ma, W. X. Wang, Z. Y. Cheng and J. Lin, *J. Solid State Sci.*, 2011, **184**, 141–148.
- 136 Z. Y. Hou, L. L. Wang, H. Z. Lian, R. T. Chai, C. M. Zhang, Z. Y. Cheng and J. Lin, *J. Solid State Chem.*, 2009, **182**, 698–708.
- 137 L. L. Wang, Z. Y. Hou, Z. W. Quan, C. X. Li, J. Yang, H. Z. Lian, P. P. Yang and J. Lin, *Inorg. Chem.*, 2009, **48**, 6731–6739.
- 138 C. Peng, G. G. Li, X. J. Kang, C. X. Li and J. Lin, *J. Colloid Interface Sci.*, 2011, **355**, 89–95.
- 139 C. Peng, X. J. Kang, G. G. Li, Z. Y. Hou, C. X. Li and J. Lin, *J. Electrochem. Soc.*, 2011, **158**, J208–J214.
- 140 C. Peng, M. M. Shang, G. G. Li, Z. Y. Hou, D. L. Geng and J. Lin, *Dalton Trans.*, 2012, **41**, 4780–4788.
- 141 Z. Y. Hou, C. X. Li, J. Yang, H. Z. Lian, P. P. Yang, R. T. Chai, Z. Y. Cheng and J. Lin, *J. Mater. Chem.*, 2009, **19**, 2737–2746.
- 142 Z. Y. Hou, Z. Y. Cheng, G. G. Li, W. X. Wang, C. Peng, C. X. Li, P. A. Ma, D. M. Yang, X. J. Kang and J. Lin, *Nanoscale*, 2011, **3**, 1568–1574.
- 143 Z. Y. Hou, H. Z. Lian, M. L. Zhang, L. L. Wang, M. F. Lv, C. M. Zhang and J. Lin, *J. Electrochem. Soc.*, 2008, **156**, J209–J214.
- 144 Z. Y. Hou, R. T. Chai, M. L. Zhang, C. M. Zhang, P. Chong, Z. H. Xu, G. G. Li and J. Lin, *Langmuir*, 2009, **25**, 12340–12348.
- 145 M. Yu, J. Lin and J. Fang, *Chem. Mater.*, 2005, **17**, 1783–1791.
- 146 W. Stöber, A. Fink and E. Bohn, *J. Colloid Interface Sci.*, 1968, **26**, 62–69.
- 147 C. K. Lin, D. Y. Kong, X. M. Liu, H. Wang, M. Yu and J. Lin, *Inorg. Chem.*, 2007, **46**, 2674–2681.
- 148 H. Wang, C. K. Lin, X. M. Liu, J. Lin and M. Yu, *Appl. Phys. Lett.*, 2005, **87**, 181907.
- 149 H. Wang, M. Yu, C. K. Lin and J. Lin, *J. Colloid Interf. Sci.*, 2006, **300**, 176–182.
- 150 G. Z. Li, Z. L. Wang, M. Yu, Z. W. Quan and J. Lin, *J. Solid State Chem.*, 2006, **179**, 2698–2706.
- 151 P. Y. Jia, X. M. Liu, Y. Luo, J. Fang and J. Lin, *Chem. Phys. Lett.*, 2006, **424**, 358–363.
- 152 P. Y. Jia, X. M. Liu, Y. Luo, M. Yu and J. Lin, *J. Electrochem. Soc.*, 2007, **154**, J39–J43.
- 153 P. Y. Jia, X. M. Liu, Li, G. Z. M. Yu, J. Fang and J. Lin, *Nanotechnology*, 2006, **17**, 734–742.
- 154 M. Yu, H. Wang, C. K. Lin, G. Z. Li and J. Lin, *Nanotechnology*, 2006, **17**, 3245–3252.
- 155 C. K. Lin, H. Wang, X. M. Liu, M. Yu, P. Y. Jia, Z. L. Wang and J. Lin, *Euro. J. Inorg. Chem.*, 2006, **2006**, 3667–3675.
- 156 X. M. Liu, G. Z. Li, P. Y. Jia and J. Lin, *J. Appl. Phys.*, 2006, **99**, 124902.
- 157 G. Z. Li, Z. L. Wang, Z. W. Quan, X. M. Liu, R. S. Wang and J. Lin, *Surf. Sci.*, 2006, **600**, 3321–3326.
- 158 G. Z. Li, Z. L. Wang, Z. W. Quan, C. X. Li and J. Lin, *Crystal Growth & Design*, 2007, **7**, 1797–1802.
- 159 G. Z. Li, M. Yu, R. S. Wang, Z. L. Wang, Z. W. Quan and J. Lin, *J. Mater. Research*, 2006, **21**, 2232–2240.
- 160 X. M. Liu and J. Lin, *J. Nanoparticle Research*, 2007, **9**, 869–875.
- 161 S. Y. Tan, P. P. Yang, C. X. Li, W. X. Wang, J. Wang, M. L. Zhang, X. Y. Jing and J. Lin, *Solid State Sci.*, 2010, **12**, 624–629.
- 162 K. Y. Jung, E. J. Kim, and Y. C. Kang *J. Electrochem. Soc.*, 2004, **151**, H69–H73.
- 163 J. E. Hubeey, *Inorganic Chemistry: Principles of Structure and Reactivity*, 2nd ed., Harper & Row, New York (1978).
- 164 M. M. Shang, G. G. Li, D. M. Yang, X. J. Kang, C. M. Zhang and J. Lin, *J. Electrochem. Soc.*, 2011, **158**, J125–J131.
- 165 C. Feldman, *Phys. Rev.*, 1960, **117**, 455–459.
- 166 A. R. West, *Solid State Chemistry and Its Applications*, John Wiley & Sons, Chichester (1992).
- 167 X. M. Liu, L. S. Yan and J. Lin, *J. Electrochem. Soc.*, 2009, **156**, P1–P6.
- 168 S. H. Yang, *J. Electron. Mater.*, 2004, **33**, L1–L4.
- 169 J. Y. Kim, D. Y. Jeon, I. Yu and H. G. Yang, *J. Electrochem. Soc.*, 2000, **147**, 3559–3563.
- 170 L. P. Xie, H. W. Song, Y. Wang, W. Xu, X. Bai, B. Dong, *J. Phys. Chem. C*, 2010, **114**, 9975–9980.
- 171 I. Yu, *Mater. Res. Bull.*, 2006, **41**, 1403–1406.
- 172 X. S. Hu, X. W. Huang, Y. S. Hu and W. D. Zhuang, *J. Rare Earth*, 2007, **25**, 11–14.
- 173 J. M. Robertson and M. T. van Tol, *Appl. Phys. Lett.*, 1980, **37**, 471–473.

- 174 S. Park, B. L. Clark, D. A. Keszler, J. P. Bender, J. F. Wager, T. A. Reynolds and G. S. Herman, *Science*, 2002, **297**, 65–65.
- 175 J. Y. Choe, D. Ravichandran, S. M. Biomquist, D. C. Morton, K. W. Kirchner, M. H. Ervin and U. Lee, *Appl. Phys. Lett.*, 2001, **78**, 3800–3802.
- 176 E. M. Rabinovich, J. Shmulovich, V. J. Fratello and N. Kopyov, *J. Am. Ceram. Soc. Bull.*, 1987, **6**, 1505–1512.
- 177 D. Ravichandran, R. Roy, A. G. Chakhovskoi, C. E. Hunt, W. B. White and S. Erdei, *J. Lumin.*, 1997, **71**, 291–298.
- 178 K. L. Frindell, M. H. Bartl, A. Popitsch and G. D. Stucky, *Angew. Chem. Int. Ed.*, 2002, **41**, 959–962.
- 179 G. R. Bai, H. Zhang and C. M. Foster, *Thin Solid Films*, 1998, **321**, 115–122.
- 180 Y. H. Lee, M. H. Song, B. K. Ju, D. K. Shin and M. H. Oh, *J. Vac. Sci. Technol. B*, 1997, **15**, 512–515.
- 181 W. Li, D. S. Mao, F. M. Zhang, X. H. Liu and S. C. Zou, Y. K. Zhu, Q. Li and J. F. Xu, *J. Vac. Sci. Technol. A*, 2000, **18**, 2295–2301.
- 182 W. Li, D. S. Mao, F. M. Zhang, X. H. Liu and S. C. Zou, Y. K. Zhu, Q. Li and J. F. Xu, *J. Vac. Sci. Technol. B*, 2001, **19**, 1004–1007.
- 183 J. H. Yum and Y. E. Sung, *J. Electrochem. Soc.*, 2004, **151**, H27–H32.
- 184 Y. E. Lee, D. P. Norton, J. D. Budai, P. D. Rack, J. Peterson and M. D. Potter, *Mat. Res. Soc. Symp. Proc.*, 2000, **621**, Q241–Q246.
- 185 M. Yu, J. Lin, Z. Wang, J. Fu, S. Wang, H. J. Zhang and Y. C. Han, *Chem. Mater.*, 2002, **14**, 2224–2231.
- 186 M. Yu, J. Lin, J. Fu, H. J. Zhang and Y. C. Han, *J. Mater. Chem.*, 2003, **13**, 1413–1419.
- 187 M. L. Pang, W. Y. Shen and J. Lin, *J. Appl. Phys.*, 2005, **97**, 033511.
- 188 P. Y. Jia and J. Lin, *J. Solid State Chem.*, 2005, **178**, 2734–2740.
- 189 C. K. Lin, M. L. Pang, M. Yu and J. Lin, *J. Lumin.*, 2005, **114**, 299–306.
- 190 M. L. Pang and J. Lin, *J. Cryst. Growth*, 2005, **284**, 262–269.
- 191 P. Y. Jia, J. Lin and X. M. Han, *Thin Solid Films*, 2005, **483**, 122–129.
- 192 M. Yu, J. Lin and S. B. Wang, *Appl. Phys. A*, 2005, **80**, 353–360.
- 193 X. M. Han, J. Lin, M. L. Pang, M. Yu and S. B. Wang, *Appl. Phys. A*, 2005, **80**, 1547–1552.
- 194 M. L. Pang, J. Lin, M. Yu and S. B. Wang, *J. Solid State Chem.*, 2004, **177**, 2236–2240.
- 195 M. Yu, J. Lin, J. Fu and Y. C. Han, *Chem. Phys. Lett.*, 2003, **371**, 178–183.
- 196 M. L. Pang, J. Lin, S. B. Wang, M. Yu, Y. H. Zhou and X. M. Han, *J. Phys.: Cond. Mat.*, 2003, **15**, 5157–5169.
- 197 M. L. Pang, J. Lin, Z. Y. Cheng, J. Fu, R. B. Xing and S. B. Wang, *Mater. Sci. Eng. B*, 2003, **100**, 124–131.
- 198 M. L. Pang, J. Lin, J. Fu, R. B. Xing, C. X. Luo and Y. C. Han, *Opt. Mater.*, 2003, **23**, 547–558.
- 199 J. E. Jang, J. H. Gwak, Y. W. Jin, S. J. Lee, S. H. Park, J. E. Jung, N. S. Lee and J. M. Kim, *J. Vac. Sci. Technol. B*, 2000, **18**, 1106–1110.
- 200 G. Y. Ying, W. B. Hu and Y. Qiu, In *The Technology of Flat Panel Displays*; Fu, J., Ed.; Post & Telecom Press: Beijing, China, 2002.
- 201 Y. Xia and G. M. Whiteside, *Annu. Rev. Mater. Sci.*, 1998, **28**, 153–184.
- 202 J. Hu, R. G. Beck and R. M. Whiteside, *Adv. Mater.*, 1998, **10**, 574–577.
- 203 S. Seraji, Y. Wu, N. E. Jewell-Larson, M. J. Forbess, S. J. Limmer, T. P. Chou and G. Cao, *Adv. Mater.*, 2000, **12**, 1421–1424.
- 204 W. X. Wang, Z. Y. Cheng, P. P. Yang, Z. Y. Hou, C. X. Li, G. G. Li, Y. L. Dai and J. Lin, *Adv. Funct. Mater.*, 2011, **21**, 456–463.
- 205 G. M. Whitesides, E. Ostuni, S. Takayama, X. Y. Jiang and D. E. Ingber, *Annu. Rev. Biomed. Eng.*, 2001, **3**, 335–373.
- 206 A. Kumar, H. A. Biebuyck and G. M. Whitesides, *Langmuir*, 1994, **10**, 1498–1511.
- 207 W. X. Wang, P. P. Yang, Z. Y. Cheng, Z. Y. Hou, C. X. Li and J. Lin, *ACS Appl Mater & Inter.*, 2011, **3**, 3921–3928.
- 208 D. Wang, P. P. Yang, Z. Y. Cheng, W. X. Wang, Z. Y. Hou, Y. L. Dai, C. X. Li and J. Lin, *J. Coll. Inter. Sci.*, 2012, **365**, 320–325.
- 209 Z. Y. Cheng, R. B. Xing, Z. Y. Hou, S. S. Huang and J. Lin, *J. Phys. Chem. C*, 2010, **114**, 9883–9888.
- 210 B. J. de Gans, P. C. Duineveld and U. S. Schubert, *Adv. Mater.*, 2004, **16**, 203–213.
- 211 E. Tekin, P. J. Smith and U. S. Schubert, *Soft Mater.*, 2008, **4**, 703–713.
- 212 M. Singh, H. M. Haverinen, P. Dhagat and G. E. Jabbour, *Adv. Mater.*, 2010, **22**, 673–685.
- 213 D. B. Van Dam and J. G. M. Kuerten, *Langmuir*, 2008, **24**, 582–589.
- 214 H. Sirringhaus, T. Kawase and R. H. Friend, *MRS Bull.*, 2001, **26**, 539–543.
- 215 Y. J. Xia and R. H. Friend, *Appl. Phys. Lett.*, 2007, **90**, 253513.
- 216 R. B. Xing, T. L. Ye, Y. Ding, D. G. Ma and Y. C. Han, *Organ. Electro.*, 2009, **10**, 313–319.
- 217 N. Mathews, Y. M. Lam, S. G. Mhaisalkar and A. C. Grimsdale, *Int. J. Mater. Res.*, 2010, **101**, 236–250.
- 218 S. C. Chang, J. Liu, J. Bharathan, Y. Yang, J. Onohara and J. Kido, *Adv. Mater.*, 1999, **11**, 734–737.
- 219 J. F. Dijkman, P. C. Duineveld, M. J. J. Hack, A. Pierik, J. Rensen, J. E. Rubingh, I. Schram and M. M. Vernhout, *J. Mater. Chem.*, 2007, **17**, 511–522.
- 220 Q. L. Niu, Y. X. Shao, W. Xu, L. Wang, S. H. Han, N. H. Liu, J. B. Peng, Y. Cao and J. Wang, *Org. Electron.*, 2008, **9**, 95–100.
- 221 E. I. Haskal, M. Büchel, P. C. Duineveld, A. Sempel and P. Van De Weijer, *MRS Bull.*, 2002, **27**, 864–869.
- 222 V. Wood, M. J. Panzer, J. Chen, M. S. Bradley, J. E. Halpert, M. G. Bawendi and V. Bulovic, *Adv. Mater.*, 2009, **21**, 2151–2155.
- 223 J. Y. Kim, C. Ingrosso, V. Fakhfour, M. Striccoli, A. Agostiano, M. L. Curri and J. Brugger, *Small*, 2009, **5**, 1051–1057.
- 224 H. M. Haverinen, R. A. Myllylä and G. E. Jabbour, *Appl. Phys. Lett.*, 2009, **94**, 073108.
- 225 S. H. Kim, Y. S. Han, Y. Kwon, Y. Hur, G. Kwak, B. K. Hur and L. S. Park, *Displays*, 2008, **29**, 333–338.
- 226 B. F. Aull and H. P. Jenssen, *Phys. Rev. B*, 1986, **34**, 6640–6646.
- 227 Z. W. Quan, D. M. Yang, C. X. Li, P. P. Yang, Z. Y. Cheng and J. Lin, *Langmuir*, 2009, **25**, 10259–10262.
- 228 Z. W. Quan, Z. L. Wang, P. P. Yang, J. Lin and J. Y. Fang, *Inorg. Chem.*, 2007, **46**, 1354–1360.
- 229 G. G. Li, D. L. Geng, M. M. Shang, Y. Zhang, C. Peng, Z. Y. Cheng and J. Lin, *J. Phys. Chem. C*, 2011, **115**, 21882–21892.
- 230 G. G. Li, Y. Zhang, D. L. Geng, M. M. Shang, C. Peng, Z. Y. Cheng and J. Lin, *ACS Appl. Mater & Interfaces*, 2012, **4**, 296–305.

- 231 G. G. Li, C. Peng, C. X. Li, P. P. Yang, Z. Y. Hou, Y. Fan and J. Lin, *J. Mater. Chem.*, 2011, **21**, 13334–13344.
- 232 M. B. Xie, H. B. Liang, Q. Su, Y. Huang, Z. H. Gao and Y. Tao, *Electrochem. Solid-State Lett.*, 2011, **14**, J69–J72.
- 5 233 D. Y. Wang, C. H. Huang, Y. C. Wu and T. M. Chen, *J. Mater. Chem.*, 2011, **21**, 10818–10822.
- 234 Y. Q. Li, A. C. A. Delsing, G. de With and H. T. Hintzen, *Chem. Mater.*, 2005, **17**, 3242–3248.
- 235 V. Bachmann, C. Ronda, O. Ceckler, W. Schnick and A. Meijerink, *Chem. Mater.*, 2009, **21**, 316–325.
- 10 236 C. H. Huang, W. R. Liu and T. M. Chen, *J. Phys. Chem. C*, 2010, **114**, 18698–18701.
- 237 C. H. Huang, P. J. Wu, J. F. Lee and T. M. Chen, *J. Mater. Chem.*, 2011, **21**, 10489–10495.
- 15 238 C. K. Chang and T. M. Chen, *Appl. Phys. Lett.*, 2007, **91**, 081902.
- 239 L. Shi and H. J. Seo, *Opt. Exp.*, 2011, **19**, 7147–7152.
- 240 C. Li, C. Zhang, Z. Hou, L. Wang, Z. Quan, H. Lian and J. Lin, *J. Phys. Chem. C*, 2009, **113**, 2332–2339.
- 20 241 M. M. Shang, C. X. Li and J. Lin, *Chem. Soc. Rev.*, 2013, DOI:10.1039/c3cs60314h.
- 242 J. Lin and Q. Su, *J. Mater. Chem.*, 1995, **5**, 1151–1154.
- 243 S. H. Yang, Y. J. Lial, N. J. Cheng and Y. H. Ling, *J. Alloys Compd.*, 2010, **489**, 689–693.
- 25 244 U. Caldiño, *J. Phys.: Condens. Matter*, 2003, **15**, 3821–3830.
- 245 S. W. S. McKeever, M. D. Brown, R. J. Abbundi, H. Chan and V. K. Mathur, *J. Appl. Phys.*, 1986, **60**, 2505–2010.
- 246 C. M. Zhang, S. S. Huang, D. M. Yang, X. J. Kang, M. M. Shang, C. Peng and J. Lin, *J. Mater. Chem.*, 2010, **20**, 6674–6680.
- 30 247 N. Guo, Y. J. Huang, H. P. You, M. Yang, Y. H. Song, K. Liu and Y. H. Zheng, *Inorg. Chem.*, 2010, **49**, 10907–10913.
- 248 C. H. Huang and T. M. Chen, *J. Phys. Chem. C*, 2011, **115**, 2349–2355.
- 35 249 R. Reisfeld, E. Greenberg, R. Velapoldi and B. Barnett, *J. Chem. Phys.*, 1972, **56**, 1698–1705.
- 250 B. M. Antipeuko, I. M. Bataev, V. L. Ermolaev, E. I. Lyubimov and T. A. Privalova, *Opt. Spectrosc.*, 1970, **29**, 177–180.
- 40 251 Blasse, G. *Philips Res. Rep.*, 1969, **24**, 131–144.
- 252 D. L. Dexter and J. A. Schulman, *J. Chem. Phys.*, 1954, **22**, 1063–1070.
- 253 W. J. Yang, L. Y. Luo, T. M. Chen and N. S. Wang, *Chem. Mater.*, 2005, **17**, 3883–3888.
- 45 254 C. H. Huang, T. W. Kuo and T. M. Chen, *ACS Appl. Mater. Interfaces*, 2010, **2**, 1395–1399.
- 255 D. L. Dexter, *J. Chem. Phys.*, 1953, **21**, 836–850.
- 256 H. P. You, J. L. Zhang, G. Y. Hong and H. J. Zhang, *J. Phys. Chem. C* 2007, **111**, 10657–10661.
- 50 257 H. Y. Chung, C. H. Lu and C. H. Hsu, *J. Am. Ceram. Soc.*, 2010, **93**, 1838–1841.
- 258 C. H. Hsu and C. H. Lu, *J. Mater. Chem.*, 2011, **21**, 2932–2939.
- 259 D. L. Geng, M. M. Shang, Y. Zhang, H. Z. Lian, Z. Y. Cheng and J. Lin, *J. Mater. Chem. C*, 2013, **1**, 2345–2353.
- 55 260 Y. Zhang, D. L. Geng, M. M. Shang, Y. Wu, X. J. Li, H. Z. Lian, Z. Y. Cheng, and J. Lin, *Eur. J. Inorg. Chem.*, 2013, **2013**, 4389–4397.
- 261 Y. Zhang, G. G. Li, D. L. Geng, M. M. Shang, C. Peng and J. Lin, *Inorg. Chem.*, 2012, **51**, 11655–11664.
- 60 262 D. L. Geng, G. G. Li, M. M. Shang, D. M. Yang, Y. Zhang, Z. Y. Cheng, J. Lin, *J. Mater. Chem.*, 2012, **22**, 14262–14271.
- 263 Y. F. Liu, X. Zhang, Z. D. Hao, X. J. Wang and J. H. Zhang, *Chem. Commun.*, 2011, **47**, 10677–10679.
- 264 C. H. Huang, T. S. Chan, W. R. Liu, D. Y. Wang, Y. C. Chiu, Y. T. Yeh, T. M. Chen, *J. Mater. Chem.*, 2012, **22**, 20210–20216.
- 265 C. H. Huang, T. M. Chen, W. R. Liu, Y. C. Chiu, Y. T. Yeh, S. M. Jang, *ACS Appl. Mater. & Interface*, 2010, **2**, 259–264.
- 70 266 C. H. Huang, W. R. Liu, T. M. Chen, *J. Phys. Chem. C*, 2010, **114**, 18698–18701.
- 267 W. Lü, Z. D. Hao, X. Zhang, Y. S. Luo, X. J. Wang and J. H. Zhang, *Inorg. Chem.*, 2011, **50**, 7846–7851.
- 75 268 G. Y. Lee, W. B. Im, A. Kirakosyan, S. H. Cheong, J. Y. Han and D. Y. Jeon, *Opt. Exp.*, 2018, **21**, 3287–3297.
- 269 S. S. Pitale, V. Kumar, I. M. Nagpure, O. M. Ntwaeaborwa, E. Coetsee and H. C. Swart, *J. Appl. Phys.*, 2011, **109**, 013105.
- 80 270 P. H. Holloway, H. C. Swart and O. M. Ntwaeaborwa, *J. Vac. Sci. Technol. A*, 2013, **31**, 050808.
- 271 D. Rag, D. Park, and Y. Kim, *J. Electrochem. Soc.*, 2004, **151**, H210–H212.
- 272 Y. H. Song, X. C. Xu, H. F. Zou, Y. Sheng and H. P. You, *J. Alloys Comp.*, 2012, **513**, 86–90.
- 85 273 C. Y. Duan, J. Chen, S. Z. Deng, N. S. Xu, J. H. Zhang, H. B. Liang and Q. Su, *J. Vac. Sci. Technol. B*, 2007, **25**, 618–622.
- 274 J. J. Hren, in *Principles of Analytical Electron Microscopy*, edited by D. C. Joy, A. D. Romig and J. I. Goldstein Plenum, New York, 1986, p.353.
- 90 275 C. H. Seager, D. R. Tallant and W. L. Warren, *J. Appl. Phys.*, 1997, **82**, 4515–4519.
- 276 Y. R. Do, D. H. Park, H. G. Yang, W. Park, B. K. Wagner, K. Yasuda and C. J. Summers, *J. Electrochem. Soc.*, 2001, **148**, G548–G551.
- 95 277 W. Hetaba, A. Mogilatenko and W. Neumann, *Micron*, 2010, **41**, 479–483.

20 displays (FEDs) and white light emitting diodes (W-LEDs) via
solid state reaction and soft chemistry methods.

5
25 Jun Lin is a professor at the Changchun Institute of Applied
Chemistry (CIAC), Chinese Academy of Sciences (CAS). He
received BSc and MSc degrees in inorganic chemistry from Jilin



Guogang Li is currently an
associate professor in China
University of Geosciences
(Wuhan). He received her BSc
10 degree from Hebei Normal
University of Science &
Technology in 2007 and then
has been a graduate student at
Changchun Institute of
15 Applied Chemistry (CIAC),

Chinese Academy of Sciences, and received a PhD degree in
2012. After graduation, he has worked as a postdoctor in Taiwan
University for one year. His current research interests mainly
include synthesis of luminescent materials for field emission



University, in 1989 and 1992,
respectively, and a PhD degree
(inorganic chemistry) from
30 CIACCAS, in 1995. He has
worked as a postdoctor for
more than 4 years in CityU
(HK, 1996), INM (Germany,
1997) and VCU/UNO (USA,
35 1998–1999). His research
interests include luminescent

materials and multifunctional composite materials together with
their applications in display, lighting and biomedical fields. He
has published more than 300 peer-reviewed journal articles in
40 related fields.